Part II

Linear response and excitation energies

7
The formal framework of linear-response TDDFT

The calculation of excited-state properties has been a long-standing goal in DFT, but it became clear early on that the ground-state theory was only of limited practical use for this purpose. As we discussed in Chapter 2, the excited-state energies E_n of an electronic many-body system are formally expressible as functionals of the ground-state density n_0, but this statement isn't terribly useful in real life.

The easiest and most obvious thing to do is to disregard all warnings, take the Kohn–Sham energy eigenvalues of the unoccupied orbitals at face value, and interpret their differences $\varepsilon_j - \varepsilon_k$ as excitation energies of the many-body system. In practice, this is a common way to analyze and interpret spectroscopic results (Körzdörfer *et al.*, 2009). Unfortunately, there is no strict formal justification for doing so, and the results often turn out to be of poor quality, especially if simple approximations to the xc functional are used. The question of the physical meaning of the Kohn–Sham eigenvalues will be addressed later, in Section 9.1, and there we will see that the Kohn–Sham energies resulting from the exact xc potential can, in fact, be very close to the true excitation energies. Of course, this works only for small systems where the exact xc potential can be numerically constructed, and is thus of no great help in practice.

Various DFT-based schemes for the calculation of excited states have been developed over the years. We give an overview of these schemes in Appendix F. Although considerable progress has been made with the formal underpinnings of DFT for excited states, the practical value of these approaches has so far remained limited, apart from simple proof-of-principle calculations for small systems.

In this chapter we shall discuss how TDDFT can be used to calculate excitation energies and optical spectra. The formal basis is linear-response theory, and we shall go over the general aspects in Sections 7.1 and 7.2. After a simple warm-up exercise in Section 7.3, the general TDDFT formalism for the calculation of excitation energies is derived in Section 7.4, based on linear-response theory. Sections 7.5–7.7 give some discussion and present some simplified schemes.

Why is TDDFT so well suited and successful for the calculation of excitation energies, and how does it work? In simple words, it is because TDDFT captures the essentially dynamical nature of an excitation process. During a transition between the ground state and an excited state, periodic charge-density fluctuations are induced, which are accompanied by dynamical many-body effects and mixing of Kohn–Sham eigenstates. Together, this leads to corrections of the static Kohn–Sham eigenvalue spectrum towards the true spectrum. The dynamical many-body effects are embodied

in the so-called xc kernel $f_{\rm xc}$, which will be introduced in Section 7.3.2. The xc kernel plays a crucial role in linear-response TDDFT, and we will dedicate Chapter 8 to the discussion of its various properties and approximations. Practical aspects and results for atomic and molecular systems will be the subject of Chapter 9.

7.1 General linear-response theory

The dynamics of electronic many-body systems is rigorously described by the time-dependent Schrödinger equation (3.5) or, alternatively, by the TDKS scheme. In Part I of this book we studied the formal aspects of these approaches, and we discussed a variety of applications.

In practice, a full solution of the time-dependent Schrödinger equation or the TDKS equation is often not necessary, or not even desirable. This is the case when the system does not deviate much from the ground state (or, more generally, from equilibrium). In such situations, calculating the full time-dependent wave function (or the full time-dependent density in the TDKS scheme) and extracting small deviations from the ground state from it would be inefficient and numerically difficult; it is vastly preferable to calculate these small differences directly. This can be accomplished using response theory.

Linear-response theory is a very widely used method, which applies whenever one is considering the response to a weak perturbation, such as in describing a spectroscopy experiment which probes the ground state of a system. As we will see, the linear response of a system contains all the information about its excitation spectrum. There also exists a large class of experiments that deal with effects beyond linear response; these situations are described by higher-order response theory.

In this section, we will give a brief overview of the basic linear-response formalism. More complete discussions of the formal aspects of response theory can be found in Pines and Nozières (1966) and Giuliani and Vignale (2005).

7.1.1 Definitions and time-dependent response

We consider a quantum mechanical observable $\hat{\alpha}$, whose ground-state expectation value is given by

$$\alpha_0 = \langle \Psi_0 | \hat{\alpha} | \Psi_0 \rangle \,, \tag{7.1}$$

where Ψ_0 is the ground-state many-body wave function associated with the static Hamiltonian $\hat{H}_0$. Now assume that the system is acted upon by a time-dependent perturbation

$$\hat{H}_1(t) = F(t)\hat{\beta} \,, \qquad t \geq t_0 \,, \tag{7.2}$$

where $F(t)$ is an external field that couples to an observable $\hat{\beta}$ and which is switched on at time t_0. This perturbation affects the wave function of the system, and thus the expectation value of the observable α, which now becomes time-dependent:

$$\alpha(t) = \langle \Psi(t) | \hat{\alpha} | \Psi(t) \rangle \,, \qquad t \geq t_0 \,. \tag{7.3}$$

The difference between the time-dependent expectation value of $\hat{\alpha}$ and its initial static value, $\alpha(t) - \alpha_0$, is called the *response* of $\hat{\alpha}$ to the perturbation (7.2). The response can be expanded in powers of the field $F(t)$:

$$\alpha(t) - \alpha_0 = \alpha_1(t) + \alpha_2(t) + \alpha_3(t) + \dots \,, \tag{7.4}$$

where $\alpha_1(t)$ is the linear response, $\alpha_2(t)$ is the quadratic (or second-order) response, $\alpha_3(t)$ is the third-order response, and so on.[1]

Using eqn (3.19) for the first-order approximation to the time evolution operator and eqn (3.18) for the interaction picture representation of the operators $\hat{\alpha}$ and $\hat{\beta}$, we obtain the linear response as

$$\alpha_1(t) = -i \int_{t_0}^{t} dt' \, F(t') \langle \Psi_0 | [\hat{\alpha}(t), \hat{\beta}(t')] | \Psi_0 \rangle \,. \tag{7.5}$$

Since the initial-state Hamiltonian $\hat{H}_0$ is time-independent, we can replace the commutator $[\hat{\alpha}(t), \hat{\beta}(t')]$ with $[\hat{\alpha}(t-t'), \hat{\beta}]$ in eqn (7.5). We now define the retarded response function

$$\chi_{\alpha\beta}(t-t') = -i\theta(t-t') \langle \Psi_0 | [\hat{\alpha}(t-t'), \hat{\beta}] | \Psi_0 \rangle \,, \tag{7.6}$$

where the word "retarded" indicates that the response at time t is due to a perturbation at an earlier time $t' \leq t$. This crucial causality requirement is ensured by the step function $\theta(t-t')$. The linear response $\alpha_1(t)$ is therefore given by

$$\alpha_1(t) = \int_{-\infty}^{\infty} dt' \, \chi_{\alpha\beta}(t-t') F(t') \,, \tag{7.7}$$

where we are allowed to replace the lower integration limit t_0 by $-\infty$ since the external field $F(t)$ is zero for all times before t_0.

It is to be emphasized that the response function $\chi_{\alpha\beta}(t-t')$ depends only on properties of the system in the absence of the probe. Another important property is that the response function does not depend on the time t_0 at which the perturbation is switched on.

Let us now consider the most important case in the context of TDDFT, namely, the density–density response. Here, the external perturbation is a scalar potential $v_1(\mathbf{r}, t)$, switched on at t_0, which couples to the density operator (3.20),

$$\hat{H}_1(t) = \int d^3r' \, v_1(\mathbf{r}', t) \hat{n}(\mathbf{r}') \,. \tag{7.8}$$

The linear response of the density is given by

$$n_1(\mathbf{r}, t) = \int_{-\infty}^{\infty} dt' \int d^3r' \, \chi_{nn}(\mathbf{r}, \mathbf{r}', t-t') v_1(\mathbf{r}', t') \,, \tag{7.9}$$

where the density–density response function is defined as

$$\chi_{nn}(\mathbf{r}, \mathbf{r}', t-t') = -i\theta(t-t') \langle \Psi_0 | [\hat{n}(\mathbf{r}, t-t'), \hat{n}(\mathbf{r}')] | \Psi_0 \rangle \,. \tag{7.10}$$

To relate eqns (7.9) and (7.10) to the general expressions (7.6) and (7.7), we notice that the linear responses to different perturbations can simply be added independently.

[1] The question remains of whether this expansion of the response in powers of $F(t)$ actually converges. The convergence of perturbation expansions is a subtle mathematical issue beyond the scope of this book; we shall content ourselves with assuming that it is guaranteed as long as the perturbing field $F(t)$ is "sufficiently weak." On the other hand, strong-field phenomena, such as the ones that will be discussed in Chapter 16, require nonperturbative approaches.

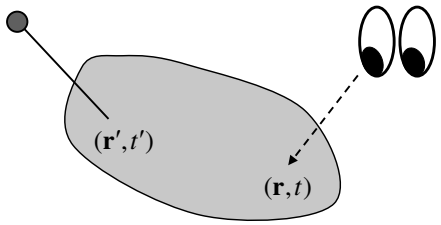

Fig. 7.1 Illustration of the linear response represented by eqn (7.9). We observe the density response of a system at position $\mathbf{r}$ and at time t, caused by the sum of small "needle pricks" at positions $\mathbf{r}'$ and earlier times t'.

Thus, the perturbing Hamiltonian (7.8) can be viewed as a sum of perturbations $v_1(\mathbf{r}', t)\hat{n}(\mathbf{r}')$ which are of the form (7.2); each gives rise to a retarded density response at all $\mathbf{r}$, and all of these are then integrated over space in eqn (7.9). An illustration is given in Fig. 7.1.

7.1.2 Frequency-dependent response and Lehmann representation

In linear-response theory, it is far more common to work in frequency space than to consider the response of the system in real time. As we will see below, replacing the time t with the frequency ω as the basic variable is the key to extracting the excitation energies of a system from its linear response.

Let us define the Fourier transform of the perturbing field, together with its inverse:[2]

$$F(t) = \int_{-\infty}^{\infty} \frac{d\omega}{2\pi} F(\omega) e^{-i\omega t} , \qquad F(\omega) = \int_{-\infty}^{\infty} dt\, F(t) e^{i\omega t} , \tag{7.11}$$

and similarly for all other time-dependent quantities. Inserting this into eqn (7.7) yields

$$\begin{aligned} \int_{-\infty}^{\infty} \frac{d\omega}{2\pi} \alpha_1(\omega) e^{-i\omega t} &= \int_{-\infty}^{\infty} dt' \int_{-\infty}^{\infty} \frac{d\omega}{2\pi} \chi_{\alpha\beta}(\omega) e^{-i\omega(t-t')} \int_{-\infty}^{\infty} \frac{d\omega'}{2\pi} F(\omega') e^{-i\omega' t'} \\ &= \int_{-\infty}^{\infty} \frac{d\omega}{2\pi} \chi_{\alpha\beta}(\omega) F(\omega) e^{-i\omega t} , \end{aligned} \tag{7.12}$$

where we have used the general relation $\int_{-\infty}^{\infty} dt'\, e^{it'(\omega-\omega')} = 2\pi\delta(\omega - \omega')$. Since all exponentials $e^{-i\omega t}$ are linearly independent, this immediately leads to the linear-response equation in frequency space,

$$\alpha_1(\omega) = \chi_{\alpha\beta}(\omega) F(\omega) . \tag{7.13}$$

Now let us take a closer look at the frequency-dependent response function,

[2]Strictly speaking, one should use a notation which distinguishes the Fourier transform of a function from the function itself, e.g., $F(t) = \int (d\omega/2\pi) \tilde{F}(\omega) e^{-i\omega t} + \text{c.c.}$ We shall ignore this subtlety in the interest of simplicity, since the distinction can be inferred from the functional arguments t and ω.

$$\chi_{\alpha\beta}(\omega) = -i \int_{-\infty}^{\infty} d\tau\, \theta(\tau) \langle \Psi_0 | [\hat{\alpha}(\tau), \hat{\beta}] | \Psi_0 \rangle e^{i\omega\tau} \,. \tag{7.14}$$

We consider the complete set of eigenfunctions $\{\Psi_n\}$, $n = 0, 1, 2, \ldots$, of the Hamiltonian $\hat{H}_0$, where Ψ_0 is the many-body ground state, with energy E_0; Ψ_1 is the first excited state, with energy E_1; and so on. We define the nth excitation energy of the system as $\Omega_n = E_n - E_0$, $n = 1, 2, \ldots$. Notice that this, in general, includes both bound states and continuum states; for the latter, all sums over states have to be converted into integrals over continua of states. Inserting the completeness relation $1 = \sum_{n=0}^{\infty} |\Psi_n\rangle\langle\Psi_n|$ into eqn (7.14) then gives

$$\begin{aligned} \chi_{\alpha\beta}(\omega) = -i \sum_{n=1}^{\infty} \int_{-\infty}^{\infty} d\tau\, \theta(\tau) e^{i\omega\tau} \Big\{ & \langle \Psi_0 | \hat{\alpha} | \Psi_n \rangle \langle \Psi_n | \hat{\beta} | \Psi_0 \rangle e^{-i\Omega_n \tau} \\ & - \langle \Psi_0 | \hat{\beta} | \Psi_n \rangle \langle \Psi_n | \hat{\alpha} | \Psi_0 \rangle e^{i\Omega_n \tau} \Big\} \,, \end{aligned} \tag{7.15}$$

where we have used the explicit form of the interaction representation (3.18) of the operator $\hat{\alpha}$. Next, we use the following integral representation of the step function $\theta(\tau)$:

$$\theta(\tau) = \lim_{\eta \to 0^+} \frac{i}{2\pi} \int_{-\infty}^{\infty} d\omega' \, \frac{e^{-i\omega'\tau}}{\omega' + i\eta} \,, \tag{7.16}$$

which can be proved by contour integration in the complex frequency plane. Using this in eqn (7.15), we obtain

$$\chi_{\alpha\beta}(\omega) = \lim_{\eta \to 0^+} \sum_{n=1}^{\infty} \left\{ \frac{\langle \Psi_0 | \hat{\alpha} | \Psi_n \rangle \langle \Psi_n | \hat{\beta} | \Psi_0 \rangle}{\omega - \Omega_n + i\eta} - \frac{\langle \Psi_0 | \hat{\beta} | \Psi_n \rangle \langle \Psi_n | \hat{\alpha} | \Psi_0 \rangle}{\omega + \Omega_n + i\eta} \right\} . \tag{7.17}$$

Equation (7.17) is called the Lehmann representation of the linear response function $\chi_{\alpha\beta}(\omega)$. It is one of the most important results in response theory because it shows explicitly how a frequency-dependent perturbation couples to the excitation spectrum of a system. This will become clear in Section 7.1.3 when we discuss the analytic behavior of $\chi_{\alpha\beta}(\omega)$ in the complex frequency plane.

The frequency-dependent density response has the following form:

$$n_1(\mathbf{r}, \omega) = \int d^3 r' \chi_{nn}(\mathbf{r}, \mathbf{r}', \omega) v_1(\mathbf{r}', \omega) \,, \tag{7.18}$$

where the Lehmann representation of the density–density response function is given by (here and in the following, $\lim_{\eta \to 0^+}$ is understood)

$$\chi_{nn}(\mathbf{r}, \mathbf{r}', \omega) = \sum_{n=1}^{\infty} \left\{ \frac{\langle \Psi_0 | \hat{n}(\mathbf{r}) | \Psi_n \rangle \langle \Psi_n | \hat{n}(\mathbf{r}') | \Psi_0 \rangle}{\omega - \Omega_n + i\eta} - \frac{\langle \Psi_0 | \hat{n}(\mathbf{r}') | \Psi_n \rangle \langle \Psi_n | \hat{n}(\mathbf{r}) | \Psi_0 \rangle}{\omega + \Omega_n + i\eta} \right\} . \tag{7.19}$$

7.1.3 Basic symmetries and analytic behavior of the response functions

In this section, we list a number of exact properties of the response functions, beginning with some basic symmetries. First of all, the density response $n_1(\mathbf{r}, t)$ must be real, which means that $\chi_{nn}(\mathbf{r}, t, \mathbf{r}', t')$ is a real function. As a consequence, we find

$$\chi_{nn}(\mathbf{r}, \mathbf{r}', \omega) = \chi^*_{nn}(\mathbf{r}, \mathbf{r}', -\omega)\,. \tag{7.20}$$

This tells us that the real part of $\chi_{nn}(\mathbf{r}, \mathbf{r}', \omega)$ is an even function of the frequency, whereas the imaginary part is an odd function. This property holds true for the general case:

$$\chi_{\alpha\beta}(\omega) = \chi^*_{\alpha\beta}(-\omega)\,, \tag{7.21}$$

which can immediately be seen from the Lehmann representation (7.17), under the assumption that $\hat{\alpha}$ and $\hat{\beta}$ are Hermitian operators.

Using the Lehmann representation (7.19) for the density–density response function together with eqn (7.20), one finds the following symmetry relation:

$$\chi_{nn}(\mathbf{r}, \mathbf{r}', \omega) = \chi_{nn}(\mathbf{r}', \mathbf{r}, \omega)\,. \tag{7.22}$$

This expression is an example of the so-called reciprocity relations, which in general are given by

$$\chi_{\alpha\beta}(\omega) = \chi_{\beta^T\alpha^T}(\omega)\,, \tag{7.23}$$

where α^T and β^T are the transposes of the operators α and β. For proofs and further discussion, see Giuliani and Vignale (2005).

Next, let us look at the behavior of $\chi_{\alpha\beta}(\omega)$ in the complex frequency plane. From the Lehmann representation (7.17), we see directly that $\chi_{\alpha\beta}(\omega)$ has poles at the excitation energies Ω_n of the system; the second term of eqn (7.17) has poles at the negatives of the excitation energies Ω_n. In both cases, the poles lie infinitesimally below the real axis, owing to the presence of the small positive parameter η. The strength of the poles is determined by the matrix elements of the operators $\hat{\alpha}$ and $\hat{\beta}$ which couple the ground state to the excited states. Thus, $\chi_{\alpha\beta}(\omega)$ is an analytic function in the upper half of the complex frequency plane.

Reviewing the derivation of eqn (7.17), we recall that the positive infinitesimal η arises from the integral representation (7.16) of the step function $\theta(\tau)$. This step function in time expresses the fact that the system responds only after a perturbation has acted on it. It thus turns out that the analytic properties of $\chi_{\alpha\beta}(\omega)$ in the complex frequency plane are a direct consequence of the causality of the time-dependent response function $\chi_{\alpha\beta}(t - t')$.

Since $\chi_{\alpha\beta}(\omega)$ is analytic in the upper half of the complex plane, we can relate its real and imaginary parts to each other. The following contour integral vanishes for real ω:

$$\oint \frac{dz}{2\pi i}\, \frac{\chi_{\alpha\beta}(z)}{z - \omega + i\eta} = 0\,, \tag{7.24}$$

where the closed contour consists of the real axis and a semicircle at infinity in the upper half of the complex plane, z is a complex integration variable, and η is real and positive. Letting $\eta \to 0^+$ and using the general relation

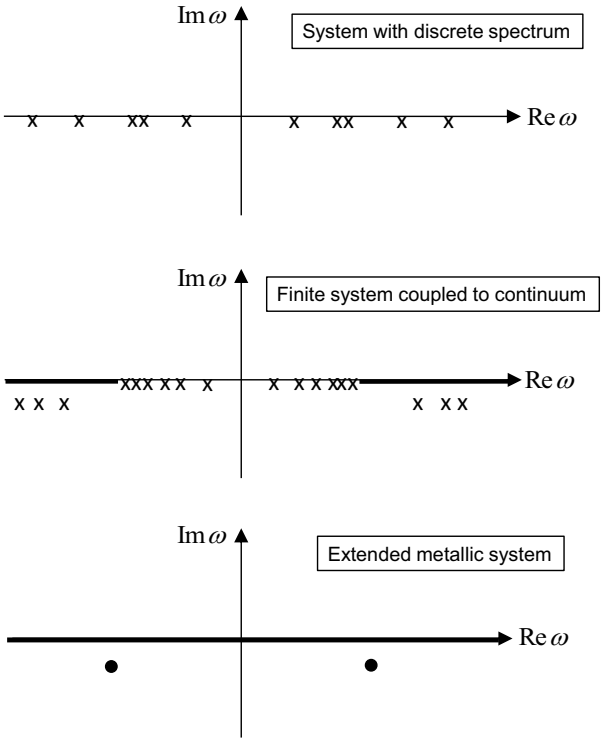

Fig. 7.2 Analytic structure of the response function (7.19) in the complex ω-plane. In a system with a discrete spectrum, the excitations are discrete poles infinitesimally below the real ω-axis. If the system is coupled to a continuum, the discrete poles give way to a branch cut at the ionization threshold, and autoionizing resonances appear embedded in the continuum. In an extended metallic system, all poles merge into a branch cut. New poles form off the real axis, indicating collective plasmon excitations.

$$\lim_{\eta\to 0^+} \frac{1}{\omega-\omega'+i\eta} = \mathcal{P}\frac{1}{\omega-\omega'} - i\pi\delta(\omega-\omega')\,, \tag{7.25}$$

where $\mathcal{P}$ denotes the principal value, and separating the real and imaginary parts using eqn (7.21), we obtain

$$\Re\chi_{\alpha\beta}(\omega) = \mathcal{P}\int_0^\infty \frac{d\omega'}{\pi}\frac{2\omega'}{\omega'^2-\omega^2}\,\Im\chi_{\alpha\beta}(\omega')\,, \tag{7.26}$$

$$\Im\chi_{\alpha\beta}(\omega) = -\mathcal{P}\int_0^\infty \frac{d\omega'}{\pi}\frac{2\omega}{\omega'^2-\omega^2}\,\Re\chi_{\alpha\beta}(\omega')\,. \tag{7.27}$$

Equations (7.26) and (7.27) are known as the Kramers–Kronig relations. They allow one to calculate the real part of the response function from the imaginary part, and vice versa.

Let us now return to the poles of the response function in the complex plane, and discuss three different cases. We first consider a system with a discrete spectrum, such as a particle in a box with infinite walls or a harmonic oscillator, where there are only excitation processes involving discrete bound states. As shown in Fig. 7.2, each excitation can be represented by a pair of poles located at $\omega = \pm\Omega_n - i\eta$. The smaller the confinement of the system, the larger the separation of the poles.

If the system is open and coupled to a continuum, such as in the case of any atom or molecule in infinite space, one obtains a Rydberg series of discrete poles, which eventually gives way to a continuum at the ionization threshold I, indicated by a branch cut just below the real axis. Inner-shell excitations that are embedded in the continuum form so-called autoionizing resonances (Stener *et al.*, 1995), which are characterized by a finite lifetime, as indicated by their distance below the real axis.[3]

Now imagine that the size of the system increases (both the physical size and the number of particles). This causes the level spacing to become smaller, and the poles on the real axis to move closer together, even at low energies. Eventually, in the thermodynamic limit of infinite system size and particle number, the poles merge together completely to form a branch cut in the complex frequency plane, located infinitesimally below the real axis. This is illustrated in the lowest panel of Fig. 7.2, where it is assumed that the extended system has the character of a metal; the excitation spectrum is therefore gapless. In addition to the merging of the poles on the real axis, new poles appear at a finite distance from the real axis. These poles correspond to *collective excitations* of the many-electron system, and their finite imaginary part indicates a finite lifetime.[4] Plasmon excitations in metals will be the subject of Section 12.2.

7.1.4 The fluctuation–dissipation theorem

Let us define the (zero-temperature) dynamical structure factor in the following way:

$$S_{\alpha\alpha^\dagger}(\omega) = \frac{1}{2\pi}\int_{-\infty}^{\infty} d\tau\, \langle\Psi_0|\hat{\alpha}(\tau)\hat{\alpha}^\dagger|\Psi_0\rangle e^{i\omega\tau}\,, \tag{7.28}$$

which should be compared to the definition (7.14) of the response function $\chi_{\alpha\beta}(\omega)$. Analogously to the Lehmann representation (7.17) of $\chi_{\alpha\beta}(\omega)$, we can write the dynamical structure factor as

$$S_{\alpha\alpha^\dagger}(\omega) = \sum_{n=0}^{\infty}\langle\Psi_0|\hat{\alpha}|\Psi_n\rangle\langle\Psi_n|\hat{\alpha}^\dagger|\Psi_0\rangle\delta(\omega-\Omega_n)\,. \tag{7.29}$$

Notice that $S_{\alpha\alpha^\dagger}(\omega) = 0$ for $\omega < 0$ and, likewise, $S_{\alpha\alpha^\dagger}(-\omega) = 0$ for $\omega > 0$. However, this is only true at zero temperature; at finite temperature T, the dynamical structure factor has a form different from eqn (7.29), where (Giuliani and Vignale, 2005)

[3]The line shape of autoionizing resonances is called the Fano profile (Fano, 1961), and can be explained as an interference effect between a discrete excitation and a continuum. For a discussion of Fano resonances in the context of TDDFT, see Hellgren and von Barth (2009) and Krueger and Maitra (2009).

[4]Plasmons are not eigenstates of the system Hamiltonian, but are classified as *quasiparticles*. We will come back to the quasiparticle concept later, in Section 13.3.

$$S_{\alpha\alpha^\dagger}(-\omega;T) = e^{-\omega/k_BT} S_{\alpha^\dagger\alpha}(\omega;T) \tag{7.30}$$

(k_B is the Boltzmann constant). At zero temperature, one finds the following expression, known as the fluctuation–dissipation theorem:

$$\Im\chi_{\alpha\alpha^\dagger}(\omega) = -\pi\Big(S_{\alpha\alpha^\dagger}(\omega) - S_{\alpha^\dagger\alpha}(-\omega)\Big)\,, \tag{7.31}$$

where we have used the relation (7.25). For the density–density response function, we have

$$\Im\chi_{nn}(\mathbf{r},\mathbf{r}',\omega) = -\pi\Big(S_{nn}(\mathbf{r},\mathbf{r}',\omega) - S_{nn}(\mathbf{r}',\mathbf{r},-\omega)\Big)\,. \tag{7.32}$$

Notice that we can write eqn (7.29) in this case as

$$S_{nn}(\mathbf{r},\mathbf{r}',\omega) = n_0(\mathbf{r})n_0(\mathbf{r}')\delta(\omega) + \sum_{n=1}^{\infty}\langle\Psi_0|\hat{n}(\mathbf{r})|\Psi_n\rangle\langle\Psi_n|\hat{n}(\mathbf{r}')|\Psi_0\rangle\delta(\omega-\Omega_n)\,. \tag{7.33}$$

This shows explicitly that the behavior of the dynamical structure factor at finite frequencies is determined by the density fluctuations (i.e., the deviations from the ground-state density n_0).

The dynamical structure factor $S_{nn}(\mathbf{r},\mathbf{r}',\omega)$ has the following important physical interpretation: for $\omega > 0$ it determines the *absorption spectrum*, and for $\omega < 0$ it determines the *stimulated-emission spectrum* (of course, stimulated emission cannot actually occur at $T = 0$, since there is no excited-state population). In turn, the imaginary part of the response function, $\Im\chi(\omega)$, is proportional to the energy dissipated in the system by a steadily oscillating probe (see Exercise 7.6).

7.1.5 High-frequency behavior

We now focus on the high-frequency behavior of the density–density response function (Giuliani and Vignale, 2005; van Leeuwen, 2001). From the Lehmann representation (7.19), we obtain the expansion

$$\chi_{nn}(\mathbf{r},\mathbf{r}',\omega\to\infty) = \frac{M(\mathbf{r},\mathbf{r}')}{\omega^2} + \mathcal{O}\left(\omega^{-4}\right)\,, \tag{7.34}$$

where

$$\begin{aligned} M(\mathbf{r},\mathbf{r}') &= \sum_{n=1}^{\infty}\Omega_n[\langle\Psi_0|\hat{n}(\mathbf{r})|\Psi_n\rangle\langle\Psi_n|\hat{n}(\mathbf{r}')|\Psi_0\rangle + \langle\Psi_0|\hat{n}(\mathbf{r}')|\Psi_n\rangle\langle\Psi_n|\hat{n}(\mathbf{r})|\Psi_0\rangle] \\ &= -\frac{1}{\pi}\int_{-\infty}^{\infty} d\omega\,\omega\Im\chi_{nn}(\mathbf{r},\mathbf{r}',\omega)\,. \end{aligned} \tag{7.35}$$

The last identity follows by using eqn (7.25) in the Lehmann representation (7.19). For the expansion (7.34) to be meaningful, the first frequency moment $M(\mathbf{r},\mathbf{r}')$ must exist and be finite, which is fortunately the case in practice. The infinite sum in eqn (7.35) converges since the matrix elements between the ground state and the nth excited states fall off rapidly for increasing n, owing to the fact that the Ψ_n become more and more rapidly oscillating functions.

One can show, furthermore, that (Goodman and Sjölander, 1973)

$$M(\mathbf{r},\mathbf{r}') = \nabla\nabla'[\delta(\mathbf{r}-\mathbf{r}')n_0(\mathbf{r})]\,, \tag{7.36}$$

so that the response equation in the high-frequency limit simply becomes

$$n_1(\mathbf{r},\omega) \longrightarrow \frac{1}{\omega^2}\,\nabla[n_0(\mathbf{r})\nabla v_1(\mathbf{r},\omega)]\,. \tag{7.37}$$

This tells us that the inverse response function, defined via

$$v_1(\mathbf{r},\omega) = \int d^3r'\;\chi^{-1}_{nn}(\mathbf{r},\mathbf{r}',\omega)n_1(\mathbf{r}',\omega)\,, \tag{7.38}$$

must have a high-frequency expansion of the form

$$\chi^{-1}_{nn}(\mathbf{r},\mathbf{r}',\omega\to\infty) = \omega^2 K(\mathbf{r},\mathbf{r}') + L(\mathbf{r},\mathbf{r}') + \mathcal{O}\left(\omega^{-2}\right)\,, \tag{7.39}$$

where the first coefficient, $K(\mathbf{r},\mathbf{r}')$, can be uniquely constructed from the ground-state density $n_0(\mathbf{r})$ (van Leeuwen, 2001). The second coefficient, $L(\mathbf{r},\mathbf{r}')$, follows in turn from the third-frequency-moment sum rule (Goodman and Sjölander, 1973). Translated into the time domain, we obtain

$$\chi^{-1}_{nn}(\mathbf{r},\mathbf{r}',t-t') = K(\mathbf{r},\mathbf{r}')\frac{\partial^2\delta(t-t')}{\partial t^2} + L(\mathbf{r},\mathbf{r}')\delta(t-t') + F(\mathbf{r},\mathbf{r}',t-t')\,, \tag{7.40}$$

where $F(\mathbf{r},\mathbf{r}',t-t')$ does not contain any delta functions in the time domain, and is in fact a causal function which vanishes for $t<t'$.

Equation (7.40) shows how the high-frequency behavior is directly connected to the short-time domain, leading to characteristic equal-time singularities in the inverse response function.

7.2 Spectroscopic observables

In practice, calculation of the photoresponse is one of the central tasks of linear-response theory. We begin by defining the first-order induced electronic dipole polarization as follows:

$$\mathbf{p}_1(t) = \int dt'\;\mathbb{\alpha}(t-t')\mathbf{E}(t')\,, \tag{7.41}$$

which can be Fourier transformed to

$$\mathbf{p}_1(\omega) = \mathbb{\alpha}(\omega)\mathbf{E}(\omega)\,. \tag{7.42}$$

Here, $\mathbb{\alpha}$ is the dynamic polarizability tensor, and $\mathbf{E}(t)$ is a time-dependent but space-independent externally applied electric field; see Appendix H for a derivation and discussion of the dipole approximation for the interaction between electromagnetic fields and matter.

To be a bit more specific, consider the external potential associated with a monochromatic electric field, assumed to be linearly polarized along the z-direction:

$$v_1(\mathbf{r},t) = \mathcal{E} z \sin(\omega t)\,, \tag{7.43}$$

where $\mathcal{E}$ is the electric field amplitude. The z-component of the dipole polarizability is obtained from the density response as[5]

$$p_{1z}(t) = -\int d^3r\; z n_1(\mathbf{r},t)\,, \tag{7.44}$$

and the zz element of the dynamic dipole polarizability tensor is given by

$$\alpha_{zz}(\omega) = -\frac{2}{\mathcal{E}}\int d^3r\; z n_1(\mathbf{r},\omega)\,. \tag{7.45}$$

Inserting eqn (7.18) for the density response, where $v_1(\mathbf{r},\omega) = (1/2)\mathcal{E}z$, we get

$$\alpha_{zz}(\omega) = -\int d^3r \int d^3r'\; z z' \chi_{nn}(\mathbf{r},\mathbf{r}',\omega)\,. \tag{7.46}$$

With the Lehmann representation (7.19) of the response function, this becomes

$$\alpha_{zz}(\omega) = \sum_{n=1}^{\infty}\left\{\frac{|\langle\Psi_n|\hat{z}|\Psi_0\rangle|^2}{\omega-\Omega_n+i\eta} - \frac{|\langle\Psi_n|\hat{z}|\Psi_0\rangle|^2}{\omega+\Omega_n+i\eta}\right\}, \tag{7.47}$$

with $\hat{z} = \sum_i^N z_i$, where z_i is the z-coordinate of the ith electron. The imaginary part of the dynamic polarizability is proportional to the Fermi's Golden Rule formula for the photoabsorption cross section,

$$\sigma_{zz}(\omega) = \frac{4\pi\omega}{c}\Im\alpha_{zz}(\omega)\,. \tag{7.48}$$

The photoabsorption cross section satisfies the following sum rule:

$$\int_0^\infty d\omega\;\frac{\sigma_{zz}(\omega)}{\omega^2} = \frac{2\pi^2}{c}\,\alpha_{zz}(0)\,, \tag{7.49}$$

where $\alpha_{zz}(0)$ is the static dipole polarizability, which follows from eqn (7.47) by setting $\omega = 0$. We can write down the following general expression for the elements of the dynamic polarizability tensor $\mathbb{\alpha}$:

$$\alpha_{\mu\nu}(\omega) = \sum_{n=1}^{\infty}\frac{2\Omega_n\langle\Psi_0|\hat{r}_\mu|\Psi_n\rangle\langle\Psi_n|\hat{r}_\nu|\Psi_0\rangle}{(\omega+i\eta)^2-\Omega_n^2}\,, \qquad \mu,\nu = 1,2,3\,, \tag{7.50}$$

where $\hat{r}_\mu = \sum_i^N r_{\mu,i}$ is the μth component of the N-electron position operator. The mean polarizability is given by

[5]The definition of $p_{1z}(t)$ accounts for the negative sign of the charge density. By contrast, the definition of $d_\mu(t)$ in eqn (5.10) refers to the dipole moment of the particle density.

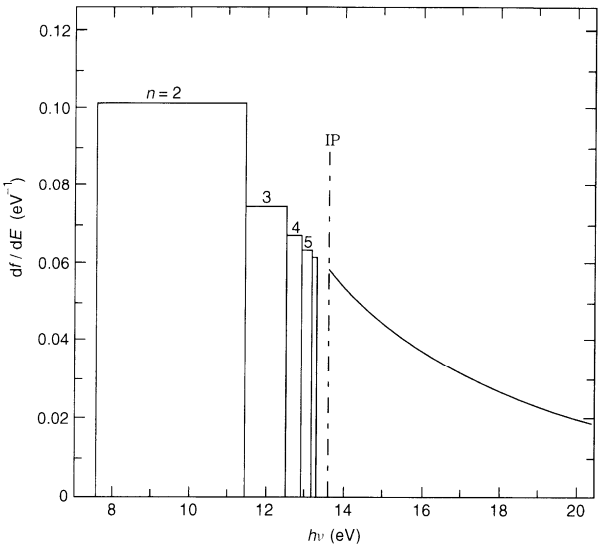

Fig. 7.3 Average oscillator strengths of atomic hydrogen close to the continuum threshold IP. [Reproduced with permission from Academic Press from Berkowitz (2002), ©2002.]

$$\bar{\alpha}(\omega) = \frac{1}{3}\mathrm{tr}\,\mathfrak{A}(\omega) = \sum_{n=1}^{\infty} \frac{f_n}{(\omega + i\eta)^2 - \Omega_n^2}\,. \tag{7.51}$$

The last equality defines the absorption oscillator strengths as the residues of the mean polarizability, where

$$f_n = \frac{2\Omega_n}{3} \sum_{\mu=1}^{3} |\langle \Psi_n | \hat{r}_\mu | \Psi_0 \rangle|^2\,. \tag{7.52}$$

The oscillator strengths are dimensionless quantities which can be defined as the ratio of the absorption rate of a given transition in an atomic or molecular system to the absorption rate of a classical, single-electron oscillator with frequency Ω_n. They satisfy the well-known Thomas–Reiche–Kuhn sum rule, also known as the f-sum rule:

$$\sum_{n=1}^{\infty} f_n = N\,. \tag{7.53}$$

We may also define a dipole strength function $\mathcal{S}(\omega)$, which integrates to the total oscillator strength:

$$\mathcal{S}(\omega) = \sum_n \delta(\omega - \Omega_n) f_n\,, \qquad \int_0^\infty d\omega\, \mathcal{S}(\omega) = N\,. \tag{7.54}$$

In general, the bound-to-bound and bound-to-continuum transitions require somewhat different treatments. Let us illustrate this using the hydrogen atom as an explicit

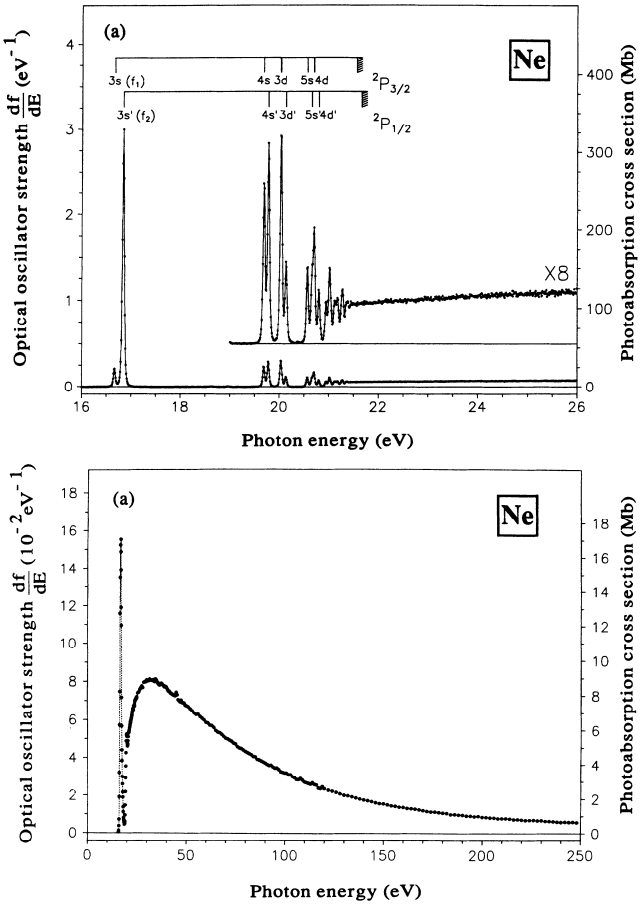

Fig. 7.4 Experimental absolute oscillator strengths for the photoabsorption of neon. Bottom: low-resolution data. Top: high-resolution data close to the ionization threshold. [Reproduced with permission from APS from Chan *et al.* (1992), ©1992.]

example, for which the oscillator strengths can be calculated analytically (Bethe and Salpeter, 1977; Berkowitz, 2002). For the Lyman series, $1s \to np$, one obtains

$$f_n = \frac{2^8 n^5 (n-1)^{2n-4}}{3(n+1)^{2n+4}} \,. \tag{7.55}$$

In the continuum, i.e., for energies above the ionization threshold of 13.6 eV, it is more meaningful to consider the oscillator strength distribution,

$$\frac{df}{dE} = \frac{16}{3(E+1/2)^4} \frac{\exp[-(4\arctan k)/k]}{[1-\exp(-2\pi/k)]} \,, \tag{7.56}$$

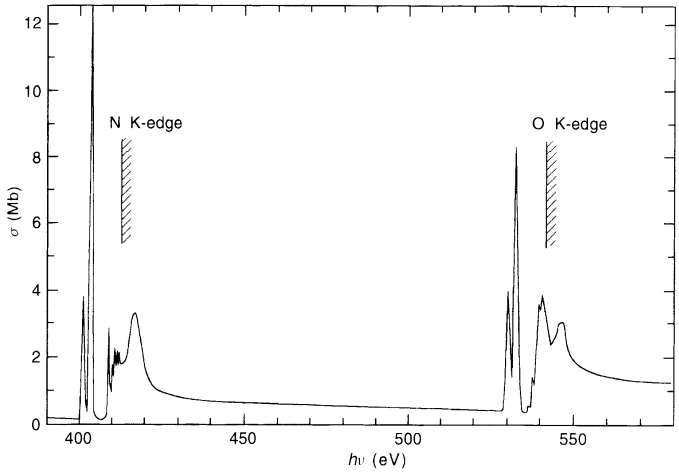

Fig. 7.5 Photoabsorption spectrum of NO_2 (Zhang *et al.*, 1990). [Reproduced with permission from Academic Press from Berkowitz (2002), ©2002.]

where k is the wavenumber of the ejected electron, which is related to the kinetic energy E of the electron by $k^2 = 2E$. The energy of the absorbed photon is $E + 1/2$, since the ionization potential of hydrogen is $1/2$ in Hartree units.

Figure 7.3 shows the average oscillator strengths for atomic hydrogen (Fano and Cooper, 1968). The strengths of the discrete transitions are represented as histograms, where the area of each rectangular block is equal to f_n. The width of the nth base is given by $dE_n/dn = 1/n^3$, where $E_n = -1/2n^2$ is the energy of the nth energy level, and n is assumed to be a continuous variable. In this way, it can be seen how the discrete transitions merge smoothly into the continuum.

Figure 7.4 shows the oscillator strength distribution for the photoabsorption of Ne, determined with electron energy loss spectroscopy (EELS) (Chan *et al.*, 1992). The spectra are normalized such that the sum rule (7.53) is satisfied. The fine structure of the atomic excitations is clearly resolved, where $^2P_{3/2}$ and $^2P_{1/2}$ represent the ground-state doublet configuration of the Ne^+ ion. A slight bump around 50 eV indicates the presence of the $2s \rightarrow np$ autoionizing resonance (Stener *et al.*, 1995).

Lastly, we give an example of the photoabsorption of a molecule. Figure 7.5 shows the photoabsorption spectrum of NO_2 (Zhang *et al.*, 1990; Berkowitz, 2002) in the spectral region close to the K-edges of the nitrogen and oxygen atoms.

From the theoretical and experimental results in Figs. 7.3–7.5, one observes several common trends in the electronic absorption spectra of atoms and molecules. Most importantly, one can distinguish discrete and continuous parts of the spectra, where the continuous parts have maxima close to their respective ionization threshold (there can be several of them, such as in Fig. 7.5) and then drop off smoothly for higher energies. The discrete absorption peaks have the highest oscillator strength for the lowest excitations; as the ionization threshold is approached, the peaks decrease in magnitude and form a Rydberg series.

7.3 Linear density response in TDDFT

7.3.1 The Runge–Gross theorem in linear response and the question of invertibility

We consider time-dependent external potentials of the form

$$v(\mathbf{r},t) = v_0(\mathbf{r}) + v_1(\mathbf{r},t)\theta(t-t_0)\,, \tag{7.57}$$

i.e., the system is in its ground state for times less than t_0, and $v_1(\mathbf{r},t)$ is a small time-dependent perturbation which is switched on at t_0. Notice that this expression is the same as eqn (4.2), but there the potential v_1 is not necessarily small.

The initial many-body ground state is uniquely determined by the Hohenberg–Kohn theorem of static DFT, and, according to the Runge–Gross theorem of Section 3.2, there exists a unique one-to-one correspondence between $v(\mathbf{r},t)$ and the time-dependent density $n(\mathbf{r},t)$. This means that we can formally write the time-dependent density as a functional of the external potential, without any dependence on the initial many-body state:

$$n(\mathbf{r},t) = n[v](\mathbf{r},t)\,. \tag{7.58}$$

Following eqn (7.4), we expand the density response in powers of the perturbation v_1:

$$n(\mathbf{r},t) - n_0(\mathbf{r}) = n_1(\mathbf{r},t) + n_2(\mathbf{r},t) + n_3(\mathbf{r},t) + \ldots\,. \tag{7.59}$$

The first-order density response is given by

$$n_1(\mathbf{r},t) = \int dt' \int d^3r'\, \chi(\mathbf{r},t,\mathbf{r}',t')v_1(\mathbf{r}',t') \tag{7.60}$$

[see eqn (7.9)], where from now on we simply write χ instead of χ_{nn} for the density–density response function.

Since eqn (7.59) represents a functional Taylor expansion of the density response, we obtain the following expression for the density–density response function of the many-body system:

$$\chi(\mathbf{r},t,\mathbf{r}',t') = \left.\frac{\delta n[v](\mathbf{r},t)}{\delta v(\mathbf{r}',t')}\right|_{v_0(\mathbf{r})}\,. \tag{7.61}$$

Via the Hohenberg–Kohn theorem, the initial potential $v_0[n_0](\mathbf{r})$ is a functional of the initial density. Equation (7.61) thus shows explicitly that the linear response function is a functional of the ground-state density only.

The one-to-one correspondence between time-dependent densities and potentials implies that one should also be able to calculate the perturbing potential from the linear density response:

$$v_1(\mathbf{r},t) = \int dt' \int d^3r'\, \chi^{-1}(\mathbf{r},t,\mathbf{r}',t')n_1(\mathbf{r}',t')\,, \tag{7.62}$$

where χ^{-1} is the inverse response function, whose existence is indeed guaranteed by the Runge–Gross theorem. Nevertheless, there are some subtle points to the question of the invertibility of the density–density response function, which we shall now discuss.

First of all, the Runge–Gross proof of Section 3.2 requires that the external time-dependent potential $v_1(\mathbf{r},t)$ which is switched on at t_0 is an analytic function of time for $t = t_0$. However, it turns out that this condition can be relaxed. As shown by van Leeuwen (2001), the density–density response function is invertible for all switch-on processes. For external perturbations $v_1(\mathbf{r},t)$ which are Laplace-transformable, it is guaranteed that no two different potentials can give the same density response. This means that in linear response, we can get away with a weaker restriction on the potential than the analyticity at $t = t_0$ that is required by the Runge–Gross theorem in the general, nonlinear case.

According to eqn (7.61), the response function is not invertible for those potential perturbations which cause zero change in the time-dependent density. For switch-on processes, this happens only in the trivial case where the perturbation is a purely time-dependent function, $v_1(\mathbf{r},t) = c(t)$. The existence of a switch-on time t_0, even if it is in the distant past, thus turns out to be crucial for the invertibility of the response function. The case of frequency-dependent perturbations which have existed at all times, on the other hand, has some potential pitfalls.[6]

Mearns and Kohn (1987) studied the question of whether there exist density responses $n_1(\mathbf{r},\omega)$ that do not come from any perturbations $v_1(\mathbf{r},\omega)$. Away from its poles, the frequency-dependent density–density response function is Hermitian and real, and one can therefore consider the eigenvalue equation

$$\int d^3r'\, \chi_{nn}(\mathbf{r},\mathbf{r}',\omega)\zeta_l(\mathbf{r}',\omega) = \lambda_l\zeta_l(\mathbf{r},\omega)\,. \tag{7.63}$$

Here, the $\zeta_l(\mathbf{r},\omega)$ are a set of orthonormal eigenfunctions, and the $\lambda_l(\omega)$ are the associated real eigenvalues. Both depend parametrically on the frequency ω. Now assume that there is some particular frequency $\bar{\omega}$ at which one of the eigenvalues $\lambda_{\bar{l}}(\bar{\omega})$ is zero, with an associated eigenfunction $\zeta_{\bar{l}}(\mathbf{r},\bar{\omega})$. This immediately tells us that there exists an external perturbation such that the density response vanishes, namely,

$$\bar{v}_1(\mathbf{r},\bar{\omega}) = \gamma\zeta_{\bar{l}}(\mathbf{r},\bar{\omega})\,, \quad \gamma \ll 1\,, \tag{7.64}$$

so that

$$\int d^3r'\, \chi_{nn}(\mathbf{r},\mathbf{r}',\bar{\omega})\bar{v}_1(\mathbf{r},\bar{\omega}) = 0\,. \tag{7.65}$$

As a consequence, the density response $\bar{n}_1(\mathbf{r},\bar{\omega}) = \gamma\zeta_{\bar{l}}(\mathbf{r},\bar{\omega})$ cannot be induced by any frequency-dependent perturbation.

Mearns and Kohn showed that this scenario does indeed happen in the explicit example of noninteracting particles in a box, and that it cannot be ruled out for general interacting or noninteracting systems; however, zero eigenvalues of the response function can only occur for isolated frequencies above the first resonance. We will reencounter this issue in Section 13.3.1.

As a final remark on this topic, it turns out that the problem of the zeros of the response function is characteristic of finite systems that are described by the time-dependent Schrödinger equation. If one instead considers large systems in thermal

[6]Strictly speaking, of course, there are in reality no perturbations which have existed forever.

equilibrium (where the second law of thermodynamics is valid, which implies some form of coupling to a heat bath), all is well and the response functions are always invertible (Ng and Singwi, 1987; Gross *et al.*, 1988*a*; Ng and Singwi, 1988). Of course, for such a scenario, the TDDFT formalism as discussed so far does not really apply, since the Schrödinger equation is time-reversible. In any case, let us emphasize again that all examples where the response function is noninvertible are for perturbations that exist at all times. In all other cases, with a switch-on time t_0, the invertibility of the response function is guaranteed.

7.3.2 Linear response of the Kohn–Sham system

As we discussed earlier, in Section 4.1, the time-dependent density $n(\mathbf{r},t)$ corresponding to the external potential (7.57) can also be reproduced in a noninteracting, time-dependent Kohn–Sham system with the effective potential

$$v_s[n](\mathbf{r},t) = v(\mathbf{r},t) + \int d^3r' \, \frac{n(\mathbf{r}',t)}{|\mathbf{r}-\mathbf{r}'|} + v_{\rm xc}[n](\mathbf{r},t) \, . \tag{7.66}$$

This can be formally inverted, and we can express the time-dependent density as a functional of the Kohn–Sham potential:

$$n(\mathbf{r},t) = n[v_s](\mathbf{r},t) \, . \tag{7.67}$$

A connection to eqn (7.58) is established by noticing that the Kohn–Sham effective potential is in turn a functional of the external potential, so that $n[v_s](\mathbf{r},t) = n[v_s[v]](\mathbf{r},t)$. Following the steps of Section 7.3.1, we expand the time-dependent density in orders of the effective potential, where the first-order term is given by

$$n_1(\mathbf{r},t) = \int dt' \int d^3r' \, \chi_s(\mathbf{r},t,\mathbf{r}',t') v_{s1}(\mathbf{r}',t') \, . \tag{7.68}$$

Here,

$$\chi_s(\mathbf{r},t,\mathbf{r}',t') = \left. \frac{\delta n[v_s](\mathbf{r},t)}{\delta v_s(\mathbf{r}',t')} \right|_{v_s[n_0](\mathbf{r})} \tag{7.69}$$

is the density–density response function for noninteracting Kohn–Sham particles, and the linearized effective potential is

$$v_{s1}[n](\mathbf{r},t) = v_1(\mathbf{r},t) + \int d^3r' \, \frac{n_1(\mathbf{r}',t)}{|\mathbf{r}-\mathbf{r}'|} + v_{\rm xc1}(\mathbf{r},t) \, . \tag{7.70}$$

The first two terms on the right-hand side are straightforward to write down; they are simply the external perturbation v_1 and the linearized time-dependent Hartree potential. The last term is the linearized xc potential, and an explicit expression for it is obtained by functional Taylor expansion:

$$v_{\rm xc1}(\mathbf{r},t) = \int dt' \int d^3r' \, \left. \frac{\delta v_{\rm xc}[n](\mathbf{r},t)}{\delta n(\mathbf{r}',t')} \right|_{n_0(\mathbf{r})} n_1(\mathbf{r}',t') \, . \tag{7.71}$$

The linearized xc potential features the so-called time-dependent xc kernel,

$$f_{\rm xc}(\mathbf{r},t,\mathbf{r}',t') = \left.\frac{\delta v_{\rm xc}[n](\mathbf{r},t)}{\delta n(\mathbf{r}',t')}\right|_{n_0(\mathbf{r})}, \tag{7.72}$$

which is a functional of the ground-state density. The xc kernel is the key quantity of TDDFT in the linear-response regime. Chapter 8 will be dedicated to a discussion of its properties and various approximations.

Equation (7.68) is the linear-response equation in TDDFT. It yields the same density response as the many-body linear-response equation (7.60). Let us insert eqn (7.70) into eqn (7.68):

$$\begin{aligned} n_1(\mathbf{r},t) = \int dt' \int d^3r'\, \chi_s(\mathbf{r},t,\mathbf{r}',t') \Bigg[v_1(\mathbf{r}',t') \\ + \int d\tau \int d^3x \left\{ \frac{\delta(t'-\tau)}{|\mathbf{r}'-\mathbf{x}|} + f_{\rm xc}(\mathbf{r}',t',\mathbf{x},\tau) \right\} n_1(\mathbf{x},\tau) \Bigg]. \end{aligned} \tag{7.73}$$

This shows that the linear density response must be calculated self-consistently, since the linearized effective potential on the right-hand side depends on $n_1(\mathbf{r},t)$. Furthermore, we can establish a relation between the interacting and noninteracting response functions by inserting eqn (7.60) into eqn (7.73):

$$\begin{aligned} \int dt' \int d^3r'\, \chi(\mathbf{r},t,\mathbf{r}',t') v_1(\mathbf{r}',t') = \int dt' \int d^3r'\, \chi_s(\mathbf{r},t,\mathbf{r}',t') \Bigg[v_1(\mathbf{r}',t') \\ + \int d\tau \int d^3x \left\{ \frac{\delta(t'-\tau)}{|\mathbf{r}'-\mathbf{x}|} + f_{\rm xc}(\mathbf{r}',t',\mathbf{x},\tau) \right\} \int d\tau' \int d^3x'\, \chi(\mathbf{x},\tau,\mathbf{x}',\tau') v_1(\mathbf{x}',\tau') \Bigg]. \end{aligned} \tag{7.74}$$

This equation holds for any perturbation v_1, whereas the response functions and the Hartree and xc integral kernels are ground-state properties of the system and thus independent of the perturbation. Therefore we obtain the following expression connecting the interacting and noninteracting response functions:

$$\begin{aligned} \chi(\mathbf{r},t,\mathbf{r}',t') = \chi_s(\mathbf{r},t,\mathbf{r}',t') \\ + \int d\tau \int d^3x \int d\tau' \int d^3x'\, \chi_s(\mathbf{r},t,\mathbf{x},\tau) \left\{ \frac{\delta(\tau-\tau')}{|\mathbf{x}-\mathbf{x}'|} + f_{\rm xc}(\mathbf{x},\tau,\mathbf{x}',\tau') \right\} \chi(\mathbf{x}',\tau',\mathbf{r}',t'). \end{aligned} \tag{7.75}$$

Integral equations of this kind, relating interacting and noninteracting quantities of a many-body system, are known as Dyson-type equations. From a purely formal point of view, eqn (7.75) can also be used to *define* the xc kernel $f_{\rm xc}$. However, eqn (7.72), which defines $f_{\rm xc}$ as a functional derivative of the time-dependent xc potential, has practical and conceptual advantages when it comes to the construction of standard approximations, as we will see later.

The interacting and noninteracting response functions depend only on the time difference $t-t'$, as shown in Section 7.1.1. Via eqn (7.75), it is therefore clear that the xc kernel also depends on the time difference only, i.e., $f_{\rm xc} = f_{\rm xc}[n_0](\mathbf{r},\mathbf{r}',t-t')$. The frequency-dependent xc kernel is thus defined as the Fourier transform of eqn (7.72),

$$f_{\rm xc}(\mathbf{r},\mathbf{r}',\omega) = \int d(t-t')\, e^{i\omega(t-t')} \left.\frac{\delta v_{\rm xc}[n](\mathbf{r},t)}{\delta n(\mathbf{r}',t')}\right|_{n_0(\mathbf{r})}, \tag{7.76}$$

or, alternatively, it can be defined via the Fourier transform of eqn (7.75):

$$f_{\rm xc}(\mathbf{r},\mathbf{r}',\omega) = \chi_s^{-1}(\mathbf{r},\mathbf{r}',\omega) - \chi^{-1}(\mathbf{r},\mathbf{r}',\omega) - \frac{1}{|\mathbf{r}-\mathbf{r}'|}\,. \tag{7.77}$$

For later reference, it is also convenient to define the combined Hartree–xc kernel as

$$f_{\rm Hxc}(\mathbf{r},\mathbf{r}',\omega) = \frac{1}{|\mathbf{r}-\mathbf{r}'|} + f_{\rm xc}(\mathbf{r},\mathbf{r}',\omega)\,. \tag{7.78}$$

With this, we can carry out the Fourier transformation of the TDDFT linear-response equation and obtain

$$n_1(\mathbf{r},\omega) = \int d^3r'\,\chi_s(\mathbf{r},\mathbf{r}',\omega)\left[v_1(\mathbf{r}',\omega) + \int d^3x\left\{\frac{1}{|\mathbf{r}'-\mathbf{x}|} + f_{\rm xc}(\mathbf{r}',\mathbf{x},\omega)\right\} n_1(\mathbf{x},\omega)\right], \tag{7.79}$$

which is the counterpart of eqn (7.18). The frequency-dependent, noninteracting Kohn–Sham response function is given by

$$\chi_s(\mathbf{r},\mathbf{r}',\omega) = \sum_{j,k=1}^{\infty}(f_k - f_j)\frac{\varphi_j^0(\mathbf{r})\varphi_k^{0*}(\mathbf{r})\varphi_j^{0*}(\mathbf{r}')\varphi_k^0(\mathbf{r}')}{\omega - \omega_{jk} + i\eta}\,, \tag{7.80}$$

where f_j and f_k are occupation numbers of the Kohn–Sham ground state (1 for occupied and 0 for unoccupied orbitals), and the quantities

$$\omega_{jk} = \varepsilon_j - \varepsilon_k \tag{7.81}$$

are differences between Kohn–Sham energy eigenvalues. The structure of the double summation in $\chi_s(\mathbf{r},\mathbf{r}',\omega)$ is such that only those terms contribute where one summation index refers to an occupied orbital and the other refers to an unoccupied orbital, i.e., $j \le N$ and $k > N$ or vice versa; all other terms cancel out. This means that the absolute values of the quantities ω_{jk} are the excitation energies of the Kohn–Sham system. We thus see that the noninteracting Kohn–Sham response function χ_s has poles at the excitation energies of the Kohn–Sham system.

At first sight, this seems to lead to a dramatic inconsistency. From eqn (7.18), one sees that the density response $n_1(\mathbf{r},\omega)$ diverges at the exact excitation energies Ω_n, since these are the poles of the full many-body response function χ [see eqn (7.19)]. On the other hand, we have shown that the exact density response $n_1(\mathbf{r},\omega)$ can also be obtained from the TDDFT expression (7.79); but from that it appears that the divergences of n_1 occur instead where the poles of χ_s are, that is, at the excitation frequencies ω_{jk} of the Kohn–Sham system (which are different from Ω_n).

To resolve this apparent contradiction, the "wrong" poles at ω_{jk} on the right-hand side of eqn (7.79) need to be somehow replaced by the "right" poles at the true excitation energies Ω_n. How does this work? There are two things in the TDDFT linear-response equation (7.79) which make sure that the poles at Ω_n come out correctly:

the self-consistency and the structure of $f_{\rm xc}$. To see this, let us for a moment treat integral operators as if they were numbers, and write eqn (7.79) symbolically as

$$n_1 = \chi_s v_1 + \chi_s f_{\rm Hxc} n_1 \,. \tag{7.82}$$

Solving for n_1, we have

$$n_1 = \frac{\chi_s v_1}{1 - \chi_s f_{\rm Hxc}} \,, \tag{7.83}$$

which demonstrates that the poles of χ_s cancel out in the self-consistent calculation of n_1. What remains is that the true poles of the density response have to be introduced on the right-hand side of eqn (7.83), which is accomplished through $f_{\rm Hxc} = \chi_s^{-1} - \chi^{-1}$, so that one recovers the many-body response equation $n_1 = \chi v_1$.

7.3.3 Spin-dependent formalism

Linear-response TDDFT is most commonly applied in an explicitly spin-dependent formulation. As we shall see, this provides more flexibility for the description of open-shell systems and various other properties. In this section, we briefly summarize the essential equations without going into any details of the existence proofs, which are for the most part straightforward generalizations of the spin-independent formalism (Liu and Vosko, 1989).

The linear spin-density response is given by

$$n_{1\sigma}(\mathbf{r},\omega) = \sum_{\sigma'} \int d^3r' \, \chi_{s,\sigma\sigma'}(\mathbf{r},\mathbf{r}',\omega) v_{s1\sigma'}(\mathbf{r}',\omega) \,, \tag{7.84}$$

with the spin-dependent linearized effective potential

$$v_{s1\sigma}(\mathbf{r},t) = v_{1\sigma}(\mathbf{r},\omega) + \sum_{\sigma'} \int d^3r' \left\{ \frac{1}{|\mathbf{r}-\mathbf{r}'|} + f_{{\rm xc},\sigma\sigma'}(\mathbf{r},\mathbf{r}',\omega) \right\} n_{1\sigma'}(\mathbf{r}',\omega) \,. \tag{7.85}$$

The noninteracting Kohn–Sham response function is diagonal in the spin indices:

$$\chi_{s,\sigma\sigma'}(\mathbf{r},\mathbf{r}',\omega) = \delta_{\sigma\sigma'} \sum_{j,k=1}^{\infty} (f_{k\sigma} - f_{j\sigma}) \frac{\varphi^0_{j\sigma}(\mathbf{r}) \varphi^{0*}_{k\sigma}(\mathbf{r}) \varphi^{0*}_{j\sigma}(\mathbf{r}') \varphi^0_{k\sigma}(\mathbf{r}')}{\omega - \omega_{jk\sigma} + i\eta} \,, \tag{7.86}$$

where $f_{j\sigma}$ and $f_{k\sigma}$ are occupation numbers of the Kohn–Sham spin orbitals, and

$$\omega_{jk\sigma} = \varepsilon_{j\sigma} - \varepsilon_{k\sigma} \tag{7.87}$$

are the Kohn–Sham excitation energies. As before, we define for notational convenience the combined Hartree–xc kernel as

$$f_{{\rm Hxc},\sigma\sigma'}(\mathbf{r},\mathbf{r}',\omega) = \frac{1}{|\mathbf{r}-\mathbf{r}'|} + f_{{\rm xc},\sigma\sigma'}(\mathbf{r},\mathbf{r}',\omega) \,. \tag{7.88}$$

The spin-dependent xc kernel is defined, in analogy to eqn (7.76), as the Fourier transform of the time-dependent kernel

$$f_{{\rm xc},\sigma\sigma'}(\mathbf{r},t,\mathbf{r}',t') = \left. \frac{\delta v_{{\rm xc}\sigma}[n_\uparrow, n_\downarrow](\mathbf{r},t)}{\delta n_{\sigma'}(\mathbf{r}',t')} \right|_{n_{0\uparrow}(\mathbf{r}), n_{0\downarrow}(\mathbf{r})} \,. \tag{7.89}$$

7.4 Warm-up exercise: TDDFT for two-level systems

Before we derive the full-fledged theory for calculating excitation energies, it is instructive to start with a warm-up exercise using a simple model system to illustrate the workings of the TDDFT approach. Let us consider a two-level system consisting of two orbitals $\varphi_1^0(\mathbf{r})$ and $\varphi_2^0(\mathbf{r})$ which are eigenstates of the static Kohn–Sham Hamiltonian

$$\hat{H}^0 = -\frac{\nabla^2}{2} + v_0(\mathbf{r}) + \int d^3r' \, \frac{n_0(\mathbf{r}')}{|\mathbf{r}-\mathbf{r}'|} + v_{\rm xc}^0[n_0](\mathbf{r}) \,, \tag{7.90}$$

where $v_{\rm xc}^0$ is the static xc potential, a functional of the ground-state density $n_0(\mathbf{r})$. We assume that initially φ_1^0 is doubly occupied and φ_2^0 is empty, and both orbitals are chosen to be real. The lowest excitation energy in the noninteracting Kohn–Sham system is given by the difference between the orbital eigenvalues,

$$\omega_{21} = \varepsilon_2 - \varepsilon_1 \,. \tag{7.91}$$

Our goal is now to determine the corresponding exact excitation energy of this two-level system using TDDFT. We consider a weak perturbation $\lambda \hat{H}'(\mathbf{r},t)$ acting on the system, where λ is a small parameter. According to time-dependent perturbation theory (Schiff, 1968), the time evolution of the wave function is given by

$$\varphi(\mathbf{r},t) = c_1(t)\varphi_1^0(\mathbf{r}) + \lambda c_2(t)\varphi_2^0(\mathbf{r}) \,, \tag{7.92}$$

where $c_1(t)$ and $c_2(t)$ are complex coefficients. Let us construct the density matrix of this time-dependent two-level system as follows:

$$\mathbb{p}(t) = \begin{pmatrix} \rho_{11} & \lambda\rho_{12} \\ \lambda\rho_{21} & \lambda^2\rho_{22} \end{pmatrix} = \begin{pmatrix} |c_1|^2 & \lambda c_1 c_2^* \\ \lambda c_1^* c_2 & \lambda^2 |c_2|^2 \end{pmatrix} , \tag{7.93}$$

where we explicitly indicate the order of the perturbation through orders of λ. The density matrix obeys the following equation of motion:

$$\frac{\partial}{\partial t}\mathbb{p} = -i[\mathbb{H},\mathbb{p}] = -i[\mathbb{H}^0 + \lambda\mathbb{H}'(t),\mathbb{p}]. \tag{7.94}$$

Dropping terms of order λ^2, this yields the linearized time evolution of the off-diagonal elements of the density matrix as follows:

$$\frac{\partial}{\partial t}\rho_{12} = -i[(H_{11}^0 - H_{22}^0)\rho_{12} - H'_{12}\rho_{11}] \tag{7.95}$$

$$\frac{\partial}{\partial t}\rho_{21} = i[(H_{11}^0 - H_{22}^0)\rho_{21} - H'_{21}\rho_{11}], \tag{7.96}$$

where $H_{11}^0 = \int d^3r \, \varphi_1^0(\mathbf{r}) H^0 \varphi_1^0(\mathbf{r})$, and similarly for all the other matrix elements of $\hat{H}^0$ and $\hat{H}'(t)$ that form the Hamiltonian matrices $\mathbb{H}^0$ and $\mathbb{H}'(t)$. Since $\rho_{11} = 1 + \mathcal{O}(\lambda^2)$, and $H_{22}^0 - H_{11}^0 = \omega_{21}$ (the bare Kohn–Sham excitation energy), this simplifies to

$$\frac{\partial}{\partial t}\rho_{12} = i[\omega_{21}\rho_{12} + H'_{12}], \tag{7.97}$$

$$\frac{\partial}{\partial t}\rho_{21} = -i[\omega_{21}\rho_{21} + H'_{21}]. \tag{7.98}$$

Next, we make the ansatz (which will be justified later)

$$\rho_{12}(t) = \widetilde{\rho}_{12}(\omega)e^{-i\omega t} + \widetilde{\rho}_{12}(-\omega)e^{i\omega t}\,, \tag{7.99}$$

and similarly for ρ_{21}, H'_{12}, and H'_{21}. This gives

$$-\omega\widetilde{\rho}_{12}(\omega) = [\omega_{21}\widetilde{\rho}_{12}(\omega) + \widetilde{H}'_{12}(\omega)], \tag{7.100}$$

$$-\omega\widetilde{\rho}_{21}(\omega) = -[\omega_{21}\widetilde{\rho}_{21}(\omega) + \widetilde{H}'_{21}(\omega)], \tag{7.101}$$

and an additional two equations for $\widetilde{\rho}_{12}(-\omega)$ and $\widetilde{\rho}_{21}(-\omega)$ which do not contain any new information. Adding eqns (7.100) and (7.101) gives

$$\widetilde{\rho}_{12}(\omega) + \widetilde{\rho}_{21}(\omega) = -\frac{\widetilde{H}'_{12}(\omega)}{\omega_{21}+\omega} - \frac{\widetilde{H}'_{21}(\omega)}{\omega_{21}-\omega}\,. \tag{7.102}$$

Let us now consider the perturbing Hamiltonian,

$$\hat{H}'(\mathbf{r},\omega) = \int d^3r' \left[\frac{1}{|\mathbf{r}-\mathbf{r}'|} + f_{\rm xc}(\mathbf{r},\mathbf{r}',\omega)\right]\delta n(\mathbf{r}',\omega)\,, \tag{7.103}$$

where $\delta n(\mathbf{r},\omega)$ is the density response. From eqns (7.92) and (7.93), we have

$$\begin{aligned} n(\mathbf{r},t) &= 2|\varphi(\mathbf{r},t)|^2 \\ &= 2\rho_{11}(t)\varphi_1^0(\mathbf{r})^2 + 2\lambda[\rho_{12}(t)+\rho_{21}(t)]\varphi_1^0(\mathbf{r})\varphi_2^0(\mathbf{r}) + 2\lambda^2\rho_{22}(t)\varphi_2^0(\mathbf{r})^2, \end{aligned} \tag{7.104}$$

where the factor 2 comes from the double occupancy of $\varphi(\mathbf{r},t)$. Taking the first-order term in λ and Fourier transforming, we get

$$\delta n(\mathbf{r},\omega) = 2\varphi_1^0(\mathbf{r})\varphi_2^0(\mathbf{r})[\widetilde{\rho}_{12}(\omega) + \widetilde{\rho}_{21}(\omega)]. \tag{7.105}$$

Notice that we do not consider an external perturbation, only the linearized Hartree and xc potentials. We are thus looking for an "eigenmode" of the system in a steady state. This justifies the ansatz (7.99) used above. We define the double matrix element

$$K_{12,12}(\omega) = \int d^3r \int d^3r'\, \varphi_1^0(\mathbf{r})\varphi_2^0(\mathbf{r}) \left[\frac{1}{|\mathbf{r}-\mathbf{r}'|} + f_{\rm xc}(\mathbf{r},\mathbf{r}',\omega)\right] \varphi_1^0(\mathbf{r}')\varphi_2^0(\mathbf{r}')\,, \tag{7.106}$$

and eqn (7.102) becomes

$$\widetilde{\rho}_{12}(\omega) + \widetilde{\rho}_{21}(\omega) = -2K_{12,12}(\omega)[\widetilde{\rho}_{12}(\omega) + \widetilde{\rho}_{21}(\omega)] \left[\frac{1}{\omega_{21}+\omega} + \frac{1}{\omega_{21}-\omega}\right]. \tag{7.107}$$

Canceling $\widetilde{\rho}_{12} + \widetilde{\rho}_{21}$ on both sides results in

$$1 = -\frac{4\omega_{21}}{\omega_{21}^2 - \omega^2}\, K_{12,12}(\omega)\,, \tag{7.108}$$

which gives the final result

$$\omega^2 = \omega_{21}^2 + 4\omega_{21}K_{12,12}(\omega)\,. \tag{7.109}$$

This is the *exact* lowest excitation energy in this two-level system. The derivation shows that eqn (7.109) accounts for both the excitation $1 \to 2$ and the deexcitation

$2 \to 1$. If we include only the excitation $1 \to 2$ by ignoring the first pole in eqn (7.107), we obtain

$$\omega = \omega_{21} + 2K_{12,12}(\omega) \,. \tag{7.110}$$

Incidentally, the same result comes out if we take the square root of eqn (7.109) and assume that $K_{12,12}$ is small compared with ω_{21}. Equations (7.109) and (7.110) show explicitly how the Kohn–Sham excitation energy is corrected by dynamical Hartree and xc effects.

7.5 Calculation of excitation energies: the Casida equation

7.5.1 Derivation

The most important application of TDDFT in the linear-response regime is in the calculation of excitation energies of finite atomic and molecular systems (Casida, 1995, 1996; Petersilka *et al.*, 1996; Elliott *et al.*, 2009). In this section we will derive the essential equations, first given by Casida (1995), which nowadays are implemented in many electronic-structure codes. As a historical note, this TDDFT formalism for excitation energies is similar to the well-known RPA approach in quantum chemistry (which, of course, does not include exchange and correlation). For an overview and references, see, for example, Schirmer and Mertins (1996).

As we discussed at length in the previous sections, the exact excitation energies Ω_n are given by the poles of the density–density response function, and the density response diverges if the system is subject to any perturbation at precisely such a frequency. In fact, an external perturbation is not even required: a system can sustain a finite response at its excitation frequencies without any external stimulation. This response has the character of an eigenmode of the system.[7] The idea is then to derive a formalism in which these eigenmodes and eigenfrequencies can be calculated directly.[8]

The starting point is the linear-response equation (7.84) without an external perturbation:

$$n_{1\sigma}(\mathbf{r},\Omega) = \sum_{\sigma'\sigma''} \int d^3r' \, \chi_{s,\sigma\sigma'}(\mathbf{r},\mathbf{r}',\Omega) \int d^3r'' f_{\mathrm{Hxc},\sigma'\sigma''}(\mathbf{r}',\mathbf{r}'',\Omega) n_{1\sigma''}(\mathbf{r}'',\Omega) \,. \tag{7.111}$$

Formally, this equation can be viewed as an eigenvalue equation of a frequency-dependent integral operator acting on $n_{1\sigma}(\mathbf{r},\omega)$, and the frequencies Ω which give the eigenvalue 1 are the excitation energies which we are looking for.

Let us introduce the following object:

$$g_{\sigma\sigma'}(\mathbf{r},\Omega) = \int d^3r' \, f_{\mathrm{Hxc},\sigma\sigma'}(\mathbf{r},\mathbf{r}',\Omega) n_{1\sigma'}(\mathbf{r}',\Omega) \,. \tag{7.112}$$

[7] One can think of a suitable initial "kick" in the distant past to get the oscillation going. In Section 9.6, we will say more about excitations in real time and how the associated eigenmodes can be triggered by an external perturbation. It will turn out that in the real-time approach one is less interested in selecting individual transitions than in exciting a broad bandwidth of the excitation spectrum.

[8] This is similar in spirit to the way small oscillations of a system of coupled oscillators are treated in classical mechanics (Goldstein *et al.*, 2002): from the equations of motion, one derives an eigenvalue equation, which yields the normal modes of the system.

Multiplying eqn (7.111) by $f_{\mathrm{Hxc},\alpha\sigma}(\mathbf{x},\mathbf{r},\Omega)$ and integrating over $\mathbf{r}$ leads to

$$g_{\alpha\sigma}(\mathbf{x},\Omega) = \sum_{\sigma'\sigma''} \int d^3r\, f_{\mathrm{Hxc},\alpha\sigma}(\mathbf{x},\mathbf{r},\Omega) \int d^3r'\, \chi_{s,\sigma\sigma'}(\mathbf{r},\mathbf{r}',\Omega) g_{\sigma'\sigma''}(\mathbf{r}',\Omega)\,. \quad (7.113)$$

Now let us look at the noninteracting Kohn–Sham response function (7.86), which we can rewrite as

$$\chi_{s,\sigma\sigma'}(\mathbf{r},\mathbf{r}',\Omega) = \delta_{\sigma\sigma'} \sum_{jk} \alpha_{jk\sigma} \frac{\Phi^*_{jk\sigma}(\mathbf{r})\Phi_{jk\sigma}(\mathbf{r}')}{\Omega - \omega_{jk\sigma} + i\eta}\,, \quad (7.114)$$

where we have defined the following quantities:

$$\alpha_{jk\sigma} = f_{k\sigma} - f_{j\sigma}\,, \quad (7.115)$$

$$\Phi_{jk\sigma}(\mathbf{r}) = \varphi^{0*}_{j\sigma}(\mathbf{r})\varphi^{0}_{k\sigma}(\mathbf{r})\,, \quad (7.116)$$

$$\omega_{jk\sigma} = \varepsilon_{j\sigma} - \varepsilon_{k\sigma}\,. \quad (7.117)$$

With all of this, eqn (7.113) becomes

$$g_{\alpha\sigma}(\mathbf{x},\Omega) = \sum_{jk} \frac{\alpha_{jk\sigma}}{\Omega - \omega_{jk\sigma}} \int d^3r\, f_{\mathrm{Hxc},\alpha\sigma}(\mathbf{x},\mathbf{r},\Omega)\Phi^*_{jk\sigma}(\mathbf{r}) \sum_{\sigma'} \int d^3r'\, \Phi_{jk\sigma}(\mathbf{r}') g_{\sigma\sigma'}(\mathbf{r}',\Omega), \quad (7.118)$$

where we are permitted to drop the infinitesimal $i\eta$ in the denominator, since the frequencies Ω will be away from the Kohn–Sham frequencies $\omega_{jk\sigma}$, as we shall see in the end. Let us now define yet another auxiliary quantity,

$$H_{jk\sigma}(\Omega) = \sum_{\sigma'} \int d^3r\, \Phi_{jk\sigma}(\mathbf{r}) g_{\sigma\sigma'}(\mathbf{r},\Omega)\,, \quad (7.119)$$

with which we can rewrite eqn (7.118) as follows:

$$H_{j'k'\alpha}(\Omega) = \sum_{\sigma} \sum_{jk} \frac{\alpha_{jk\sigma}}{\Omega - \omega_{jk\sigma}} \int d^3x \int d^3r\, \Phi_{j'k'\alpha}(\mathbf{x}) f_{\mathrm{Hxc},\alpha\sigma}(\mathbf{x},\mathbf{r},\Omega)\Phi^*_{jk\sigma}(\mathbf{r}) H_{jk\sigma}(\Omega)\,. \quad (7.120)$$

Next, we define the coupling-matrix elements

$$K_{jk\sigma,j'k'\sigma'}(\Omega) = \int d^3r \int d^3r'\, \Phi_{jk\sigma}(\mathbf{r}) f_{\mathrm{Hxc},\sigma\sigma'}(\mathbf{r},\mathbf{r}',\Omega)\Phi^*_{j'k'\sigma'}(\mathbf{r}')\,, \quad (7.121)$$

and eqn (7.120) becomes

$$H_{jk\sigma}(\Omega) = \sum_{\sigma'} \sum_{j'k'} \frac{\alpha_{j'k'\sigma'}}{\Omega - \omega_{j'k'\sigma'}} K_{jk\sigma,j'k'\sigma'}(\Omega) H_{j'k'\sigma'}(\Omega)\,. \quad (7.122)$$

Finally, the most compact form is achieved by defining

$$\beta_{j'k'\sigma'}(\Omega) = \frac{H_{j'k'\sigma'}(\Omega)}{\Omega - \omega_{j'k'\sigma'}}\,, \quad (7.123)$$

which gives the final expression

$$\sum_{\sigma'}\sum_{j'k'}\Big[\delta_{jj'}\delta_{kk'}\delta_{\sigma\sigma'}\omega_{j'k'\sigma'}+\alpha_{j'k'\sigma'}K_{jk\sigma,j'k'\sigma'}(\Omega)\Big]\beta_{j'k'\sigma'}(\Omega)=\Omega\beta_{jk\sigma}(\Omega)\,. \quad (7.124)$$

This has the form of an eigenvalue equation (of infinite dimension, since it runs over all bound and continuum Kohn–Sham states), and yields in principle the exact excitation energies Ω of the system. From the eigenvectors $\beta_{j'k'\sigma'}(\Omega)$, the associated eigenmode profiles follow as

$$n_{1\sigma}(\mathbf{r},\Omega)=\sum_{jk}\alpha_{jk\sigma}\Phi^*_{jk\sigma}(\mathbf{r})\beta_{jk\sigma}(\Omega)\,, \quad (7.125)$$

which is obtained by plugging eqns (7.112) and (7.119) into eqn (7.123), and comparing the result with eqn (7.111).

Equation (7.124) is defined only for $\alpha_{j'k'\sigma'}\neq 0$, which means of course that in setting up the linear-response matrix we consider only transitions between an occupied and an unoccupied Kohn–Sham state. In the following, we label occupied states by i,i' and unoccupied states by a,a'. Thus, eqn (7.124) can be rewritten as two coupled equations,

$$\sum_{\sigma'}\sum_{j'k'}\Big[\delta_{ij'}\delta_{ak'}\delta_{\sigma\sigma'}\omega_{j'k'\sigma'}+\alpha_{j'k'\sigma'}K_{ia\sigma,j'k'\sigma'}(\Omega)\Big]\beta_{j'k'\sigma'}(\Omega)=\Omega\beta_{ia\sigma}(\Omega), \quad (7.126)$$

$$\sum_{\sigma'}\sum_{j'k'}\Big[\delta_{aj'}\delta_{ik'}\delta_{\sigma\sigma'}\omega_{j'k'\sigma'}+\alpha_{j'k'\sigma'}K_{ai\sigma,j'k'\sigma'}(\Omega)\Big]\beta_{j'k'\sigma'}(\Omega)=\Omega\beta_{ai\sigma}(\Omega), \quad (7.127)$$

or, in more detail (dropping, for brevity, the frequency arguments of β and K),

$$\sum_{i'a'\sigma'}\Big\{\Big[\delta_{ii'}\delta_{aa'}\delta_{\sigma\sigma'}\omega_{i'a'\sigma'}-K_{ia\sigma,i'a'\sigma'}\Big]\beta_{i'a'\sigma'}+K_{ia\sigma,a'i'\sigma'}\beta_{a'i'\sigma'}\Big\}=\Omega\beta_{ia\sigma}, \quad (7.128)$$

$$\sum_{i'a'\sigma'}\Big\{-K_{ai\sigma,i'a'\sigma'}\beta_{i'a'\sigma'}+\Big[\delta_{aa'}\delta_{ii'}\delta_{\sigma\sigma'}\omega_{a'i'\sigma'}+K_{ai\sigma,a'i'\sigma'}\Big]\beta_{a'i'\sigma'}\Big\}=\Omega\beta_{ai\sigma}. \quad (7.129)$$

Now, notice that $\omega_{a'i'\sigma'}>0$ and $\omega_{i'a'\sigma'}=-\omega_{a'i'\sigma'}<0$. Furthermore, we let

$$X_{ia\sigma}=-\beta_{ia\sigma}\,,\qquad Y_{ia\sigma}=\beta_{ai\sigma}\,, \quad (7.130)$$

which puts eqns (7.128) and (7.129) in the form

$$\sum_{i'a'\sigma'}\Big\{\Big[\delta_{ii'}\delta_{aa'}\delta_{\sigma\sigma'}\omega_{a'i'\sigma'}+K_{ia\sigma,i'a'\sigma'}\Big]X_{i'a'\sigma'}+K_{ia\sigma,a'i'\sigma'}Y_{i'a'\sigma'}\Big\}=-\Omega X_{ia\sigma}, \quad (7.131)$$

$$\sum_{i'a'\sigma'}\Big\{K_{ai\sigma,i'a'\sigma'}X_{i'a'\sigma'}+\Big[\delta_{aa'}\delta_{ii'}\delta_{\sigma\sigma'}\omega_{a'i'\sigma'}+K_{ai\sigma,a'i'\sigma'}\Big]Y_{i'a'\sigma'}\Big\}=\Omega Y_{ia\sigma}\,. \quad (7.132)$$

From eqn (7.125), one obtains the eigenmode associated with a given frequency Ω:

$$n_{1\sigma}(\mathbf{r},\Omega)=\sum_{ia}\left[\Phi^*_{ia\sigma}(\mathbf{r})X_{ia\sigma}(\Omega)+\Phi_{ia\sigma}(\mathbf{r})Y_{ia\sigma}(\Omega)\right]. \quad (7.133)$$

In practice, the spatial profiles of the eigenmodes $n_{1\sigma}(\mathbf{r},\Omega_n)$ (also known as transition densities) can be of interest if one wants to obtain a visualization of the density changes

induced during a particular excitation. However, of more practical importance are observables such as the dynamic polarizability and the oscillator strengths associated with a given excitation, which we shall discuss below.

Let us assume that the Kohn–Sham orbitals are real, which is permitted if the ground-state Hamiltonian has time-reversal symmetry. The set of coupled eigenvalue equations (7.131) and (7.132) can then be written in the following compact matrix form, known as the Casida equation (Casida, 1995):

$$\begin{pmatrix} \mathbb{A} & \mathbb{B} \\ \mathbb{B} & \mathbb{A} \end{pmatrix} \begin{pmatrix} \mathbf{X} \\ \mathbf{Y} \end{pmatrix} = \Omega \begin{pmatrix} -\mathbb{1} & 0 \\ 0 & \mathbb{1} \end{pmatrix} \begin{pmatrix} \mathbf{X} \\ \mathbf{Y} \end{pmatrix}, \tag{7.134}$$

where the matrix elements of $\mathbb{A}$ and $\mathbb{B}$ are given by

$$A_{ia\sigma,i'a'\sigma'}(\Omega) = \delta_{ii'}\delta_{aa'}\delta_{\sigma\sigma'}\omega_{a'i'\sigma'} + K_{ia\sigma,i'a'\sigma'}(\Omega)\,, \tag{7.135}$$

$$B_{ia\sigma,i'a'\sigma'}(\Omega) = K_{ia\sigma,i'a'\sigma'}(\Omega)\,. \tag{7.136}$$

$\mathbb{A}$ and $\mathbb{B}$ are sometimes called the orbital rotation Hessians (Furche and Ahlrichs, 2002). Notice that $\mathbb{A}^\dagger(\omega) = \mathbb{A}(-\omega)$ and $\mathbb{B}^\dagger(\omega) = \mathbb{B}(-\omega)$, which follows from the properties (8.1) and (8.2) of the frequency-dependent xc kernel (see Section 8.1). Because of this, eqn (7.134) has the mathematical structure of an infinite-dimensional anti-Hermitian eigenvalue problem.[9] We shall present numerical applications of the Casida formalism to atomic and molecular excitation energies in Chapter 9.

Strictly speaking, the excitation frequencies Ω are not eigenvalues, and the vectors $\mathbf{X}$ and $\mathbf{Y}$ are therefore not orthonormal in the usual sense; the solutions of eqn (7.134) come in pairs as $\mathbf{X}_n, \mathbf{Y}_n, \Omega_n$ and $\mathbf{Y}_n^*, \mathbf{X}_n^*, -\Omega_n$. It can be shown (McLachlan and Ball, 1964) that the frequencies are all real and that the vectors can be chosen such that

$$\langle \mathbf{X}_n | \mathbf{X}_m \rangle - \langle \mathbf{Y}_n | \mathbf{Y}_m \rangle = \pm\delta_{mn} \tag{7.137}$$

for positive and negative Ω_n, respectively.

7.5.2 Discussion

The Casida equation (7.134) yields, in principle, the exact excitation energies Ω_n of any many-body system, under the following conditions:

- First, the exact Kohn–Sham ground state of the system must be calculated, which requires knowledge of the exact $v_{\rm xc}^0[n_0]$. All occupied and unoccupied Kohn–Sham orbitals and energy eigenvalues $\varphi_{j\sigma}^0(\mathbf{r})$ and $\varepsilon_{j\sigma}$ are needed, including the continuum states.
- The exact frequency-dependent xc kernel $f_{{\rm xc},\sigma\sigma'}[n_0](\mathbf{r},\mathbf{r}',\omega)$ is required.
- The infinite-dimensional pseudo-eigenvalue equation (7.134) has to be solved. Since the elements of the matrices $\mathbb{A}$ and $\mathbb{B}$ depend on the frequency via $f_{{\rm xc},\sigma\sigma'}$, this requires not just one diagonalization but some sort of an iterative scheme.

[9] In other words, taking the Hermitian conjugate (i.e., the transpose and complex conjugate) of eqn (7.134) leads to the same eigenvalue equation, but with the eigenvalue Ω replaced with $-\Omega$. If the xc kernel is approximated by a frequency-independent, real expression, the eigenvalue problem (7.134) becomes Hermitian.

Needless to say, in practice none of these requirements can be satisfied exactly, only to varying degrees of approximation. We shall discuss these approximations later in more detail. In the meantime, let us imagine that we have perfect approximations to the xc functionals and unlimited computational resources at our disposal, and discuss the properties of the exact TDDFT linear-response scheme.

If we set the coupling-matrix elements $K_{ia\sigma,i'a'\sigma'}$ to zero, eqn (7.134) simply reproduces the Kohn–Sham excitation energies $\omega_{ai\sigma}$ as eigenvalues, which are the poles of the noninteracting Kohn–Sham response function (7.114). Notice that the $\omega_{ai\sigma}$ are *single* excitation energies; in a noninteracting system, there are no double or multiple excitations in linear response. The poles Ω_n of the many-body response function (7.19), on the other hand, include not just single excitations, but also multiple excitations. In order to reproduce these, the frequency dependence of the coupling-matrix elements $K_{ia\sigma,i'a'\sigma'}$ via the xc kernel $f_{\rm xc}$ is essential, since this makes it possible for eqn (7.134) to have more solutions than the dimension of the eigenvalue problem. In general, the concept of single, double, or multiple excitations in a many-body system needs some clarification; we will discuss this in more detail in Section 9.3.

The TDDFT linear-response formalism which we have presented here can determine all excitations Ω_n, even if they are dipole forbidden, as long as there exists a corresponding pole in the density–density response function (7.19). This requires the associated matrix element $\langle\Psi_n|\hat{n}(\mathbf{r})|\Psi_0\rangle$ to differ from zero at least at some value of $\mathbf{r}$. If this is not the case, i.e., if $\langle\Psi_n|\hat{n}(\mathbf{r})|\Psi_0\rangle$ happens to vanish for all $\mathbf{r}$, then the excited state Ψ_n cannot be reached by any perturbation that couples to the density, and the TDDFT linear-response formalism is "blind" to such excitations. Such situations can indeed occur in practice. An explicit example is the $\pi \to \pi^*$ excitation from the $^1\Sigma_g^+$ ground state of the N_2 molecule to the $^1\Sigma_u^-$ excited state, where the matrix element $\langle\Psi(^1\Sigma_g^+)|\hat{n}(\mathbf{r})|\Psi(^1\Sigma_u^-)\rangle$ is equal to 0 independent of $\mathbf{r}$, owing to symmetry (Heßelmann and Görling, 2009). To capture such excitations, one needs to resort to a response theory where the two states Ψ_0 and Ψ_n are coupled in a different way, for example via the current-density operator (see Section 10.3).

In practice, the Casida equation (7.134) is often cast into the alternative form

$$\mathbb{C}\mathbf{Z} = \Omega^2\mathbf{Z}\,. \tag{7.138}$$

To arrive at this expression, one assumes that the Kohn–Sham orbitals are real. Some elementary matrix algebra then shows that

$$\mathbb{C} = (\mathbb{A}-\mathbb{B})^{1/2}(\mathbb{A}+\mathbb{B})(\mathbb{A}-\mathbb{B})^{1/2}\,, \tag{7.139}$$

$$\mathbf{Z} = (\mathbb{A}-\mathbb{B})^{1/2}(\mathbf{X}-\mathbf{Y})\,. \tag{7.140}$$

Using the explicit forms of the matrix elements (7.135) and (7.136), one finds

$$\sum_{i'a'\sigma'}\left[\delta_{ii'}\delta_{aa'}\delta_{\sigma\sigma'}\omega^2_{a'i'\sigma'} + 2\sqrt{\omega_{ai\sigma}\omega_{a'i'\sigma'}}K_{ia\sigma,i'a'\sigma'}\right]Z_{i'a'\sigma'} = \Omega^2 Z_{ia\sigma}\,. \tag{7.141}$$

This version of the Casida equation is computationally simpler than eqn (7.134) and is therefore implemented in most TDDFT computer codes (see Appendix O).[10]

Using a derivation similar to that leading to eqn (7.134), and assuming that the Kohn–Sham orbitals are real, the TDDFT linear-response equation (7.84) can be recast into (Casida, 1995)

$$\left[\begin{pmatrix} \mathbb{A} & \mathbb{B} \\ \mathbb{B} & \mathbb{A} \end{pmatrix} - \omega \begin{pmatrix} -\mathbb{1} & 0 \\ 0 & \mathbb{1} \end{pmatrix}\right] \begin{pmatrix} \mathbf{X} \\ \mathbf{Y} \end{pmatrix} = - \begin{pmatrix} \mathbf{v}_1 \\ \mathbf{v}_1 \end{pmatrix}, \tag{7.142}$$

where the elements of the vector $\mathbf{v}_1$ are given by $v_{1,ia\sigma} = \int d^3r\, \Phi_{ia\sigma}(\mathbf{r}) v_1(\mathbf{r},\omega)$. It is then straightforward to show from eqn (7.142) that

$$\mathbf{X} + \mathbf{Y} = 2(\mathbb{A} - \mathbb{B})^{1/2} (\mathbb{C} - \omega^2)^{-1} (\mathbb{A} - \mathbb{B})^{1/2} \mathbf{v}_1 \,. \tag{7.143}$$

Using this in eqn (7.133) for $n_1(\mathbf{r},\omega)$ and comparing the result with eqn (7.45) gives the following expression for the dynamic polarizability:

$$\alpha_{zz}(\omega) = 2\mathbf{z}^T (\mathbb{A} - \mathbb{B})^{1/2} (\mathbb{C} - \omega^2)^{-1} (\mathbb{A} - \mathbb{B})^{1/2} \mathbf{z} \,, \tag{7.144}$$

where the elements of $\mathbf{z}$ are given by $z_{ia\sigma} = \int d^3r\, z \Phi_{ia\sigma}(\mathbf{r})$. We now use the spectral expansion

$$(\mathbb{C} - \omega^2)^{-1} = \sum_n \frac{\mathbf{Z}_n \mathbf{Z}_n^T}{\Omega_n^2 - \omega^2} \,, \tag{7.145}$$

which is implied by the completeness $\sum_n \mathbf{Z}_n \mathbf{Z}_n^T = \mathbb{1}$ of the eigenvectors of eqn (7.138). Comparing the result with eqn (7.50), we find the following expression for the oscillator strengths:

$$f_n = \frac{2}{3} \sum_{i=1}^{3} |\mathbf{x}_i^T (\mathbb{A} - \mathbb{B})^{1/2} \mathbf{Z}_n|^2 \,. \tag{7.146}$$

7.5.3 The Casida formalism for spin-unpolarized systems

The Casida formalism can be simplified if the electronic ground state is not spin-polarized, so that $\Phi_{ia\uparrow}(\mathbf{r}) = \Phi_{ia\downarrow}(\mathbf{r}) \equiv \Phi_{ia}(\mathbf{r})$ and $\omega_{ia\uparrow} = \omega_{ia\downarrow} \equiv \omega_{ia}$ (Bauernschmitt and Ahlrichs, 1996; Furche *et al.*, 2000). In that case we can define

$$X_{ia}^{\pm} = X_{ia\uparrow} \pm X_{ia\downarrow} \,, \qquad Y_{ia}^{\pm} = Y_{ia\uparrow} \pm Y_{ia\downarrow} \,, \tag{7.147}$$

$$A_{ia,i'a'}^{\pm} = \delta_{ii'}\delta_{aa'}\omega_{a'i'} + K_{ia\uparrow,i'a'\uparrow} \pm K_{ia\uparrow,i'a'\downarrow} \,, \tag{7.148}$$

$$B_{ia,i'a'}^{\pm} = K_{ia\uparrow,i'a'\uparrow} \pm K_{ia\uparrow,i'a'\downarrow} \,, \tag{7.149}$$

and eqn (7.134) decouples into two independent eigenvalue equations

$$\begin{pmatrix} \mathbb{A}^{\pm} & \mathbb{B}^{\pm} \\ \mathbb{B}^{\pm} & \mathbb{A}^{\pm} \end{pmatrix} \begin{pmatrix} \mathbf{X}^{\pm} \\ \mathbf{Y}^{\pm} \end{pmatrix} = \Omega_{\pm} \begin{pmatrix} -\mathbb{1} & 0 \\ 0 & \mathbb{1} \end{pmatrix} \begin{pmatrix} \mathbf{X}^{\pm} \\ \mathbf{Y}^{\pm} \end{pmatrix}. \tag{7.150}$$

[10] In cases where one uses hybrid xc functionals that contain a portion of exact HF exchange eqn (7.138) does not reduce to the simple form (7.141) and therefore has no advantage over eqn (7.134). Refer to Section 7.7 for more details.

The explicit expressions for the matrix elements of $\mathbb{B}^{\pm}$ are

$$B^{+}_{ia,i'a'} = 2\int d^3r \int d^3r'\, \Phi_{ia}(\mathbf{r}) \left[\frac{1}{|\mathbf{r}-\mathbf{r}'|} + f_{\rm xc}(\mathbf{r},\mathbf{r}',\Omega)\right] \Phi_{i'a'}(\mathbf{r}')\,, \qquad (7.151)$$

$$B^{-}_{ia,i'a'} = 2\int d^3r \int d^3r'\, \Phi_{ia}(\mathbf{r}) g_{\rm xc}(\mathbf{r},\mathbf{r}',\Omega) \Phi_{i'a'}(\mathbf{r}')\,, \qquad (7.152)$$

and similarly for $A^{\pm}_{ia,i'a'}$, where we define

$$f_{\rm xc}(\mathbf{r},\mathbf{r}',\omega) = = \frac{1}{2}\left[f_{{\rm xc}\uparrow\uparrow}(\mathbf{r},\mathbf{r}',\omega) + f_{{\rm xc}\uparrow\downarrow}(\mathbf{r},\mathbf{r}',\omega)\right]\,, \qquad (7.153)$$

$$g_{\rm xc}(\mathbf{r},\mathbf{r}',\omega) = = \frac{1}{2}\left[f_{{\rm xc}\uparrow\uparrow}(\mathbf{r},\mathbf{r}',\omega) - f_{{\rm xc}\uparrow\downarrow}(\mathbf{r},\mathbf{r}',\omega)\right]\,. \qquad (7.154)$$

Here we have used the fact that $f_{{\rm xc}\uparrow\uparrow} = f_{{\rm xc},\downarrow\downarrow}$ and $f_{{\rm xc}\uparrow\downarrow} = f_{{\rm xc},\downarrow\uparrow}$ for spin-unpolarized systems.

The two independent sets of solutions $\Omega_{\pm}$ correspond to the singlet and triplet excitation energies of the system. In the singlet case, one has $n_{1\uparrow}(\mathbf{r},\Omega_+) = n_{1\downarrow}(\mathbf{r},\Omega_+)$, i.e., the response of the system is such that the spin-up and spin-down eigenmodes are in phase. In the triplet case, on the other hand, one has $n_{1\uparrow}(\mathbf{r},\Omega_-) = -n_{1\downarrow}(\mathbf{r},\Omega_-)$, which means that the spin-up and spin-down eigenmodes are out of phase. Notice that, in general, triplet excitations can involve both spin-conserving and spin-flip transitions. However, spin-flip transitions are beyond the formalism presented in this chapter: this requires a linear-response framework for systems with noncollinear spins. See Appendix G for further details, and Exercise 7.14 for a simple example.

7.6 The Tamm–Dancoff approximation and other simplifications

In practice, the full Casida equation (7.134) is often replaced by schemes which are simplified or truncated to various degrees. The motivation for doing so is usually the resulting reduction in computational cost, but it sometimes turns out that there can be benefits in accuracy, or even new physical insights.

The eigenvalues of eqn (7.141) are the squares of the excitation energies; this means that for each excitation energy Ω_n the Casida formalism also delivers the corresponding negative value, $-\Omega_n$. The excitation energies thus come in pairs, $(\Omega_n, -\Omega_n)$, which is also evident from the pole structure of the response function (7.19). Physically, the pair $(\Omega_n, -\Omega_n)$ corresponds to the excitations and deexcitations of the system.[11]

The approximation to the exact TDDFT linear-response scheme (7.134) in which all deexcitation processes are neglected is called the Tamm–Dancoff approximation (TDA). The TDA has been known for a long time in nuclear physics, where it is introduced as an approximation to the polarization propagator, limited to single particle–hole pairs that are propagating forward in time (Fetter and Walecka, 2003). In the

[11] "Deexcitation" is used here synonymously with "stimulated emission." Spontaneous emission in closed systems cannot occur in our formal framework based on the time-dependent Schrödinger equation with classical fields, but would require field quantization in the framework of quantum electrodynamics, or coupling to some other form of a bath of external degrees of freedom such as phonons.

context of the TDHF approach and using the language of quantum chemistry, this approximation is formally identical to the configuration interaction singles (CIS) method (see Section 7.7). The TDA has been adopted in TDDFT (Hirata and Head-Gordon, 1999), but with a somewhat different meaning from that originally used in nuclear physics: one simply sets the off-diagonal matrices $\mathbb{B}$ in eqn (7.134) to zero, but keeps the matrix $\mathbb{A}$ as it is [see eqn (7.135)]. This results in the simpler eigenvalue problem

$$\mathbb{A}\mathbf{X} = \Omega\mathbf{X}\,. \tag{7.155}$$

The TDA occasionally has some technical advantages over the full TDDFT linear-response formalism, for example for open-shell systems away from the ground-state equilibrium geometry (Casida *et al.*, 2000). This will be discussed further in Sections 9.2 and 17.1.

If the poles of the full response function (7.19) are well separated, then it is possible to just focus on a single excitation energy and expand around this particular pole (Petersilka *et al.*, 1996; Appel *et al.*, 2003). This is aided by the fact that the coupling-matrix elements $K_{ia\sigma,i'a'\sigma'}$ decay relatively rapidly away from the diagonal, because the overlap of increasingly different orbitals becomes smaller and smaller by cancellation of oscillations. Thus, under the condition

$$\left| \sum_{i'a'\sigma' \neq ia\sigma} \frac{K_{ia\sigma,i'a'\sigma'}}{\omega_{ai\sigma} - \omega_{a'i'\sigma'}} \right| \ll 1\,, \tag{7.156}$$

one can dramatically reduce the dimension of the Casida equation (7.134) by ignoring all off-diagonal elements of the matrices $\mathbb{A}$ and $\mathbb{B}$ with $ia \neq i'a'$. The result is the so-called small-matrix approximation (SMA),[12]

$$\Omega_{\pm}^2 = \omega_{ia\sigma}^2 + 2\omega_{ia\sigma}[K_{ia\sigma,ia\sigma}(\Omega) \pm K_{ia\sigma,ia\bar{\sigma}}(\Omega)]\,, \tag{7.157}$$

where $\bar{\sigma}$ denotes the opposite of the spin σ. Equation (7.157) is sometimes also called the dressed[13] SMA (Maitra *et al.*, 2004; Cave *et al.*, 2004) to emphasize the self-consistent dependence of the xc kernel in $K_{ia\sigma,ia\sigma}$ on the excitation frequency Ω. We will get back to this issue when we discuss double excitations later, in Section 9.3.

The SMA, eqn (7.157), can be simplified further by making the TDA, i.e., by including only the positive excitation energy, which leads to

$$\Omega_{\pm} = \omega_{ia\sigma} + [K_{ia\sigma,ia\sigma}(\Omega) \pm K_{ia\sigma,ia\bar{\sigma}}(\Omega)]\,. \tag{7.158}$$

A similar relation can be obtained in an alternative way by directly expanding the TDDFT linear-response equation (7.111) about the Kohn–Sham excitation energy $\omega_{ia\sigma}$ (Petersilka *et al.*, 1996; Appel *et al.*, 2003), resulting in

[12] The condition (7.156) holds in the special case where the SMA correction is small compared with the particular Kohn–Sham transition itself. The SMA remains valid even when the corrections to the Kohn–Sham excitations are large, provided the poles are well separated (Appel *et al.*, 2003).

[13] In the language of many-body physics, $\omega_{ia\sigma}$ would be referred to as the "bare" excitation energy, in contrast with "dressed" excitation energies. However, this language can lead to confusion if one does not clearly specify what the dressing consists of. Usually it means that a particle is surrounded by clouds of virtual photons, phonons, or other elementary excitations, which affect how the particle moves or interacts with other particles.

$$\Omega_\pm = \omega_{ia\sigma} + [K_{ia\sigma,ia\sigma}(\omega_{ia\sigma}) \pm K_{ia\sigma,ia\bar{\sigma}}(\omega_{ia\sigma})] \,. \tag{7.159}$$

Equation (7.159) is known as the single-pole approximation (SPA), and it differs from eqn (7.158) only in the frequency argument of the xc kernel. For frequency-independent xc kernels, the two expressions are identical.

To see the structure of the SPA most clearly, let us assume that the Kohn–Sham ground state is not spin-polarized, so that $\omega_{ia\uparrow} = \omega_{ia\downarrow} = \omega_{ia}$, and that the orbitals are real. With the explicit form of the coupling-matrix elements (7.121), the SPA equation (7.159) then has the following two solutions:

$$\Omega_+ = \omega_{ia} + 2\int d^3r \int d^3r' \; \Phi_{ia}(\mathbf{r}) \left[\frac{1}{|\mathbf{r}-\mathbf{r}'|} + f_{\rm xc}(\mathbf{r},\mathbf{r}',\omega_{ia})\right] \Phi_{ia}(\mathbf{r}') \,, \tag{7.160}$$

$$\Omega_- = \omega_{ia} + 2\int d^3r \int d^3r' \; \Phi_{ia}(\mathbf{r}) g_{\rm xc}(\mathbf{r},\mathbf{r}',\omega_{ia}) \Phi_{ia}(\mathbf{r}') \,, \tag{7.161}$$

where the spin-independent xc kernels $f_{\rm xc}$ and $g_{\rm xc}$ are defined in eqns (7.153) and (7.154).

As we have seen in Section 7.4, the SMA becomes exact for a two-level system, see eqns (7.109) and (7.110). In general, the SMA and the SPA are useful approximations in situations where the excitations under consideration are well separated from other excitations, and in that case constitute the leading corrections to the bare Kohn–Sham excitations (Vasiliev *et al.*, 1999). Later, in Section 9.1, we will illustrate this for closed-shell atoms.

7.7 Excitation energies with time-dependent Hartree–Fock theory

We conclude this chapter with a brief summary of the TDHF approach to calculating excitation energies. As we shall see, there are many similarities to the TDDFT treatment, but also important differences. For simplicity, we ignore the spin index in this section. For an introduction to HF theory, see Appendix D.

Let us first consider the real-time domain. The basic idea of the TDHF approach is that the time-dependent many-body wave function $\Psi(t)$ is assumed to have the form of a single Slater determinant. Using this form of $\Psi(t)$ in the time-dependent Schrödinger equation (3.5), the TDHF equations are obtained[14] as follows:

$$\begin{aligned} i\frac{\partial}{\partial t}\varphi_j^{\rm HF}(\mathbf{r},t) = \left[-\frac{\nabla^2}{2} + v(\mathbf{r},t)\right]\varphi_j^{\rm HF}(\mathbf{r},t) + \sum_{l=1}^{N}\int d^3r' \; \frac{\varphi_l^{*\rm HF}(\mathbf{r}',t)\varphi_l^{\rm HF}(\mathbf{r}',t)}{|\mathbf{r}-\mathbf{r}'|}\,\varphi_j^{\rm HF}(\mathbf{r},t) \\ - \sum_{l=1}^{N}\int d^3r' \; \frac{\varphi_l^{*\rm HF}(\mathbf{r}',t)\varphi_j^{\rm HF}(\mathbf{r}',t)}{|\mathbf{r}-\mathbf{r}'|}\,\varphi_l^{\rm HF}(\mathbf{r},t) \,. \end{aligned} \tag{7.162}$$

Here, the second term on the right-hand side is recognized to be the Hartree potential acting on the TDHF single-particle orbitals $\varphi_j^{\rm HF}(\mathbf{r},t)$, and the third term is the nonlocal exchange potential, featuring $\varphi_j^{\rm HF}(\mathbf{r}',t)$ under the integral.

[14] The derivation of the TDHF equations can, for instance, be accomplished using a time-dependent variational principle (Langhoff *et al.*, 1972).

Like the TDKS equation, the TDHF equation (7.162) is an initial-value problem, where the system at the initial time is described by the static HF equation

$$\varepsilon_j^{\rm HF}\varphi_j^{\rm HF0}(\mathbf{r}) = \left[-\frac{\nabla^2}{2} + v_0(\mathbf{r})\right]\varphi_j^{\rm HF0}(\mathbf{r}) + \sum_{l=1}^{N}\int d^3r'\,\frac{\varphi_l^{\rm HF0}(\mathbf{r}')\varphi_l^{\rm HF0}(\mathbf{r}')}{|\mathbf{r}-\mathbf{r}'|}\,\varphi_j^{\rm HF0}(\mathbf{r}) - \sum_{l=1}^{N}\int d^3r'\,\frac{\varphi_l^{\rm HF0}(\mathbf{r}')\varphi_j^{\rm HF0}(\mathbf{r}')}{|\mathbf{r}-\mathbf{r}'|}\,\varphi_l^{\rm HF0}(\mathbf{r})\,. \tag{7.163}$$

We assume here that the static HF single-particle orbitals are real.

Time-dependent perturbation theory leads to the TDHF formalism for calculating excitation energies (Dreuw and Head-Gordon, 2005), which can be written in a matrix form that formally resembles the Casida equation (7.134):

$$\begin{pmatrix} \mathbb{A}^{\rm HF} & \mathbb{B}^{\rm HF} \\ \mathbb{B}^{\rm HF} & \mathbb{A}^{\rm HF} \end{pmatrix}\begin{pmatrix} \mathbf{X} \\ \mathbf{Y} \end{pmatrix} = \Omega^{\rm HF}\begin{pmatrix} -\mathbb{1} & 0 \\ 0 & \mathbb{1} \end{pmatrix}\begin{pmatrix} \mathbf{X} \\ \mathbf{Y} \end{pmatrix}. \tag{7.164}$$

The matrix elements of $\mathbb{A}^{\rm HF}$ and $\mathbb{B}^{\rm HF}$ are defined as

$$A^{\rm HF}_{ia,i'a'} = \delta_{ii'}\delta_{aa'}(\varepsilon_a^{\rm HF} - \varepsilon_i^{\rm HF}) + (ia||i'a')\,, \tag{7.165}$$

$$B^{\rm HF}_{ia,i'a'} = (ia||a'i')\,, \tag{7.166}$$

where

$$(ia||i'a') = \int d^3r\int d^3r'\,\frac{\varphi_i^{\rm HF0}(\mathbf{r})\varphi_a^{\rm HF0}(\mathbf{r})\varphi_{i'}^{\rm HF0}(\mathbf{r}')\varphi_{a'}^{\rm HF0}(\mathbf{r}')}{|\mathbf{r}-\mathbf{r}'|} - \int d^3r\int d^3r'\,\frac{\varphi_i^{\rm HF0}(\mathbf{r})\varphi_{i'}^{\rm HF0}(\mathbf{r})\varphi_a^{\rm HF0}(\mathbf{r}')\varphi_{a'}^{\rm HF0}(\mathbf{r}')}{|\mathbf{r}-\mathbf{r}'|}\,. \tag{7.167}$$

Since $A^{\rm HF}_{ia,i'a'} - B^{\rm HF}_{ia,i'a'} \neq \delta_{ii'}\delta_{aa'}(\varepsilon_a^{\rm HF} - \varepsilon_i^{\rm HF})$ there is less practical computational advantage in recasting eqn (7.164) into a form similar to eqn (7.138).

Making the TDA, one obtains what is known as the CIS equation for the excitation energies:

$$\mathbb{A}^{\rm HF}\mathbf{X} = \Omega^{\rm CIS}\mathbf{X}\,. \tag{7.168}$$

The TDHF formalism briefly outlined in this section becomes relevant to the practical implementation of TDDFT whenever one uses hybrid xc functionals which contain an admixture of the exact HF exchange. In our review of static DFT in Chapter 2, we gave some examples of popular hybrid xc potentials.

Exercise 7.1 Carry out the steps leading to the relation (7.5) for $\alpha_1(t)$, using eqn (3.19) for the first-order approximation to the time evolution operator.

Exercise 7.2 Derive the Lehmann representation of the response function, eqn (7.17), from eqn (7.14).

Exercise 7.3 Verify how the Kramers–Kronig relations (7.26) and (7.27) follow from eqn (7.24).

Exercise 7.4 Show that the Kramers–Kronig relations (7.26) and (7.27) can be written as

$$\Re\chi_{\alpha\beta}(\omega) = -\mathcal{P}\int_{-\infty}^{\infty}\frac{d\omega'}{\pi}\frac{\Im\chi_{\alpha\beta}(\omega')}{\omega-\omega'}\,,$$
$$\Im\chi_{\alpha\beta}(\omega) = \mathcal{P}\int_{-\infty}^{\infty}\frac{d\omega'}{\pi}\frac{\Re\chi_{\alpha\beta}(\omega')}{\omega-\omega'}\,.$$

Verify these relations explicitly, using the following representation of the delta function:

$$\delta(y-y') = \frac{1}{\pi^2}\int_{-\infty}^{\infty}\frac{dx}{(x-y)(x-y')}\,.$$

Exercise 7.5 Prove that the connection between the dynamical structure factor $S_{\alpha\alpha^\dagger}(\omega)$ and the response function $\chi_{\alpha\alpha^\dagger}(\omega)$ given in eqn (7.31) follows from eqns (7.17) and (7.29).

Exercise 7.6 Find the energy that is transferred to a system per unit time, and show that it is determined by the imaginary part of the response function. Start with the expression

$$\frac{dE}{dt} = \int d^3r\,\mathbf{F}(\mathbf{r},t)\cdot\mathbf{j}_1(\mathbf{r},t)\,, \tag{7.169}$$

where $\mathbf{F}(\mathbf{r})$ is the force density associated with an external perturbation, and $\mathbf{j}(\mathbf{r})$ is the current response. Recast this in terms of a scalar perturbing potential and a density response,

$$\frac{dE}{dt} = \int d^3r\,v_1(\mathbf{r},t)\frac{\partial}{\partial t}n_1(\mathbf{r},t)\,, \tag{7.170}$$

and assume that the perturbation has the form $v_1(\mathbf{r},t) = v_1(\mathbf{r},\omega)e^{-i\omega t}+\text{c.c.}$, and similarly for $n_1(\mathbf{r},t)$. Show that this gives the following expression for the steady rate of energy dissipation:

$$\left.\frac{dE}{dt}\right|_{\text{diss}} = -2\omega\int d^3r\int d^3r'\,v_1(\mathbf{r},\omega)v_1^*(\mathbf{r}',\omega)\Im\chi(\mathbf{r},\mathbf{r}',\omega)\,. \tag{7.171}$$

Exercise 7.7 Find examples of time-dependent perturbations $v_1(\mathbf{r},t)$ which are Laplace-transformable for $t\geq t_0$ but nonanalytic at t_0.

Exercise 7.8 To get a feeling for response functions, calculate the static density–density response function of a one-particle system using simple static perturbation theory. From any introductory quantum mechanics textbook, e.g., Schiff (1968), we know that the first-order correction to the kth single-electron orbital due to a static perturbation $\delta v(\mathbf{r})$ is given by

$$\delta\varphi_k^0(\mathbf{r}) = \sum_{j\neq k}\frac{\varphi_j^0(\mathbf{r})}{\varepsilon_k-\varepsilon_j}\int d^3r'\,\varphi_j^{0*}(\mathbf{r}')\delta v(\mathbf{r}')\varphi_k^0(\mathbf{r}')\,.$$

Show that the static density–density response function follows as

$$\chi^0(\mathbf{r},\mathbf{r}') = \sum_{j=2}^{\infty}\frac{\varphi_1^0(\mathbf{r})\varphi_j^{0*}(\mathbf{r})\varphi_1^{0*}(\mathbf{r}')\varphi_j^0(\mathbf{r}')}{\varepsilon_1-\varepsilon_j}+\text{c.c.}$$

Convince yourself that this expression can also be obtained from the static limit of the frequency-dependent Kohn–Sham response function (7.80).

Exercise 7.9 Prove the f-sum rule (7.53).

Exercise 7.10 Calculate the oscillator strength of the lowest transition of the H atom.

Exercise 7.11 Derive eqn (7.80) for the frequency-dependent Kohn–Sham response function from the full many-body response function (7.19) by assuming that the many-body wave functions Ψ_n are given by single Slater determinants.

Exercise 7.12 Extend the formalism of Section 7.4 to the case of spin-dependent two-level systems. Assuming that the ground state is spin-unpolarized, show that one finds

$$\omega_{\pm}^2 = \omega_{21}^2 + 2\omega_{21}[K_{12\sigma,12\sigma}(\omega) \pm K_{12\sigma,12\bar{\sigma}}(\omega)] \,,$$

where the spin-dependent matrix elements $K_{12\sigma,12\sigma'}(\omega)$ are given by eqn (7.121).

Exercise 7.13 Extend the formalism of Section 7.4 to three-level systems. The doubly occupied time-dependent Kohn–Sham orbital is $\varphi(\mathbf{r},t) = c_1(t)\varphi_1^0(\mathbf{r}) + \lambda c_2(t)\varphi_2^0(\mathbf{r}) + \lambda c_3(t)\varphi_3^0(\mathbf{r})$, which gives the following density matrix:

$$\rho(t) = \begin{pmatrix} \rho_{11} & \lambda\rho_{12} & \lambda\rho_{13} \\ \lambda\rho_{21} & \lambda^2\rho_{22} & \lambda^2\rho_{23} \\ \lambda\rho_{31} & \lambda^2\rho_{32} & \lambda^2\rho_{33} \end{pmatrix} = \begin{pmatrix} |c_1|^2 & \lambda c_1 c_2^* & \lambda c_1 c_3^* \\ \lambda c_1^* c_2 & \lambda^2|c_2|^2 & \lambda^2 c_2 c_3^* \\ \lambda c_1^* c_3 & \lambda^2 c_2^* c_3 & \lambda^2|c_3|^2 \end{pmatrix} .$$

Going through a similar procedure to that for two-level systems, show that the exact excitation energies in this three-level system are obtained from the following system of equations:

$$\begin{aligned} (\omega_{21}^2 + 4\omega_{21}K_{12,12})\xi_{12} + 4\sqrt{\omega_{21}\omega_{31}}K_{12,13}\xi_{13} &= \omega^2\xi_{12} \,, \\ 4\sqrt{\omega_{21}\omega_{31}}K_{13,12}\xi_{12} + (\omega_{31}^2 + 4\omega_{31}K_{13,13})\xi_{13} &= \omega^2\xi_{13} \,. \end{aligned}$$

Verify that this can also be directly obtained from eqn (7.141) in the case of three spin-unpolarized Kohn–Sham levels.

Exercise 7.14 In Appendix G, we discuss spin-conserving versus spin-flip excitations from a more general point of view, based on the linear response of the spin-density matrix. The SPA in this case yields two pairs of spin-conserving excitations and two spin-flip excitations, $\omega_{1,2}^{\mathrm{sc}}$ and $\omega_{1,2}^{\mathrm{sf}}$ [see eqns (G.31) and (G.32)]. The SPA for these excitations involves only the highest occupied and lowest unoccupied single-particle levels for each spin.

Now consider a closed-shell system whose ground state is spin-unpolarized. In this case, three of the four SPA excitation energies become identical, $\omega_2^{\mathrm{sc}} = \omega_1^{\mathrm{sf}} = \omega_2^{\mathrm{sf}}$, representing the triplet excitation. The fourth one, ω_1^{sc}, is the singlet excitation energy. This reveals that for closed-shell systems, triplet excitations can come in both spin-conserving and spin-flip flavors, whereas singlet excitations are spin-conserving.

Show explicitly, using the LSDA xc kernels (G.23)–(G.26), that in the spin-unpolarized case one obtains $\omega_1^{\mathrm{sc}} = \Omega_+$ and $\omega_2^{\mathrm{sc}} = \omega_1^{\mathrm{sf}} = \omega_2^{\mathrm{sf}} = \Omega_-$, where Ω_+ and Ω_- are given in eqns (7.160) and (7.161).

8
The frequency-dependent xc kernel

The key quantity in linear-response TDDFT is the xc kernel $f_{\rm xc}(\mathbf{r},\mathbf{r}',\omega)$. In the previous chapter, we have given its definition, and we have shown how the linear-response formalism allows us to calculate the excitation energy spectra of atoms and molecules in principle exactly using the Casida equations, assuming the exact $f_{\rm xc}$ is known.

We will now study the xc kernel in more detail, beginning with an overview of those of its exact properties which are known to date. To a certain extent, one might expect the situation to be somewhat easier for the xc kernel than for the time-dependent xc potential: $v_{\rm xc}(\mathbf{r},t)$ is a functional of the time-dependent density $n(\mathbf{r},t)$ at all times $t' \leq t$, whereas $f_{\rm xc}(\mathbf{r},\mathbf{r}',\omega)$ is a functional only of the ground-state density $n_0(\mathbf{r})$.

However, the spatial behavior of the xc kernel is more complicated: it is a nonlocal function of $\mathbf{r}$ and $\mathbf{r}'$ which enters as an integral kernel in the response equation, whereas the xc potential is a local operator in the TDKS equation. And, as far as the dynamical aspects are concerned, both the xc potential and the xc kernel of linear response have to deal with similar issues related to causality and memory. We will soon discover how the frequency dependence of $f_{\rm xc}$ is crucial for reproducing certain features of the excitation spectra of finite and extended systems.

Most of the applications of linear-response TDDFT use the adiabatic approximation for $f_{\rm xc}$, whereby the frequency dependence is ignored. We will give examples of commonly used approximate xc kernels, but will defer the question of how well they work until Chapter 9, where we discuss applications and results.

There exists a sizable body of work on the xc kernel of the homogeneous electron liquid, $f_{\rm xc}(q,\omega)$, and we can take advantage of this knowledge in constructing new xc kernels for inhomogeneous systems. Section 8.3 of this chapter will be dedicated to an overview of the properties of $f_{\rm xc}(q,\omega)$ and will give several explicit parametrizations.

8.1 Exact properties

8.1.1 Basic symmetries, analyticity, and high-frequency and static limits

The frequency-dependent xc kernel $f_{\rm xc}(\mathbf{r},\mathbf{r}',\omega)$ was defined in Section 7.3.2 as the Fourier transform of the time-dependent kernel $f_{\rm xc}(\mathbf{r},t,\mathbf{r}',t')$. The latter must be a real-valued quantity, since the density response $n_1(\mathbf{r},t)$ is real. As a consequence, we have

$$f_{\rm xc}(\mathbf{r},\mathbf{r}',\omega) = f^*_{\rm xc}(\mathbf{r},\mathbf{r}',-\omega)\,. \tag{8.1}$$

Furthermore, from the symmetry property (7.22) of the interacting response function, which also holds for the noninteracting response function, it follows that

$$f_{\rm xc}(\mathbf{r},\mathbf{r}',\omega) = f_{\rm xc}(\mathbf{r}',\mathbf{r},\omega)\,. \tag{8.2}$$

The definition of the xc kernel in eqn (7.77) involves the inverses of the interacting and noninteracting response functions. As we discussed in Section 7.1.3, the density–density response function is analytic in the upper half of the complex plane; moreover, it is also nonvanishing in the upper complex plane and thus invertible. Therefore, the xc kernel itself is an analytic function in the upper complex plane, and we can derive Kramers–Kronig relations for it:

$$\Re f_{\rm xc}(\mathbf{r},\mathbf{r}',\omega) = \Re f_{\rm xc}(\mathbf{r},\mathbf{r}',\infty) + \mathcal{P}\int_{-\infty}^{\infty}\frac{d\omega'}{\pi}\frac{\Im f_{\rm xc}(\mathbf{r},\mathbf{r}',\omega')}{\omega'-\omega}\,, \tag{8.3}$$

$$\Im f_{\rm xc}(\mathbf{r},\mathbf{r}',\omega) = -\mathcal{P}\int_{-\infty}^{\infty}\frac{d\omega'}{\pi}\frac{\Re f_{\rm xc}(\mathbf{r},\mathbf{r}',\omega') - \Re f_{\rm xc}(\mathbf{r},\mathbf{r}',\infty)}{\omega'-\omega}\,. \tag{8.4}$$

Here we have taken account of the fact that the xc kernel does not vanish in the limit of infinite frequencies, but instead approaches a real function $f_{\rm xc}(\mathbf{r},\mathbf{r}',\infty)$. To show this, we consider eqn (7.77) for the xc kernel and insert the high-frequency limits of the interacting and noninteracting inverse response functions, given in eqn (7.39):

$$f_{\rm xc}(\mathbf{r},\mathbf{r}',\omega\to\infty) = L_s(\mathbf{r},\mathbf{r}') - L(\mathbf{r},\mathbf{r}') - \frac{1}{|\mathbf{r}-\mathbf{r}'|} + \mathcal{O}\left(\omega^{-2}\right)\,, \tag{8.5}$$

where $L(\mathbf{r},\mathbf{r}')$ and $L_s(\mathbf{r},\mathbf{r}')$ follow from the third-frequency-moment sum rule (Goodman and Sjölander, 1973) applied to the interacting and the noninteracting system, respectively. Notice that the functions $K(\mathbf{r},\mathbf{r}')$ and $K_s(\mathbf{r},\mathbf{r}')$ [see eqn (7.39)] are identical and thus cancel out in eqn (8.5). The reason for this is that $K(\mathbf{r},\mathbf{r}')$ and $K_s(\mathbf{r},\mathbf{r}')$ are functionals of the ground-state density $n_0(\mathbf{r})$ only, which is the same in the interacting and the noninteracting system. Recently, Nazarov *et al.* (2010*a*) derived an explicit expression for the infinite-frequency limit $f_{\rm xc}(\mathbf{r},\mathbf{r}',\infty)$ (the "antiadiabatic limit" of the xc kernel) in terms of $n_0(\mathbf{r})$, $v^0_{\rm xc}(\mathbf{r})$, the kinetic xc stress tensor, and the pair correlation function.

The static (zero-frequency) limit of the xc kernel is given by

$$f_{\rm xc}(\mathbf{r},\mathbf{r}',0) = \frac{\delta v^0_{\rm xc}[n_0](\mathbf{r})}{\delta n_0(\mathbf{r}')} = \frac{\delta E_{\rm xc}[n_0]}{\delta n_0(\mathbf{r})\delta n_0(\mathbf{r}')}\,, \tag{8.6}$$

which follows directly from a linearization of the static Kohn–Sham equation for a system under the influence of a static perturbation.

8.1.2 The zero-force theorem and the long-range property

Let us now consider the zero-force theorem of TDDFT, eqn (6.9), and linearize the time-dependent density and xc potential as $n(\mathbf{r},t) = n_0(\mathbf{r}) + n_1(\mathbf{r},t)$ and $v_{\rm xc}(\mathbf{r},t) = v^0_{\rm xc}(\mathbf{r}) + v_{\rm xc1}(\mathbf{r},t)$. Inserting this into eqn (6.9) and dropping terms of second order gives

$$\int d^3r\,[n_0(\mathbf{r})\nabla v^0_{\rm xc}(\mathbf{r}) + n_0(\mathbf{r})\nabla v_{\rm xc1}(\mathbf{r},t) + n_1(\mathbf{r},t)\nabla v^0_{\rm xc}(\mathbf{r})] = 0\,. \tag{8.7}$$

The first term is nothing but the zero-force theorem of static DFT, and therefore vanishes independently. We thus get, using the definitions (7.71) and (7.72) of the linearized xc potential,

$$\int d^3r\, n_0(\mathbf{r})\nabla \int dt' \int d^3r' f_{\rm xc}(\mathbf{r},t,\mathbf{r}',t')n_1(\mathbf{r}',t') + \int d^3r\, n_1(\mathbf{r},t)\nabla v^0_{\rm xc}(\mathbf{r}) = 0\,. \quad (8.8)$$

This relation must hold for arbitrary density responses $n_1(\mathbf{r},t)$, and we arrive at

$$\int d^3r\, n_0(\mathbf{r})\nabla f_{\rm xc}(\mathbf{r},t,\mathbf{r}',t') = -\nabla' v^0_{\rm xc}(\mathbf{r}')\delta(t-t')\,, \quad (8.9)$$

where ∇' denotes the gradient operator with respect to $\mathbf{r}'$. Fourier transformation of eqn (8.9) leads to

$$\int d^3r\, n_0(\mathbf{r})\nabla f_{\rm xc}(\mathbf{r},\mathbf{r}',\omega) = -\nabla' v^0_{\rm xc}(\mathbf{r}')\,, \quad (8.10)$$

or, since the xc kernel is symmetric in $\mathbf{r}$ and $\mathbf{r}'$ [see eqn (8.2)],

$$\int d^3r'\, n_0(\mathbf{r}')\nabla' f_{\rm xc}(\mathbf{r},\mathbf{r}',\omega) = -\nabla v^0_{\rm xc}(\mathbf{r})\,. \quad (8.11)$$

If we multiply both sides by $n_0(\mathbf{r})$ and integrate over all space, we obtain

$$\int d^3r \int d^3r'\, n_0(\mathbf{r})n_0(\mathbf{r}')\nabla' f_{\rm xc}(\mathbf{r},\mathbf{r}',\omega) = 0\,, \quad (8.12)$$

which is the zero-force theorem for the xc kernel. This ensures that Newton's third law is satisfied for many-body systems in the case of linear response. There also exists a related zero-torque theorem, which we will discuss later.

Let us now come back to eqn (8.11). There seems to be a peculiar feature to this equation: the left-hand side contains a frequency dependence, whereas the right-hand side does not. This puts a stringent requirement on the frequency dependence of $f_{\rm xc}$: it must be such that an ω-independent, real quantity is obtained upon integrating $n_0(\mathbf{r}')\nabla' f_{\rm xc}(\mathbf{r},\mathbf{r}',\omega)$ over all space. In other words, the frequency dependence somehow averages out. This is, of course, trivially satisfied for any adiabatic (i.e., frequency-independent) approximation to $f_{\rm xc}$, but it is a crucial constraint on any nonadiabatic approximation and not so easy to satisfy, as we will see later.

A partial integration of eqn (8.11) gives

$$\int d^3r'\, f_{\rm xc}(\mathbf{r},\mathbf{r}',\omega)\nabla' n_0(\mathbf{r}') = \nabla v^0_{\rm xc}(\mathbf{r})\,. \quad (8.13)$$

From this relation, we can get some insight into the important question of the spatial range of $f_{\rm xc}$, closely following an argument made by Vignale (2006). Let us assume that the xc kernel has a finite spatial range, which would imply that the integral

$$\int d^3r'\, f_{\rm xc}(\mathbf{r},\mathbf{r}',\omega) \quad (8.14)$$

has a finite value for all $\mathbf{r}$. For instance, this is satisfied if $f_{\rm xc}(\mathbf{r},\mathbf{r}',\omega)$, if viewed as a matrix in space, is dominant along the diagonal ($\mathbf{r}=\mathbf{r}'$) and has rapidly decreasing

off-diagonal elements. The decrease of $f_{\rm xc}$ as $\mathbf{r}'$ moves away from a given $\mathbf{r}$ must be fast enough (e.g., exponential) for the integral (8.14) to exist and be finite.

Next, we consider the case where the ground-state density $n_0(\mathbf{r})$ varies slowly on a length scale given by the spatial range of $f_{\rm xc}(\mathbf{r},\mathbf{r}',\omega)$, so that it can be pulled out in front of the integral in eqn (8.13). We obtain

$$[\nabla n_0(\mathbf{r})] \int d^3r'\, f_{\rm xc}(\mathbf{r},\mathbf{r}',\omega) = \nabla v^0_{\rm xc}(\mathbf{r})\,. \tag{8.15}$$

Let us look at this equation in the limit where the system becomes more and more uniform. Both $\nabla n_0(\mathbf{r})$ and $\nabla v^0_{\rm xc}(\mathbf{r})$ are then small quantities of first order in the wave vector $\mathbf{k}$ characterizing the nonuniformity. The integral over the xc kernel approaches

$$\int d^3r'\, f_{\rm xc}(\mathbf{r},\mathbf{r}',\omega) \longrightarrow f_{\rm xc}(\mathbf{k}=0,\omega)\,, \tag{8.16}$$

where $f_{\rm xc}(\mathbf{k},\omega)$ is the frequency-dependent xc kernel of the homogeneous electron liquid. We will discuss this quantity in more detail in Section 8.3. We thus arrive an equation where the left-hand side is explicitly frequency-dependent, whereas the right-hand side is not. This contradiction means that we must have made a wrong assumption: the integral (8.14) cannot be finite in general, but must diverge in the weakly inhomogeneous case. This means that the xc kernel for a general nonuniform system has a long spatial range, i.e., it does *not* fall off rapidly for $\mathbf{r} \neq \mathbf{r}'$.

The fact that $f_{\rm xc}(\mathbf{r},\mathbf{r}',\omega)$ has a long spatial range is closely related to the *ultranonlocality problem*, which will be discussed in Section 10.2. This issue plays an important role in TDDFT whenever one attempts to go beyond the adiabatic approximation and construct frequency-dependent xc kernels. As we will see in Chapter 10, there is an elegant way to circumvent the ultranonlocality problem, namely, by switching from densities to currents as basic variables.

For weakly inhomogeneous extended systems, the long spatial range of $f_{\rm xc}$ can be made explicit in the following form:

$$\lim_{\mathbf{q}\to 0} f_{\rm xc}(\mathbf{q},\mathbf{q},\omega) = \frac{\alpha(\omega)}{q^2}\,. \tag{8.17}$$

The frequency-dependent coefficient $\alpha(\omega)$ can be shown (Nazarov *et al.*, 2009) to depend only on the average ground-state density and the frequency-dependent xc kernel of a uniform electron liquid at that average density. As we will see later in Chapter 12, this $1/q^2$ dependence of the xc kernel has profound implications for the description of excitonic properties of bulk insulators, and we will give a more detailed discussion there.

8.1.3 Variational principle and causality

In Section 6.6, we explained that there is no stationary-action principle associated with the TDDFT action (6.66); the definition of the xc potential, eqn (6.78), therefore contains boundary terms in addition to the functional derivative of the xc action functional that one would have naively expected, and which was originally proposed by Runge and Gross (1984).

To emphasize this point and put it in the present context of linear response, let us for a moment pretend that

$$v_{\rm xc}(\mathbf{r},t) = \frac{\delta \mathcal{A}_{\rm xc}[n]}{\delta n(\mathbf{r},t)}\,, \tag{8.18}$$

and calculate the xc kernel from this, using its definition (7.72):

$$f_{\rm xc}(\mathbf{r},t,\mathbf{r}',t') = \left.\frac{\delta^2 \mathcal{A}_{\rm xc}[n]}{\delta n(\mathbf{r},t)\delta n(\mathbf{r}',t')}\right|_{n_0(\mathbf{r})}\,. \tag{8.19}$$

This expression, although nice and compact, has a serious problem: it violates causality! This is easily seen by noticing that the right-hand side of eqn (8.19) is symmetric under interchange of $(\mathbf{r},t)$ and $(\mathbf{r}',t')$. $f_{\rm xc}(\mathbf{r},t,\mathbf{r}',t')$, on the other hand, must vanish for $t<t'$, which leads to a clear contradiction.[1] One concludes from this that eqn (8.18) cannot be correct, and the xc potential cannot be expressed as a simple functional derivative. Indeed, as we saw in Section 6.5, eqn (8.18) misses some crucial boundary terms. We'll now discuss how this affects the xc kernel, and what corrections have to be made to eqn (8.19) (Vignale, 2008).

We begin by writing the xc kernel as

$$f_{\rm xc}(\mathbf{r},t,\mathbf{r}',t') = \frac{\delta v_s(\mathbf{r},t)}{\delta n(\mathbf{r}',t')} - \frac{\delta v(\mathbf{r},t)}{\delta n(\mathbf{r}',t')} - \frac{\delta(t-t')}{|\mathbf{r}-\mathbf{r}'|}\,, \tag{8.20}$$

where the right-hand side has to be evaluated at the ground-state density. Now, from eqn (6.71) we have

$$\begin{aligned}\frac{\delta v(\mathbf{r},t)}{\delta n(\mathbf{r}',t')} = \frac{\delta^2 \mathcal{A}_0[n]}{\delta n(\mathbf{r},t)\delta n(\mathbf{r}',t')} &- i\left\langle \Psi[n](t_1)\left|\frac{\delta^2\Psi[n](t_1)}{\delta n(\mathbf{r},t)\delta n(\mathbf{r}',t')}\right.\right\rangle \\ &-i\left\langle \frac{\delta\Psi[n](t_1)}{\delta n(\mathbf{r}',t')}\left|\frac{\delta\Psi[n](t_1)}{\delta n(\mathbf{r},t)}\right.\right\rangle .\end{aligned} \tag{8.21}$$

Interchanging $(\mathbf{r},t)$ and $(\mathbf{r}',t')$ gives

$$\begin{aligned}\frac{\delta v(\mathbf{r}',t')}{\delta n(\mathbf{r},t)} = \frac{\delta^2 \mathcal{A}_0[n]}{\delta n(\mathbf{r},t)\delta n(\mathbf{r}',t')} &- i\left\langle \Psi[n](t_1)\left|\frac{\delta^2\Psi[n](t_1)}{\delta n(\mathbf{r},t)\delta n(\mathbf{r}',t')}\right.\right\rangle \\ &-i\left\langle \frac{\delta\Psi[n](t_1)}{\delta n(\mathbf{r},t)}\left|\frac{\delta\Psi[n](t_1)}{\delta n(\mathbf{r}',t')}\right.\right\rangle ,\end{aligned} \tag{8.22}$$

where the left-hand side vanishes for $t>t'$. Thus, subtracting eqn (8.22) from eqn (8.21) gives

$$\begin{aligned}\frac{\delta v(\mathbf{r},t)}{\delta n(\mathbf{r}',t')} &= -i\left\langle \frac{\delta\Psi[n](t_1)}{\delta n(\mathbf{r}',t')}\left|\frac{\delta\Psi[n](t_1)}{\delta n(\mathbf{r},t)}\right.\right\rangle + i\left\langle \frac{\delta\Psi[n](t_1)}{\delta n(\mathbf{r},t)}\left|\frac{\delta\Psi[n](t_1)}{\delta n(\mathbf{r}',t')}\right.\right\rangle \\ &= 2\Im\left\langle \frac{\delta\Psi[n](t_1)}{\delta n(\mathbf{r}',t')}\left|\frac{\delta\Psi[n](t_1)}{\delta n(\mathbf{r},t)}\right.\right\rangle .\end{aligned} \tag{8.23}$$

[1] This argument, which triggered much of the subsequent work on action principles in TDDFT, was at the time referred to as the "causality paradox." It was originally put forward by U. J. Gossmann in 1994 and first appeared in the literature in Gross *et al.* (1995).

As we discussed in Section 6.6, the right-hand side does not depend on the choice of the upper time limit t_1 as long as it is (infinitesimally) larger than both t and t'. A similar relation can be derived for the functional derivative of v_s:

$$\frac{\delta v_s(\mathbf{r},t)}{\delta n(\mathbf{r}',t')} = 2\Im \left\langle \frac{\delta\Phi[n](t_1)}{\delta n(\mathbf{r}',t')} \middle| \frac{\delta\Phi[n](t_1)}{\delta n(\mathbf{r},t)} \right\rangle . \tag{8.24}$$

Notice that eqns (8.23) and (8.24) are both valid for $t > t'$, which leaves the case $t = t'$ undetermined. Indeed, we have seen that there are equal-time singularities in the response functions, related to the high-frequency behavior. It thus follows that

$$\begin{aligned} f_{\rm xc}(\mathbf{r},t,\mathbf{r}',t') = 2\Im \left[\left\langle \frac{\delta\Phi[n](t_1)}{\delta n(\mathbf{r}',t')} \middle| \frac{\delta\Phi[n](t_1)}{\delta n(\mathbf{r},t)} \right\rangle - \left\langle \frac{\delta\Psi[n](t_1)}{\delta n(\mathbf{r}',t')} \middle| \frac{\delta\Psi[n](t_1)}{\delta n(\mathbf{r},t)} \right\rangle \right] \theta(t-t') \\ + f_{\rm xc}(\mathbf{r},\mathbf{r}',\omega=\infty)\delta(t-t') . \end{aligned} \tag{8.25}$$

The first two terms on the right-hand side of eqn (8.25) have to be evaluated at $n_0(\mathbf{r})$, and we recall from Section 6.6.2 that t_1 can be replaced by t_+.

We make the intriguing observation that the first two terms of eqn (8.25) have the appearance of a Berry curvature, for the noninteracting and the interacting system. The Berry phase γ, also known as the geometric phase, is an important quantum mechanical concept that arises from the adiabatic time evolution of a system along a path in parameter space (Xiao *et al.*, 2010). The Berry phase is defined as follows:

$$\gamma = i \oint_{\mathcal{C}} d\mathbf{R} \cdot \langle \Psi_{\mathbf{R}} | \nabla_{\mathbf{R}} | \Psi_{\mathbf{R}} \rangle , \tag{8.26}$$

where $\mathbf{R}$ denotes some time-dependent parameter, which could for instance be a nuclear position, but more abstract types of parameters are also possible. $\Psi_{\mathbf{R}}$ is the eigenstate of the system for each value of the parameter $\mathbf{R}$, and $\mathcal{C}$ is a closed loop in parameter space. As the system moves slowly through the parameter space and comes back to its initial configuration, it picks up a phase factor γ upon its return. The integral in eqn (8.26) can be transformed into a surface integral,

$$\gamma = \frac{1}{2} \sum_{\mu\nu} \oint_{\mathcal{S}} dR_\mu \, dR_\nu \, \Omega_{\mu\nu} , \tag{8.27}$$

where R_μ and R_ν are components of the vector $\mathbf{R}$ in the parameter space, and $\Omega_{\mu\nu}$ is the Berry curvature,

$$\Omega_{\mu\nu} = 2\Im \left\langle \frac{\partial\Psi}{\partial R_\mu} \middle| \frac{\partial\Psi}{\partial R_\mu} \right\rangle . \tag{8.28}$$

The physical interpretation of the Berry curvature is that it plays the role of a local "magnetic field" in the parameter space.

Coming back to eqn (8.25), we see that here the parameter space is obviously given by the time-dependent density. The noninteracting and interacting wave functions $\Phi[n](t_1)$ and $\Psi[n](t_1)$ themselves are not adiabatic eigenstates, but their functional derivatives are to be evaluated at the ground-state density. This shows that the first two terms of eqn (8.25) can indeed be viewed as a generalized Berry curvature (8.28).

8.2 Approximations

In any practical application of linear-response TDDFT one needs to rely on suitable approximations to the xc kernel. These can, in principle, be generated from any given approximation to the time-dependent xc potential via

$$f_{\rm xc}^{\rm app}(\mathbf{r},\mathbf{r}',\omega) = \int d(t-t')\, e^{i\omega(t-t')}\, \left.\frac{\delta v_{\rm xc}^{\rm app}[n](\mathbf{r},t)}{\delta n(\mathbf{r}',t')}\right|_{n_0(\mathbf{r})}\,, \tag{8.29}$$

which follows from eqn (7.76). Of course, approximate xc kernels can also be directly constructed by other means, without the input of an approximate $v_{\rm xc}(\mathbf{r},t)$. We will encounter examples of both kinds throughout this book.

As we discussed earlier at the end of Section 4.1, an essential requirement for any approximate time-dependent xc potential is that it has to match the approximate static xc potential $v_{\rm xc}^{0,{\rm app}}(\mathbf{r})$ that was used to generate the initial ground state of the system. In other words, $v_{\rm xc}^{\rm app}(\mathbf{r},t_0) = v_{\rm xc}^{0,{\rm app}}(\mathbf{r})$ at the initial time. Furthermore, $v_{\rm xc}^{\rm app}(\mathbf{r},t)$ needs to reduce to $v_{\rm xc}^{0,{\rm app}}(\mathbf{r})$ in the static limit when there is no time-dependent external potential for $t \leq t_0$.

These requirements carry over to the xc kernel, which also has to match the static xc potential that was used to calculate the ground state of the system. This is guaranteed if the static limit of the approximate frequency-dependent xc kernel satisfies eqn (8.6).

If one chooses, for whatever reason, an approximate xc kernel that does not match the static xc potential that was used for the ground-state calculation, basic theorems of linear response such as the f-sum rule (7.53) and the zero-force theorem (see Section 8.1.2) may be violated (Liebsch, 1985). The basic reason is that choosing an ill-fitting xc kernel introduces spurious internal forces. Response properties such as excitation energies and oscillator strengths may then come out incorrectly.

The simplest and most drastic treatment of the xc kernel, known as the random-phase approximation (RPA), is to set it equal to zero:

$$f_{\rm xc}^{\rm RPA} = 0\,. \tag{8.30}$$

This means that all dynamical xc effects are ignored in the linear response. As we shall see, the RPA typically leads to an overestimation of excitation energies in finite systems, but it often tends to give reasonable to good results for plasmon-type collective excitations in large metallic systems.

The most commonly used approximations to the xc kernel fall into the class of the adiabatic approximation:

$$f_{\rm xc}^{\rm A}(\mathbf{r},\mathbf{r}') = \frac{\delta v_{\rm xc}^{0}[n_0](\mathbf{r})}{\delta n_0(\mathbf{r}')} = \frac{\delta^2 E_{\rm xc}[n_0]}{\delta n_0(\mathbf{r})\delta n_0(\mathbf{r}')}\,, \tag{8.31}$$

which is frequency-independent and purely real. This approximation can be viewed as replacing the xc kernel at each frequency with its static limit [see eqn (8.6)]. Any approximate static xc potential will automatically give the corresponding adiabatic xc kernel. Of particular interest is the adiabatic LDA:

$$f_{\rm xc}^{\rm ALDA}(\mathbf{r},\mathbf{r}') = \left.\frac{d^2 e_{\rm xc}^{h}(\bar{n})}{d\bar{n}^2}\right|_{\bar{n}=n_0(\mathbf{r})} \delta(\mathbf{r}-\mathbf{r}')\,. \tag{8.32}$$

The ALDA is not only frequency-independent, it is also local in space. For completeness, the spin-dependent ALDA xc kernel is

$$f_{\mathrm{xc},\sigma\sigma'}^{\mathrm{ALDA}}(\mathbf{r},\mathbf{r}') = \left.\frac{d^2 e_{\mathrm{xc}}^h(\bar{n}_\uparrow,\bar{n}_\downarrow)}{d\bar{n}_\sigma d\bar{n}_{\sigma'}}\right|_{\substack{\bar{n}_\uparrow=n_{0\uparrow}(\mathbf{r})\\ \bar{n}_\downarrow=n_{0\downarrow}(\mathbf{r})}} \delta(\mathbf{r}-\mathbf{r}')\,. \tag{8.33}$$

From eqn (8.31), it is straightforward (although often tedious in practice) to derive the adiabatic xc kernel associated with any approximate static xc density functional, such as one of the GGAs.

A number of more sophisticated xc kernels have been developed in recent years. In Part III of this book, we will discuss various approaches that lead to frequency-dependent and nonlocal approximations to f_{xc}. In Chapter 10, we will show how a local, frequency-dependent xc functional can be constructed using time-dependent current-DFT (TDCDFT). Orbital-dependent xc functionals will be the subject of Chapter 11, and in Section 11.3 we will discuss how approximate nonlocal xc kernels can be derived using the linearized TDOEP approach. Finally, in Chapter 13, we will discuss the definition of $f_{\mathrm{xc}}(\mathbf{r},\mathbf{r}',\omega)$ in the context of diagrammatic many-body perturbation theory and consider several explicit, frequency-dependent approximations.

8.3 The xc kernels of the homogeneous electron liquid

The LDA for the xc potential of static DFT, eqn (2.81), uses the xc energy density $e_{\mathrm{xc}}^h(n)$ of a homogeneous electron liquid of a given uniform density n as input. As we discussed in Section 2.2.4, very accurate numerical results for $e_{\mathrm{xc}}^h(n)$ are available, which means that the modern functional forms of the static LDA xc energy are very close to being numerically exact (Vosko *et al.*, 1980; Perdew and Wang, 1992; Tanatar and Ceperley, 1989; Attaccalite *et al.*, 2002).

In the dynamical case, the situation is much more complicated, and we will review the current state of knowledge in TDDFT for homogeneous systems in this section [for an exhaustive presentation of this topic, the reader is referred to Giuliani and Vignale (2005)]. The key quantities are the longitudinal and transverse xc kernels $f_{\mathrm{xc}}^{L,T}(q,\omega)$ of the homogeneous electron liquid, and we will discuss some of their exact properties. The zero-wave-vector limits $f_{\mathrm{xc}}^{L,T}(0,\omega)$ will be needed as input for local approximations in TDDFT, and we will give an overview of the available parametrizations in two and three dimensions.

8.3.1 Definitions

The xc kernel $f_{\mathrm{xc}}(q,\omega)$ of a homogeneous electron liquid is a complex, frequency- and wavevector-dependent quantity, defined via

$$\chi(q,\omega) = \frac{\chi_0(q,\omega)}{1-[v(q)+f_{\mathrm{xc}}(q,\omega)]\chi_0(q,\omega)}\,. \tag{8.34}$$

Here, $\chi_0(q,\omega)$ is the density–density response function of a noninteracting homogeneous electron liquid, also known as the Lindhard function. It can be calculated analytically in 2D and 3D (Giuliani and Vignale, 2005). The Coulomb interaction is given

by $v(q) = 2\pi/q$ in 2D and $v(q) = 4\pi/q^2$ in 3D, and $\chi(q,\omega)$ is the density–density response function of an interacting homogeneous electron liquid. Equation (8.34) can be recast in the following way:

$$\frac{1}{\chi(q,\omega)} = \frac{1}{\chi_0(q,\omega)} + v(q) + f_{\rm xc}(q,\omega)\,. \tag{8.35}$$

We will soon see (Chapter 10) that in addition to studying $f_{\rm xc}(q,\omega)$, it is of great interest to discuss the xc kernels of TDCDFT, $f_{\rm xc}^{L,T}(q,\omega)$, where L and T stand for "longitudinal" and "transverse." These are defined similarly to eqn (8.34):

$$\chi^{L,T}(q,\omega) = \frac{\chi_0^{L,T}(q,\omega)}{1-(q^2/\omega^2)[v^{L,T}(q)+f_{\rm xc}^{L,T}(q,\omega)]\chi_0^{L,T}(q,\omega)}\,. \tag{8.36}$$

Here, $\chi^{L,T}(q,\omega)$ and $\chi_0^{L,T}(q,\omega)$ are the longitudinal and transverse current–current response functions of the interacting and noninteracting electron liquids, respectively, and $v^L(q) = v(q)$ and $v^T(q) = 0$.

The response functions of TDDFT and TDCDFT are connected via the following simple relation:

$$\chi(q,\omega) = \frac{q^2}{\omega^2}\,\chi^L(q,\omega)\,, \tag{8.37}$$

and similarly for $\chi_0(q,\omega)$ and $\chi_0^L(q,\omega)$. The transverse current–current response function, on the other hand, is unique to TDCDFT and has no correspondence in TDDFT (the physical reasons for this will become clear later, in Chapter 10). From eqn (8.37), one immediately sees that the density xc kernel and the longitudinal current xc kernel are identical:

$$f_{\rm xc}(q,\omega) = f_{\rm xc}^L(q,\omega)\,. \tag{8.38}$$

In the following we will discuss the properties of the xc kernels $f_{\rm xc}^{L,T}$, and this will automatically include $f_{\rm xc}$.

The exact form of $f_{\rm xc}^{L,T}(q,\omega)$ as a function of the density n is unknown. There exists a sizable body of accurate numerical results for the static, wave-vector-dependent xc kernel $f_{\rm xc}(q,0)$ (Moroni *et al.*, 1992, 1995; Corradini *et al.*, 1998; Davoudi *et al.*, 2001). These results take advantage of quantum Monte Carlo calculations of the ground state of the homogeneous electron liquid; however, this methodology does not carry over to the dynamical case.

Since we don't have precise numerical benchmark results for $f_{\rm xc}^{L,T}(q,\omega)$, we need to rely on other methods to obtain explicit approximations and density functionals. The idea is to collect all the exact properties of $f_{\rm xc}^{L,T}(q,\omega)$ which are known (such as sum rules and asymptotic and limiting behavior), and try to come up with an approximate functional form that obeys as many of the known constraints as possible, and then hope for the best.

8.3.2 Exact properties

General analytic behavior. The xc kernels are analytic functions in the upper half of the complex ω-plane. Similarly to eqns (8.3) and (8.4), the Kramers–Kronig relations are given by

$$\Re f_{\rm xc}^{L,T}(q,\omega) = f_{\rm xc}^{L,T}(q,\infty) + \mathcal{P}\int_{-\infty}^{\infty}\frac{d\omega'}{\pi}\frac{\Im f_{\rm xc}^{L,T}(q,\omega')}{\omega'-\omega}\,, \tag{8.39}$$

$$\Im f_{\rm xc}^{L,T}(q,\omega) = -\mathcal{P}\int_{-\infty}^{\infty}\frac{d\omega'}{\pi}\frac{\Re f_{\rm xc}^{L,T}(q,\omega') - f_{\rm xc}^{L,T}(q,\infty)}{\omega'-\omega}\,, \tag{8.40}$$

which hold for each value of q. Thus, any approximation to the imaginary part of the xc kernel will automatically yield an expression for the real part, and vice versa. The real and imaginary parts satisfy the symmetry relations

$$\Re f_{\rm xc}^{L,T}(q,\omega) = \Re f_{\rm xc}^{L,T}(q,-\omega)\,, \tag{8.41}$$

$$\Im f_{\rm xc}^{L,T}(q,\omega) = -\Im f_{\rm xc}^{L,T}(q,-\omega)\,. \tag{8.42}$$

Infinite-frequency limits. In the infinite-frequency limit, $f_{\rm xc}^{L,T}(q,\infty)$ becomes a real function. This can be seen from the high-frequency expansions of the interacting and noninteracting response functions in eqn (8.35) (see also Section 7.1.5). The leading terms in the expansion involve the first-frequency-moment sum rule or f-sum rule, which are the same for the interacting and noninteracting response functions and therefore cancel out. The infinite-frequency limit of $f_{\rm xc}^{L,T}(q,\infty)$ is therefore determined by the next term in the expansion, which involves the third-moment sum rule for the interacting and noninteracting response functions. More details and plots of $f_{\rm xc}^{L,T}(q,\infty)$ for various values of r_s can be found in Nazarov *et al.* (2010*a*).

In the limit $q \to 0$, it is possible to derive relatively simple expressions for the infinite-frequency xc kernels:

$$f_{\rm xc}^{L}(0,\infty) = -\frac{1}{2}(1+3\beta_D)n^{2/D}\frac{d}{dn}\left(\frac{e_{\rm xc}^h}{n^{1+2/D}}\right) + 6n^{1/D}\frac{d}{dn}\left(\frac{e_{\rm xc}^h}{n^{1+1/D}}\right), \tag{8.43}$$

$$f_{\rm xc}^{T}(0,\infty) = \frac{1}{2}(1-\beta_D)n^{2/D}\frac{d}{dn}\left(\frac{e_{\rm xc}^h}{n^{1+2/D}}\right) + 2n^{1/D}\frac{d}{dn}\left(\frac{e_{\rm xc}^h}{n^{1+1/D}}\right). \tag{8.44}$$

Here, $D = 2$ or 3 is the dimensionality of the system, and $\beta_3 = 1/5$ and $\beta_2 = 1/2$. In the following, we use the abbreviated notation $f_{\rm xc}^{L,T}(0,\infty) \equiv f_{\rm xc}^{L,T}(\infty)$.

The imaginary part of the xc kernels vanishes in the limit of high frequencies. For $q = 0$, one finds

$$\Im f_{\rm xc}^{L,T}(0,\omega\to\infty) = -c_D^{L,T}\,\frac{\pi^{4-D}}{\omega^{D/2}}\,, \tag{8.45}$$

with the coefficients $c_3^L = 23/15$, $c_3^T = 16/15$ and $c_2^L = 11/32$, $c_2^T = 9/32$. These results follows from the second-order perturbation theory of the irreducible polarization propagator (Glick and Long, 1971; Holas and Singwi, 1989) or from an equation-of-motion approach (Nifosì *et al.*, 1998; Giuliani and Vignale, 2005).

Low-frequency behavior. The imaginary part of $f_{\rm xc}^{L,T}(0,\omega)$ approaches zero for low frequencies, with a linear frequency dependence:

$$\Im f_{\rm xc}^{L,T}(0,\omega\to 0) = -\frac{k_F^{D-2}}{n^2\pi^2}S_D^{L,T}\omega\,, \tag{8.46}$$

where k_F is the Fermi wave vector, and the dimensionless constants $S_D^{L,T}$ have been derived by Qian and Vignale (2002); we give them here for completeness:

$$S_3^L = -\frac{1}{45\pi}\left\{5 - \left(\lambda + \frac{5}{\lambda}\right)\tan^{-1}\lambda - \frac{2}{\lambda}\sin^{-1}\frac{\lambda}{\sqrt{1+\lambda^2}} + \frac{2}{\lambda\sqrt{2+\lambda^2}}\left[\frac{\pi}{2} - \tan^{-1}\frac{1}{\lambda\sqrt{2+\lambda^2}}\right]\right\}, \tag{8.47}$$

$$S_2^L = \frac{1}{6}\left\{-\frac{\pi}{4} + \frac{3-\lambda^2}{2-\lambda^2}\ln(\lambda+1) - \frac{\lambda}{1+\lambda} + \frac{f(\lambda)}{2-\lambda^2}\right\}. \tag{8.48}$$

The transverse constants are related in a simple manner to the longitudinal ones by $S_3^T = (3/4)S_3^L$ and $S_2^T = S_2^L$. In 3D, we have $\lambda = \sqrt{\pi k_F}$, and in 2D, we have $\lambda = k_F$. The function $f(\lambda)$ in eqn (8.48) is given by

$$f(\lambda) = \begin{cases} 2\sqrt{1-\lambda^2}\tan^{-1}\sqrt{\dfrac{1-\lambda}{1+\lambda}}, & \lambda < 1, \\ \sqrt{\lambda^2-1}\ln\left[\dfrac{\sqrt{\lambda+1}-\sqrt{\lambda-1}}{\sqrt{\lambda+1}+\sqrt{\lambda-1}}\right], & \lambda > 1. \end{cases} \tag{8.49}$$

Static, long-wavelength limits. It is of particular interest to consider the limiting case of $f_{\rm xc}^{L,T}(q,\omega)$ where both of the arguments q and ω go to zero, i.e., the long-wavelength static limit. It turns out, quite remarkably, that the result depends on the order in which those two limits are taken! In other words, the xc kernel is nonanalytic as a function of q and ω. This was first pointed out by Conti and Vignale (1999), who also introduced two characteristic elasticity parameters of the electron liquid, the xc bulk modulus $K_{\rm xc}$ and the xc shear modulus $\mu_{\rm xc}$.

The xc bulk modulus is related to the compressibility of the electron liquid and follows in a simple manner from the xc energy density:

$$K_{\rm xc} = n^2\frac{d^2 e_{\rm xc}^h(n)}{dn^2}\,. \tag{8.50}$$

The xc shear modulus $\mu_{\rm xc}$, on the other hand, accounts for the fact that the Fermi surface of the electron liquid resists deformations of its equilibrium spherical shape. Unfortunately, $\mu_{\rm xc}$ is much less well known than $K_{\rm xc}$; one can express it in terms of the so-called Landau parameters F_1 and F_2 (Pines and Nozières, 1966):

$$\mu_{\rm xc} = \frac{2E_F n}{25}\frac{3F_2 - 5F_1}{3+F_1} \quad \text{(3D)}, \qquad \mu_{\rm xc} = \frac{E_F n}{2}\frac{F_2 - F_1}{2+F_1} \quad \text{(2D)}\,, \tag{8.51}$$

where E_F is the Fermi energy of the electron liquid of density n. The Landau parameters are only approximately known, and only for a handful of values of r_s; the resulting values for $\mu_{\rm xc}$ are listed in Table 8.1.

The long-wavelength limit of the static xc kernels (where the $\omega \to 0$ limit is taken first) has the following form:

Table 8.1 Values of the xc shear modulus $\mu_{\rm xc}$ of the homogeneous electron liquid in 3D (in units of $2\omega_{pl}n$) and 2D (in Hartree units), and the dimensionless fitting parameters $\Gamma_D^{L,T}$ for the Qian–Vignale parametrizations (8.66) and (8.70).

r_s	$\mu_{\rm xc}^{3D}/(2\omega_{pl}n)$	Γ_3^L	Γ_3^T	$\mu_{\rm xc}^{2D}$	Γ_2^L	Γ_2^T
1	0.00738	1.656	1.821	0.118	0.763	0.651
2	0.00770	1.368	1.533	−0.198	0.927	0.861
3	0.00801	1.215	1.380	−0.763	1.08	1.03
4	0.00837	1.112	1.277			
5	0.00869	1.033	1.198	−1.84	1.31	1.29

$$\lim_{q\to 0} f_{\rm xc}^L(q,0) \equiv f_{\rm xc}^L(0) = K_{\rm xc}/n^2 \,, \tag{8.52}$$

$$\lim_{q\to 0} f_{\rm xc}^T(q,0) \equiv f_{\rm xc}^T(0) = 0 \,. \tag{8.53}$$

The opposite case, i.e., the static limit of the zero-wave-vector xc kernels, is

$$\lim_{\omega\to 0} f_{\rm xc}^L(0,\omega) = \frac{1}{n^2}\left[K_{\rm xc} + \left(2 - \frac{2}{D}\right)\mu_{\rm xc}\right], \tag{8.54}$$

$$\lim_{\omega\to 0} f_{\rm xc}^T(0,\omega) = \mu_{\rm xc}/n^2 \,. \tag{8.55}$$

The fact that the xc shear modulus $\mu_{\rm xc}$ appears in eqns (8.54) and (8.55) but not in eqns (8.52) and (8.53) clearly illustrates that the $\omega \to 0$ and $q \to 0$ limits of the xc kernels do not commute. This surprising fact has some very important practical consequences, as we will see later in Chapter 10.

The reason why the xc shear modulus does not vanish in the static limit is quite simple, at least at first glance: taking the $q = 0$ limit first means that we consider perturbations of infinite spatial extent, and it would take an infinite amount of time for the system to "iron out" these perturbations and reach local equilibrium. As long as ω is still finite, there is not enough time to establish equilibrium and the system remains "dynamical" all the way down to zero frequency.[2]

There is, however, another aspect which we have so far not taken into account, namely, the system can also relax towards equilibrium because of intrinsic electron–electron collisions. These collisions operate at a characteristic relaxation rate τ^{-1}, which depends on the temperature T of the electron liquid. At low temperatures, τ^{-1} vanishes as T^2 (this is a result of Fermi liquid theory). For $\omega \ll \tau^{-1}$, the system is thus always in thermodynamic equilibrium owing to collision processes, no matter how large the spatial wavelength of the perturbation. However, it turns out that in practice even very small frequencies (with $\omega \ll E_F$) are still very large compared with τ^{-1}.

Figure 8.1 illustrates the physical regime in which the static limit of the zero-wave-vector xc kernels is taken. The shaded region is the electron–hole continuum of

[2]By contrast, in the opposite situation considered in eqns (8.52) and (8.53), which takes place exactly at $\omega = 0$, the system is always in a state of thermodynamic equilibrium at each value of q.

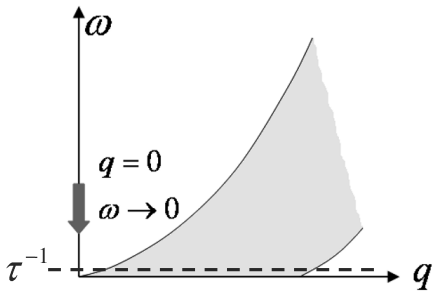

Fig. 8.1 Illustration of the static limit of $f_{\rm xc}^{L,T}(0,\omega)$. Perturbations with $q=0$ have infinite spatial extent, and it takes an infinite time to reach thermodynamic equilibrium: the system remains "dynamical" all the way down to $\omega = 0$, at least for frequencies above τ^{-1}, the characteristic relaxation rate due to electron collisions (τ^{-1} vanishes at zero temperature).

a homogeneous electron liquid, and here one approaches the origin from above this region. As long as the frequency is above the characteristic relaxation rate τ^{-1} (which vanishes at zero temperature), the system does not reach its true static limit, and the xc shear modulus remains present in eqns (8.54) and (8.55).

8.3.3 Parametrizations

In the following, we shall use the convention $f_{\rm xc}^{L,T}(0,\omega) \equiv f_{\rm xc}^{L,T}(\omega)$, i.e., we suppress the wave vector argument whenever it is zero.

Gross–Kohn (GK) and Holas–Singwi (HS) parametrizations. The oldest and best-known parametrization of the xc kernel (Gross and Kohn, 1985; Iwamoto and Gross, 1987) was originally derived for $f_{\rm xc}$ only, but it can easily be extended to $f_{\rm xc}^{L,T}$. The GK parametrization has the following simple functional form for a 3D system:

$$\Im f_{\rm xc}^{L,T}(\omega) = \frac{a_3^{L,T}\omega}{(1+b_3^{L,T}\omega^2)^{5/4}}\,, \tag{8.56}$$

with

$$a_3^{L,T} = -\pi c_3^{L,T}\left(\gamma/\pi c_3^{L,T}\right)^{5/3}\left[f_{\rm xc}^{L,T}(\infty) - f_{\rm xc}^{L,T}(0)\right]^{5/3}, \tag{8.57}$$

$$b_3^{L,T} = \left(\gamma/\pi c_3^{L,T}\right)^{4/3}\left[f_{\rm xc}^{L,T}(\infty) - f_{\rm xc}^{L,T}(0)\right]^{4/3}, \tag{8.58}$$

and the numerical constant $\gamma = \Gamma(1/4)^2/4\sqrt{2\pi}$, where $\Gamma(1/4) = 3.625610$. The coefficients $c_3^{L,T}$ are defined after eqn (8.45). We should also mention that there exists an extension of the GK formula to finite wave vectors (Dabrowski, 1986).

The analogous formula for the 2D case is due to Holas and Singwi (1989):

$$\Im f_{\rm xc}^{L,T}(\omega) = \frac{a_2^{L,T}\omega}{\left(b_2^{L,T}\right)^2 + \omega^2}\,, \tag{8.59}$$

with

$$a_2^{L,T} = -c_2^{L,T}\pi^2 \,, \tag{8.60}$$

$$b_2^{L,T} = -a_2^{L,T}\left[f_{\rm xc}^{L,T}(\infty) - f_{\rm xc}^{L,T}(0)\right]^{-1} \,. \tag{8.61}$$

It is straightforward to see that the parametrizations (8.56) and (8.59) satisfy the high-frequency limit (8.45). To fix the coefficients $a_D^{L,T}$ and $b_D^{L,T}$, a second condition is required, which is given by the Kramers–Kronig relation (8.39) with $\omega = 0$ and $q \to 0$.

The main advantage of eqns (8.56) and (8.59) clearly lies in their simplicity, which makes them practically useful. However, it is also clear that these simple interpolation formulas contain only a bare minimum of physical input and thus leave much room for improvement.

Nifosì–Conti–Tosi (NCT) parametrization. A different and somewhat more systematic approach to the construction of $f_{\rm xc}^{L,T}(\omega)$ was taken by Nifosì, Conti and Tosi (Nifosì *et al.*, 1998). The starting point is an exact representation of the xc kernels in terms of four-point response functions (following from the equation of motion for the current–current response function); these are then approximated using a decoupling scheme, which casts $f_{\rm xc}^{L,T}(\omega)$ into a convolution of two spectral functions:

$$\begin{aligned}\Im f_{\rm xc}^{L,T}(\omega) = -g_{\rm x}(\omega)\int_0^\omega \frac{d\omega'}{\pi}\int \frac{d^Dq}{(2\pi)^D n^2}[v^L(q)]^2\,\frac{q^2}{(\omega-\omega')}\Im\chi^L(q,\omega-\omega') \\ \times\left[a_D^{L,T}\frac{q^2}{\omega'^2}\Im\chi^L(q,\omega') + b_D^{L,T}\frac{q^2}{\omega^2}\Im\chi^T(q,\omega')\right],\end{aligned} \tag{8.62}$$

where $a_3^L = 23/30$, $a_3^T = 8/15$, $a_2^L = 11/16$, $a_2^T = 9/16$, and $b_3^L = 8/15$, $b_3^T = 2/5$, $b_2^L = b_2^T = 1/2$. To account for the exchange interaction between the final states of two-pair excitations, which reduces the spectral strength by a factor of 2 in the high-frequency limit in a perturbative treatment, the phenomenological factor $g_{\rm x}(\omega)$ is defined as follows:[3]

$$g_{\rm x}(\omega) = \frac{1+\omega/4E_F}{1+\omega/2E_F} \,. \tag{8.63}$$

Equation (8.62) still requires the imaginary parts of the interacting longitudinal and transverse response functions as input, which can be evaluated within the RPA. In Conti *el.* (1997) and Nifosì *et al.* (1998), simple analytical interpolation formulas are given which make the numerical implementation of eqn (8.62) straightforward. In 3D, we have

$$\Im f_{\rm xc}^{L}(\omega) = -g_{\rm x}(\omega)\begin{cases} c_0\widetilde{\omega} + c_2\dfrac{\widetilde{\omega}-1}{e^{7/\widetilde{\omega}-5}+1} \,, & (\widetilde{\omega}<2)\,, \\ \dfrac{d_0\sqrt{\widetilde{\omega}-2}+d_1}{\widetilde{\omega}(\widetilde{\omega}-\omega_1\sqrt{\widetilde{\omega}}-\omega_2)} \,, & (\widetilde{\omega}>2)\,, \end{cases} \tag{8.64}$$

[3] In an earlier version of their approximation, Conti *et al.* (1997) used the slightly different definition $g(x) = (\beta+\omega/4E_F)/(1+\omega/2E_F)$. The purpose of the adjustable parameter β was to make the limits $q \to 0$ and $\omega \to 0$ interchangeable. However, in the light of the discussion of Section 8.3.2, this appears to be an unphysical constraint, and it should be removed by setting $\beta = 1$ as in eqn (8.63).

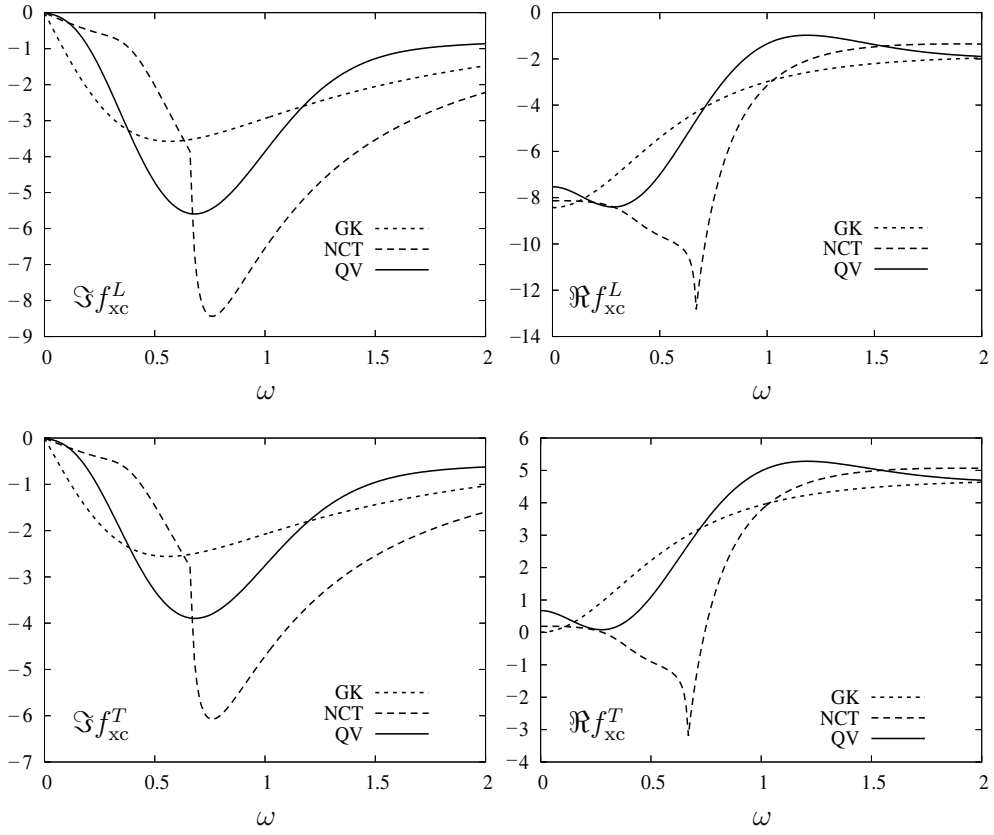

Fig. 8.2 3D parametrizations of the frequency-dependent longitudinal and transverse xc kernels of a homogeneous system with $r_s = 3$. All quantities are in atomic units.

where $\widetilde{\omega} = \omega/\omega_{pl}$; the plasma frequency is defined as $\omega_{pl} = \sqrt{4\pi n}$, and $\Im f_{\rm xc}^L$ is given in units of $2\omega_{pl}/n$. The fitting parameters c_0, c_1, d_0, d_1, ω_1, and ω_2 have been tabulated for a range of values of r_s in conti *et al.* (1997). The transverse xc kernel is given, to within a very good approximation, as $\Im f_{\rm xc}^T(\omega) = 0.72\Im f_{\rm xc}^L(\omega)$ for all frequencies and all values of r_s.

The 2D interpolation formula reads

$$\Im f_{\rm xc}^L(\omega) = -g_{\rm x}(\omega)\frac{c_1\omega + c_2\omega^2 + c_3\omega^3 + c_{\rm HS}\omega^5}{c_0 + c_4\omega^4 + \omega^6}\,, \tag{8.65}$$

where the coefficients c_0, c_1, c_2, c_3, and c_4 are tabulated in Nifosì *et al.* (1998), and $c_{\rm HS} = 11\pi/8r_s^2$. Similarly to the 3D case, the transverse kernel is approximated as being proportional to the longitudinal kernel, $\Im f_{\rm xc}^T(\omega) = 0.85\Im f_{\rm xc}^L(\omega)$. In eqn (8.65), ω is given in Ry, and $\Im f_{\rm xc}$ in units of Ry$/n$.

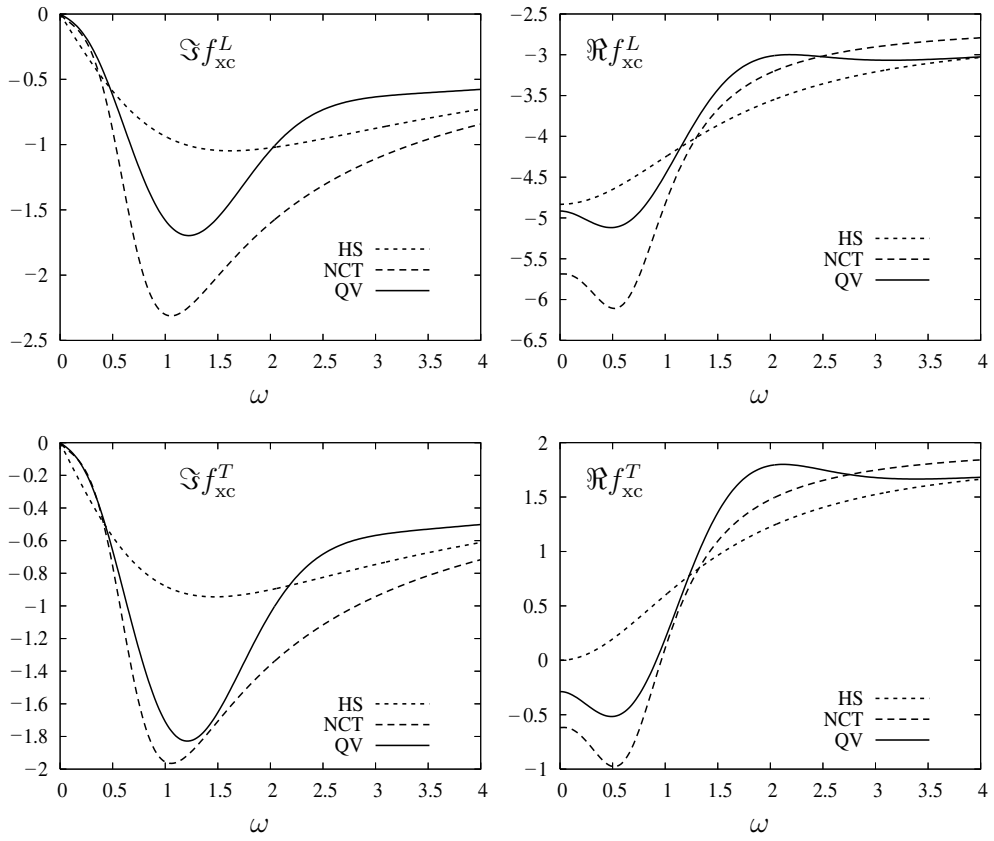

Fig. 8.3 2D parametrizations of the frequency-dependent longitudinal and transverse xc kernels of a homogeneous system with $r_s = 3$. All quantities are in atomic units.

Qian–Vignale (QV) parametrization. Qian and Vignale (2002) gave the following interpolation formula (for 3D systems):

$$\Im f_{\rm xc}^{L,T}(\omega) = -\frac{\omega}{n}\left[\frac{a_3^{L,T}}{(1+b_3^{L,T}\widetilde{\omega}^2)^{5/4}} + \widetilde{\omega}^2 \exp\left(-\frac{(|\widetilde{\omega}| - \Omega_3^{L,T})^2}{\Gamma_3^{L,T}}\right)\right], \tag{8.66}$$

where $\widetilde{\omega} = \omega/2\omega_{pl}$. The parameters $a_3^{L,T}$ and $b_3^{L,T}$ are determined by the high- and low-frequency relations (8.45) and (8.46) as

$$a_3^{L,T} = \left(\frac{16}{3\pi^2}\right)^{1/3} r_s^2 S_3^{L,T}, \tag{8.67}$$

$$b_3^{L,T} = 16\left(\frac{2^{10}}{3\pi^8}\right)^{1/15} r_s \left(\frac{S_3^{L,T}}{c_3^{L,T}}\right)^{4/5}, \tag{8.68}$$

and $c_3^{L,T}$ is given after eqn (8.45). The parameters $\Omega_3^{L,T}$ and $\Gamma_3^{L,T}$ are defined in an implicit manner by solving a transcendental equation; they are related via

$$\Omega_3^{L,T} = 1 - \frac{3\Gamma_3^{L,T}}{2} \,. \tag{8.69}$$

Selected values of $\Gamma_3^{L,T}$ are given in Table 8.1. In 2D, we have

$$\Im f_{\rm xc}^{L,T}(\omega) = -\frac{\widetilde{\omega}}{2n}\left[\frac{a_2^{L,T}}{1+b_2^{L,T}\widetilde{\omega}^2} + \widetilde{\omega}^2 \exp\left(-\frac{(|\widetilde{\omega}| - \Omega_2^{L,T})^2}{\Gamma_2^{L,T}}\right)\right] , \tag{8.70}$$

where $\widetilde{\omega} = \omega(2^7 r_s^2)^{-1/3} E_F^{-1}$, and

$$a_2^{L,T} = \left(\frac{2^5 r_s}{\pi^{3/2}}\right)^{2/3} S_2^{L,T} \,, \tag{8.71}$$

$$b_2^{L,T} = \left(\frac{2^7 r_s^2}{\pi^3}\right)^{2/3} \frac{S_2^{L,T}}{c_2^{L,T}} \,, \tag{8.72}$$

and $c_2^{L,T}$ is given after eqn (8.45). As in the 3D case, the parameters $\Omega_2^{L,T}$ and $\Gamma_2^{L,T}$ follow from a transcendental equation and are related in the same way as in eqn (8.69). Some selected values are given in Table 8.1.

The three parametrizations for the xc kernels are compared in Figs. 8.2 (3D) and 8.3 (2D). All approximations have been constructed so as to satisfy their respective high-frequency limits (8.45), and they all satisfy $\lim_{\omega\to 0} \Im f_{\rm xc}^{L,T}(\omega) = 0$ with a linear slope; however, only the QV parametrization has the correct slope (8.46) at low frequencies.

There are sharp features in the NCT parametrization in 3D (a kink in the imaginary part and a spike in the real part), located at $2\omega_{pl}$ ($= 0.67$ for $r_s = 3$). The physical origin is the large spectral strength of the plasmon mode compared with the single-particle excitations; therefore, the pair-excitation spectrum is dominated by two-plasmon processes in this region. Because of its simple nature as an interpolation formula, the GK parametrization does not have these features. However, the two-plasmon contribution in the NCT parametrization is probably exaggerated owing to the lack of self-consistency in the decoupling procedure (Qian and Vignale, 2002). In the QV parametrization, the plasmon contribution is included as a Gaussian with a finite width, centered at $2\omega_{pl}$ [see eqns (8.66) and (8.66)].

In 2D, the plasmon contributions to $f_{\rm xc}^{L,T}(\omega)$ are much less pronounced because the plasmon dispersion goes to zero as $\sqrt{q}$ in the large-wavelength limit.

Finally, we observe that $\Re f_{\rm xc}^{L,T}(\omega)$ has different zero-frequency limits in the three parametrizations. The GK and HS parametrizations assume that the xc shear modulus vanishes, i.e., $\mu_{\rm xc} = 0$, and thus $\Re f_{\rm xc}^{T}(0) = 0$. The NCT and QV parametrizations, on the other hand, work with a finite $\mu_{\rm xc}$.[4] As we will see later in Chapter 10, this leads to frequency-dependent local approximations for the xc kernel which do not reduce to the ALDA in the static limit. This will have important practical consequences.

[4]Notice that NCT uses values for $\mu_{\rm xc}$ that are different from the ones given in Table 8.1. Thus, the values of $\Re f_{\rm xc}^{T}(0)$ in QV and NCT do not agree. See also footnote 3.

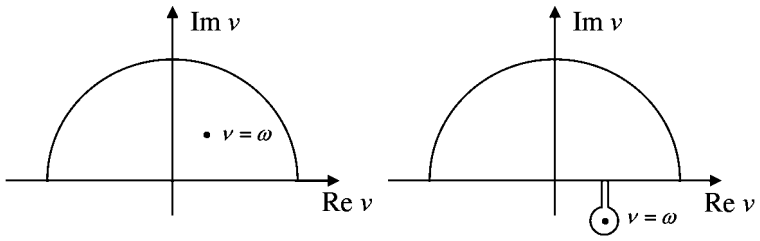

Fig. 8.4 Integration contours for the analytic continuation of $f_{\rm xc}(\omega)$.

8.3.4 Analytic continuation

The xc kernel $f_{\rm xc}(\omega)$ (we drop the superscripts L, T here) is an analytic function of the frequency in the upper half of the complex frequency plane. All the parametrizations that we discussed in Section 8.3.3 were defined for frequencies infinitesimally above the real axis. In practice, however, we are often interested in evaluating $f_{\rm xc}(\omega)$ *below* the real frequency axis: a frequency with a negative imaginary part corresponds to an excitation with a finite lifetime. We shall discuss the physics of such excitations in much more detail when we deal with extended systems in Chapter 12. For the time being let us simply consider the problem of how $f_{\rm xc}(\omega)$ (or rather, a particular approximation to the xc kernel in the form of an explicit parametrization) is to be continued into the lower half of the complex frequency plane (Dobson *et al.*, 1990).

Let ω denote a complex frequency with $\Im\omega > 0$. Then, using Cauchy's theorem and the analyticity of the xc kernel in the upper complex plane, we can write

$$f_{\rm xc}(\omega) - f_{\rm xc}(\infty) = \frac{1}{2\pi i} \oint \frac{f_{\rm xc}(\nu) - f_{\rm xc}(\infty)}{\nu - \omega}\, d\nu \tag{8.73}$$

and

$$0 = \frac{1}{2\pi i} \oint \frac{f_{\rm xc}(\nu) - f_{\rm xc}(\infty)}{\nu - \omega^*}\, d\nu\,, \tag{8.74}$$

where the contour integration is over the infinite semicircle shown in the left part of Fig. 8.4. Combining eqns (8.73) and (8.74), one obtains

$$f_{\rm xc}^{\rm up}(\omega) = f_{\rm xc}(\infty) + \frac{1}{\pi} \int_{-\infty}^{\infty} \frac{\Im f_{\rm xc}(\nu^+)}{\nu - \omega}\, d\nu\,, \qquad \Im\omega > 0\,, \tag{8.75}$$

where $\nu^+ = \nu + i\delta$ (δ is a positive infinitesimal), and $f_{\rm xc}^{\rm up}$ is defined in the upper complex plane.

To continue into the lower half, we deform the contour to include the pole in the lower half-plane (see the right part of Fig. 8.4). This gives an additional contribution from the small circle $\mathcal{C}$ around this pole:

$$\begin{aligned} f_{\rm xc}^{\rm lo}(\omega) &= f_{\rm xc}(\infty) + \frac{1}{\pi} \int_{-\infty}^{\infty} \frac{\Im f_{\rm xc}(\nu^+)}{\nu - \omega}\, d\nu + \frac{1}{\pi} \oint_{\mathcal{C}} \frac{\Im f_{\rm xc}(\nu)}{\nu - \omega}\, d\nu \\ &= f_{\rm xc}^{\rm up}(\omega) + 2i\, \Im f_{\rm xc}(\omega)\,, \qquad \Im\omega < 0\,. \end{aligned} \tag{8.76}$$

In carrying out this procedure, one needs to make sure that the contour does not run over a branch cut of $\Im f_{\rm xc}(\omega)$. Let us check this for the GK parametrization, given in eqn (8.56). In this approximation, the function $\Im f_{\rm xc}^{L,T}(\omega)$ has two poles, sitting on the imaginary axis at $\pm i/(b_3^{L,T})^{1/2}$, with associated branch cuts in the negative direction of the real axis.[5] Therefore, none of the branch cuts of $\Im f_{\rm xc}$ interferes with the analytic continuation as long as we take frequencies with $\Re\omega > 0$.

Exercise 8.1 Prove that the f-sum rule is violated if the xc kernel and the static xc potential don't match.

Exercise 8.2 Work out the spin-dependent ALDA xc kernels $f_{{\rm xc},\uparrow\uparrow}$, $f_{{\rm xc},\uparrow\downarrow}$, $f_{{\rm xc},\downarrow\uparrow}$, $f_{{\rm xc},\downarrow\downarrow}$, starting from eqn (8.33). To make things simpler, do this only for the exchange part. The energy densities of the homogeneous electron liquid are given in Section 2.2.4, i.e., you need to work with the variables n, ζ instead of $n_\uparrow, n_\downarrow$.

Exercise 8.3 Show that the parameters a_3, a_2, b_3, b_2 of the GK and HS parametrizations (8.56) and (8.59) are determined by the high-frequency limit (8.45) and the Kramers–Kronig relation (8.39) with $\omega = 0$ and $q \to 0$.

Exercise 8.4 Show that the real part corresponding to the 2D HS parametrization (8.59) of $\Im f_{\rm xc}^{L}(0,\omega)$ is given by

$$\Re f_{\rm xc}^{L}(0,\omega) = f_{\rm xc}^{L}(0,\infty) + \frac{a_2 b_2}{b_2^2 + \omega^2}\,. \tag{8.77}$$

Exercise 8.5 Write a computer program to calculate the real part of the homogeneous xc kernel, $\Re f_{\rm xc}^{L,T}$, from a given parametrization of $\Im f_{\rm xc}^{L,T}$ by numerically evaluating the Kramers–Kronig relation (8.39). Reproduce the plots shown in Figs. 8.2 and 8.3 and also explore other values of r_s. You can limit yourself to the GK and HS parametrizations, since they are the easiest to implement.

To deal with the singularity in the principal-value integral in eqn (8.39), you can introduce a small imaginary part into the denominator, $\omega' \to \omega' + i\delta$, so that

$$\Re f_{\rm xc}^{L,T}(q,\omega) = f_{\rm xc}^{L,T}(q,\infty) + \lim_{\eta\to 0}\int_{-\infty}^{\infty}\frac{d\omega'}{\pi}\frac{(\omega'-\omega)\Im f_{\rm xc}^{L,T}(q,\omega')}{(\omega'-\omega)^2+\eta^2}\,. \tag{8.78}$$

With a small but finite η, this can be easily evaluated using any standard numerical integration routine, such as Gaussian quadrature.

Exercise 8.6 Verify that $f_{\rm xc}^{\rm lo}$ [eqn (8.76)] is indeed the analytic continuation of $f_{\rm xc}^{\rm up}$ [eqn (8.75)] by showing that the two functions become identical on the real axis. Hint: try to show that

$$\lim_{\delta\to 0^+}\Big\{f_{\rm xc}^{\rm up}(\omega+i\delta) - f_{\rm xc}^{\rm lo}(\omega - i\delta)\Big\} = 0\,.$$

[5] Note that this does not contradict the statement that the xc kernel is analytic in the upper frequency plane. The real and imaginary parts can be nonanalytic by themselves; together, the analyticity of $f_{\rm xc} = \Re f_{\rm xc} + i\Im f_{\rm xc}$ is enforced through the Kramers–Kronig relations.

9

Applications to atomic and molecular systems

Today, the vast majority of applications of TDDFT are in the linear-response regime, with the general objective of describing excited-state properties of a wide variety of systems. This has made a large impact in the area of theoretical chemistry, where TDDFT methods are unrivaled when it comes to treating medium-sized and large molecules. In the preceding chapters, we have laid the theoretical foundations for the TDDFT approach to calculating excitation energies. In this chapter, we will give evidence for the various successes of the method and discuss the underlying reasons; but we will also point out current challenges and problems.

It is appropriate to begin this chapter by mentioning the work of Zangwill and Soven (1980), who were the first to carry out TDDFT calculations of photoabsorption in rare-gas atoms using the ALDA. Since then, linear-response TDDFT has come a long way and its use has now become routine in the calculation of excited-state properties in physics, (bio)chemistry, and materials science, with a rapidly growing number of applications. The chronology of the development of linear-response TDDFT from its humble beginnings to today has been summarized in a recent review by Casida (2009).

The calculation of excitation energies with TDDFT has now become a standard ingredient of many widely used computer codes (see Appendix O). For many practical purposes, these codes serve as a "black box" requiring relatively little formal training in (TD)DFT. The computational tools of electronic-structure theory and quantum chemistry have thus become accessible to a broad scientific community. However, a healthy dose of caution is required: one needs to be aware that there are some tasks which TDDFT handles very well (with the existing approximate xc functionals), and others where it doesn't seem to work at all. We will try to provide sufficient information in this chapter to help prospective and current TDDFT users to make an informed judgment. The following topics will be covered:

- an illustration of how the Casida equation (7.134) and its approximations (TDA, SMA, and SPA) correct the bare Kohn–Sham excitation spectrum for simple systems;
- an assessment of the performance of various approximate xc functionals;
- a discussion of some of the practical and computational aspects;
- tough cases for TDDFT, such as multiple and charge-transfer excitations;
- alternative methods to obtain excitation energies and spectra, such as real-time propagation, and the Sternheimer equation approach.

In this chapter, we will only consider applications to excitations in finite atomic and molecular systems. Electron dynamics in extended systems will be discussed in Chapter 12. Furthermore, we will treat the nuclei as fixed, and will worry about coupled electron–nuclear dynamics later, in Chapter 17.

A word about notation: when discussing linear-response TDDFT calculations, we need to specify which approximation has been used for the xc kernel, and also for the ground-state xc potential. For instance, by "ALDA/LDA" we will indicate that we have used the ALDA for the xc kernel and the LDA for the ground-state calculation.

9.1 Excitation energies of small systems: basic trends and features

As we explained in Chapter 7, calculating excitation energies is a two-step process: first we need to do a ground-state DFT calculation to get the Kohn–Sham orbitals and energy eigenvalues for all occupied and unoccupied states, and then we need to "shift" the Kohn–Sham excitation spectrum towards the true spectrum using TDDFT.[1]

9.1.1 The exact Kohn–Sham spectrum

The first question that naturally arises is this: how good (or bad) are the Kohn–Sham excitation energies really? In our overview of DFT in Chapter 2, we emphasized that the Kohn–Sham eigenvalues ε_j have no true physical meaning, except for that of the highest occupied orbital, whose absolute value equals the ionization energy of the system. In other words, in general, we have

$$\omega_{\rm KS} = \varepsilon_a - \varepsilon_i \;\neq\; \Omega_j = E_j - E_0 \,. \tag{9.1}$$

But how large are the deviations of the *exact* Kohn–Sham excitations, $\omega_{\rm KS}^{\rm exact}$, from the true excitations Ω_j? Savin *et al.* (1998) studied this question for small atomic systems where exact Kohn–Sham solutions could be obtained by inversion (see Appendix E) from numerically quasi-exact ground-state densities that were calculated using quantum Monte Carlo methods.

Table 9.1 shows results for the lowest transitions of the Be atom, comparing experimental results with exact Kohn–Sham excitation energies.[2] The ground state of Be has a closed shell, so the single-electron Kohn–Sham energies do not resolve the multiplet splitting. Looking at the data, we find a remarkable trend: the $\omega_{\rm KS}^{\rm exact}$ always fall right in between the experimental singlet and triplet excitation energies. For the low-lying excitations, where the singlet–triplet splitting is large, this produces sizable errors. The agreement becomes much better for higher excitations, and the Kohn–Sham excitations then merge with the exact Rydberg series of the atom.[3]

The results shown here for the Be atom are quite generic and have been observed for other systems as well. We conclude from this that the *exact* Kohn–Sham energy

[1] This also implies that additional excitations, not present in the Kohn–Sham spectrum, must be produced. We will come back to this when we discuss double excitations in Section 9.3.

[2] A more rigorous comparison with experiment would require taking into account the finite nuclear mass and relativistic effects. Fortunately, these lead to only very minor corrections for light atoms.

[3] The "quantum defect" is a very accurate measure for assessing the quality of high-lying and continuum states. It is found that the exact Kohn–Sham quantum defects fall between the exact singlet and triplet quantum defects (van Faassen and Burke, 2006, 2009).

Table 9.1 Excitation energies of the Be atom (in a.u.), comparing exact Kohn–Sham excitation energies with experiment. From Savin *et al.* (1998).

Transition	Final state	Experiment	$\omega_{\rm KS}^{\rm exact}$
$2s \to 2p$	1^3P	0.100153	0.1327
	1^1P	0.193941	
$2s \to 3s$	2^3S	0.237304	0.2444
	2^1S	0.249127	
$2s \to 3p$	2^3P	0.267877	0.2694
	2^1P	0.274233	
$2s \to 3d$	1^3D	0.282744	0.2833
	1^1D	0.293556	
$2s \to 4s$	3^3S	0.293921	0.2959
	3^1S	0.297279	
$2s \to 4p$	3^3P	0.300487	0.3046
	3^1P	0.306314	
$2s \to 4d$	2^3D	0.309577	0.3098
	2^1D	0.313390	
$2s \to 5s$	4^3S	0.314429	0.3153
	4^1S	0.315855	

eigenvalues are not that meaningless after all! In fact, they constitute an excellent approximation to the exact excitation energies, in the sense that they form an "average" over a singlet–triplet pair (for closed-shell systems).

Several formal arguments can be made why this shouldn't come as a complete surprise. Since the exact Kohn–Sham xc potential has the correct $-1/r$ asymptotic behavior, it is to be expected that the high-lying excitations should be well described. This was demonstrated in an impressive manner by Al-Sharif *et al.* (1998) for the Rydberg states of the Ne atom. Beyond that, Savin *et al.* (1998) showed that the Kohn–Sham orbitals and the neutral quasiparticle amplitudes—a concept of many-body physics related to excitations of an interacting N-electron system—agree to within terms of order r^{-4}. Görling (1996) developed a DFT perturbation theory for excited states in which the Kohn–Sham excitation energies emerge as the zero-order approximation in a series expansion in terms of the electron–electron interaction.

In general, of course, we do not have the luxury of knowing the exact Kohn–Sham eigenvalues of a system, apart from in a few simple cases. As we will see below, the popular semilocal xc functionals usually lead to quite poor approximations for $\omega_{\rm KS}$.

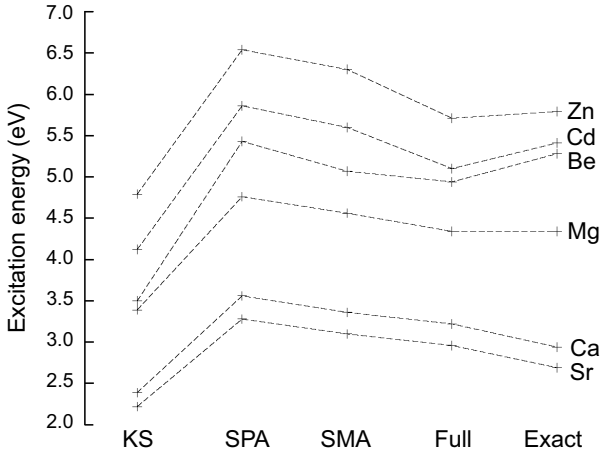

Fig. 9.1 Lowest singlet excitation energies for various closed-shell atoms (Vasiliev *et al.*, 1999), calculated with the LDA/ALDA, using various TDDFT schemes.

9.1.2 Results for closed-shell atoms and N_2

Let us now consider some TDDFT calculations of the excitation energies of simple, closed-shell systems. This will serve as a first illustration of the following questions:

1. How well does the ALDA/LDA perform?
2. How important is the asymptotic behavior of the ground-state xc potential?
3. How good are approximate schemes such as the SMA and SPA?

Figure 9.1 shows the lowest singlet $^1S \rightarrow {}^1P$ excitation energies of various closed-shell atoms (Vasiliev *et al.*, 1999), comparing the bare LDA Kohn–Sham excitations, TDDFT excitation energies, and experimental values. The TDDFT excitation energies were calculated within the ALDA, using the full Casida approach [eqn (7.134)], the SMA [eqn (7.157)], and the SPA [eqn (7.159)].

The bare LDA Kohn–Sham excitations are found to be significantly too low, with errors ranging from around 0.5 eV (Ca and Sr) to 1.78 eV (Be). This is a very typical observation, and is related to the wrong asymptotic behavior of the LDA (and most other semilocal xc potentials); we will talk more about this shortly.

Figure 9.1 then shows how the Kohn–Sham excitations are corrected by TDDFT: using the full Casida formalism gives much better agreement with experiment, with a maximum deviation of not more than around 0.3 eV. The simplified TDDFT approaches are seen to somewhat overcorrect: the SMA gives excitation energies that are typically around 0.4 to 0.5 eV too high, and the SPA overshoots a little more. But the bottom line is that even the simplest TDDFT correction to the bare Kohn–Sham excitation energies gives a significant improvement, often reducing the error by half.

Let us carry the analysis of atomic excitation energies a bit further, taking advantage of the fact that for these simple systems one can compare the above results with exact theoretical results and very precise spectroscopic data (Gross *et al.*, 1996; Petersilka *et al.*, 1998, 2000; Vasiliev and Martin, 2004). One of the main questions is

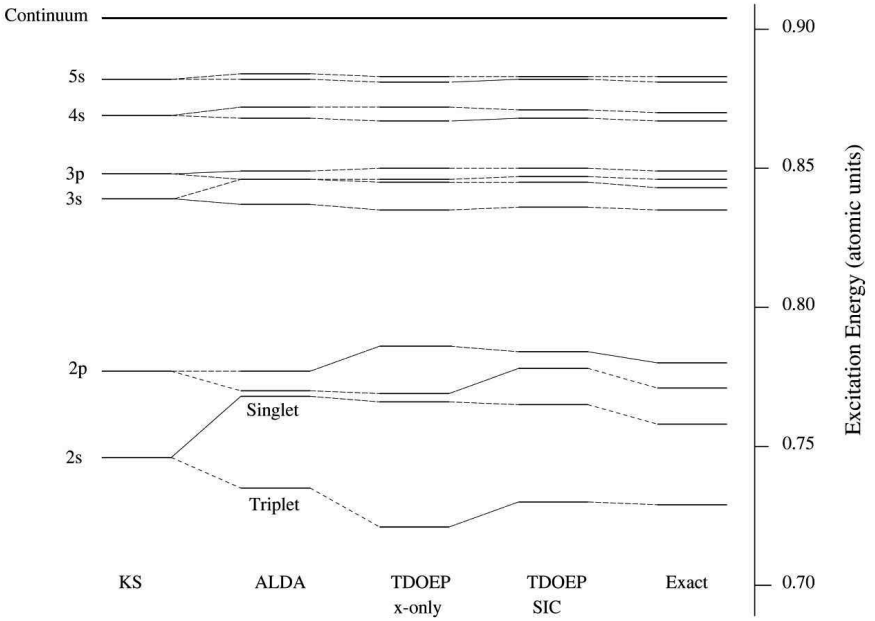

Fig. 9.2 Excitation energies of the He atom: Kohn–Sham excitations, TDDFT corrections, and exact results. [Reproduced with permission from John Wiley & Sons, Inc. from Petersilka *et al.* (2000), ©2000.]

the following: given that we have to rely on approximations to both the ground-state xc potential and the TDDFT xc kernel, which one is more important, and where can we get away with simpler approximations? It turns out that it is usually the approximation to $v_{\rm xc}$ which has the strongest influence on the quality of the results, but we will sharpen this statement a bit more after looking at some results.

Figure 9.2 shows singlet and triplet excitation energies for the He atom (Petersilka *et al.*, 2000), starting from the exact ground-state DFT solution and using various approximate TDDFT xc kernels: the ALDA, TDOEP x-only, and TDOEP SIC functionals (these functionals will be explained in Chapter 11). Since we are already starting from the exact bare Kohn–Sham excitations, we can focus on how well the singlet–triplet splitting is reproduced by TDDFT.

The first observation is that the singlet excitation energy is always above the bare Kohn–Sham excitation, whereas the triplet excitation is always below, for all approximate xc kernels. This can easily be understood in the light of the discussion in Section 7.6; see eqns (7.160) and (7.161). For Ω_+ (the singlet energy), the Hartree part gives a large positive correction, whereas $f_{\rm xc}$ produces a smaller negative contribution. For Ω_-, there is no Hartree contribution, and the only effect comes from $g_{\rm xc}$, which is negative. Strictly speaking, this argument is valid if the SPA is used for calculating the excitation energies; however, it carries over to the full calculation since the SPA gives the dominating contribution in this case (Petersilka *et al.*, 2000).

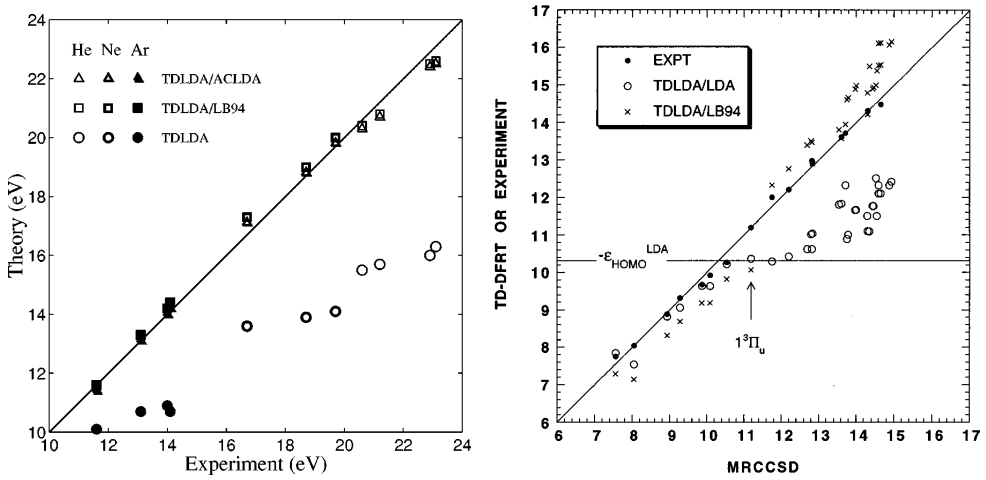

Fig. 9.3 Left: lowest singlet excitation energies of rare-gas atoms calculated with TDDFT in the ALDA. [Reproduced with permission from APS from Vasiliev and Martin (2004), ©2004.] Right: the first 35 vertical excitation energies of N_2 (in eV), compared with multireference coupled-cluster singles and doubles (MRCCSD) calculations. [Reproduced with permission from AIP from Casida *et al.* (1998*b*), ©1998.]

The three different approximate xc kernels which are compared in Fig. 9.2 give rather similar results, and are all in very good agreement with experiment. The x-only kernel somewhat exaggerates the singlet–triplet splitting, which points to the importance of correlation effects.

The lowest few singlet excitation energies of the rare-gas atoms He, Ne, and Ar, calculated with TDDFT in the ALDA, are compared with experimental results in the left panel of Fig. 9.3 (Vasiliev and Martin, 2004). The ground-state calculations were done using the LDA and two xc functionals which produce the correct $-1/r$ long-range behavior of the xc potential, LB94 [see eqn (2.96)] and ACLDA (van Leeuwen and Baerends, 1994; Casida and Salahub, 2000). It is quite striking to observe how much better the agreement becomes if the asymptotically correct ground-state xc functionals are used.

The right-hand panel of Fig. 9.3 shows the first 35 vertical excitation energies (not counting degeneracies) of the N_2 molecule (Casida *et al.*, 1998*b*). Here, the TDDFT calculations are compared with high-level theoretical results obtained using a multireference coupled-cluster singles and doubles (CCSD) approach (Ben-Shlomo and Kaldor, 1990); a few experimental values are also indicated. Looking at the results, a clear trend emerges: the ALDA/LDA calculations agree quite well with the quasi-exact benchmark results as long as the excitation energies are not too high. In fact, one observes that the energy of the highest occupied LDA orbital, $\varepsilon_{\rm HOMO}^{\rm LDA}$, seems to set a threshold: the ALDA/LDA excitation energies above this threshold are significantly underestimated. By contrast, the ALDA/LB94 excitation energies are more consistent, and much better for the higher transitions.

9.1.3 Discussion

From the few simple examples we have discussed above, several trends emerge, and we can draw a number of preliminary conclusions.

- TDDFT, even using simple xc functionals, gives a significant improvement relative to the bare Kohn–Sham excitation spectra of finite systems. Overall, the ground-state xc potential appears to be the most important factor which determines the quality of the TDDFT excitation energies.
- Even the most basic ALDA/LDA calculations can give good results, as long as one limits oneself to low-lying transitions.[4] The reason is that the LDA, as well as many other (semi)local functionals, has the wrong asymptotic behavior, and thus yields outer levels that are too weakly bound or not bound at all. As long as the transitions are below the HOMO level and do not involve any major contributions from virtual transitions close to or above that threshold, TDDFT results with local or semilocal approximations are fine. If higher excitations are desired, one should use an asymptotically corrected xc functional such as the LB94, LDA–SIC, or x-only KLI functional (see Chapter 11). Hybrid functionals provide a partial cure, since their asymptotic behavior is like $-a/r$, where a is a constant.
- The choice of the xc kernel seems relatively less important than the choice of $v_{\rm xc}^0$, but plays a more important role when "first-order" effects cancel. This happens, for instance, when one calculates the singlet–triplet splitting associated with a given transition. A proper treatment of correlation then becomes more important.
- Simplifications of the full Casida matrix equation are less accurate, but can still be useful. The SPA, in general, gives the dominant correction to the bare Kohn–Sham excitation energies and can be used to get a reasonable estimate of the full TDDFT excitation energies. The TDA can often be used as a simple cure for some unphysical effects caused by approximate xc kernels, such as triplet instabilities in open-shell molecules (see below).

9.2 Molecular excited-state properties with TDDFT: an overview

The quality of TDDFT results depends strongly on the xc functionals used to calculate the ground state (including optimization of the molecular geometry) and the excitation energies.[5] This obviously leads to the dilemma of which functional to choose in order to get the most accurate results for the property of interest. A straightforward recommendation is not always possible, since the performance of different xc functionals can vary between different systems; what works for a particular type of electronic transition in one particular molecule may not work so well elsewhere.

But this doesn't mean at all that TDDFT is completely unsystematic and relies only on guesswork. Just as for static DFT, extensive tests of different xc functionals

[4] However, there exists a clever way to calculate Rydberg excitations and their oscillator strengths quite accurately with the ALDA/LDA. The trick is to use quantum defect theory, exploiting the fact that the overall shape of the LDA xc potential is quite similar to the exact xc potential, and runs almost parallel to it in the valence region (Wasserman *et al.*, 2003; Wasserman and Burke, 2005).

[5] There is, of course, also a dependence on the basis set used to carry out the calculation. A meaningful comparison between different xc functionals must be carried out with the same basis set.

Table 9.2 Overview of wave-function-based methods suitable for calculating excited states. The formal scaling of the computational cost with the number of electrons N is indicated for each method. In state-of-the-art numerical implementations, a somewhat better scaling can often be achieved. In multireference approaches, the computational cost is determined by the size of the active space, which is strongly problem-dependent. By comparison, TDDFT scales as N^2 to N^3, depending on the implementation.

Method	Single-reference (SR)	Multireference (MR)
SCF (self-consistent field)	TDHF [N^3]	CASSCF[a]
CI (configuration interaction)	CIS [N^3], CISD [N^6] CISDT [N^8], full CI [e^N]	MR-CISD, CAS-CI
CC (coupled cluster)	CCS [N^4], CC2 [N^5], CCSD [N^6], CC3 [N^7], CCSDT [N^8]	MR-CC
PT (perturbation theory)		CASPT2[b]

[a] Complete-active-space self-consistent field.
[b] Complete-active-space second-order perturbation theory.

have been performed in the literature, and a wealth of data has been collected over the past years. Based on comparisons with available experimental data or high-accuracy benchmark results, several clear trends have begun to emerge. We now know pretty well where standard xc functionals can be expected to work, and at what level of accuracy; on the other hand, we also know where difficulties can arise, and there are intense efforts under way to find cures for these problems.

9.2.1 Quantum chemical methods and their computational cost

The vast majority of applications of TDDFT in chemistry are concerned with low-lying excitation energies in medium-size to large molecules, both organic and inorganic. Of course, what is considered large today may be small by tomorrow's standards, owing to the continuing rapid increase in our computational capabilities. At the present time, high-accuracy wave-function-based approaches such as CC3 are limited to systems with about 15 atoms; with other high-end approaches such as CC2 or CASPT2 one can go to about 2–3 times that size, but 50 atoms seems to be the current limit (Grimme, 2004; Dreuw and Head-Gordon, 2005; Jacquemin *et al.*, 2009). TDDFT, by contrast, delivers an excellent compromise between computational efficiency and accuracy, and allows the treatment of molecules containing hundreds of atoms.

Table 9.2 gives a schematic overview of the most common ab initio wave-function-based methods in theoretical chemistry that can be used to calculate excitation ener-

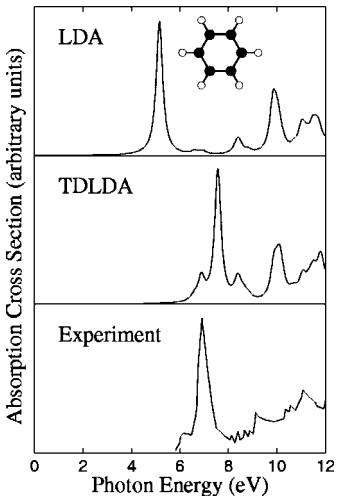

Fig. 9.4 Calculated and experimental optical spectra for benzene (the theoretical spectra are broadened by 0.1 eV). [Reproduced with permission from APS from Vasiliev *et al.* (2002), ©2009.]

gies. A more detailed review of the various quantum chemical approaches is beyond the scope of this book, but can be found in more specialized textbooks (Szabo and Ostlund, 1996; Helgaker *et al.*, 2000) or review articles (Grimme, 2004; Dreuw and Head-Gordon, 2005; Friesner, 2005).

In general, we distinguish between single-reference and multireference methods. The former can be treated essentially as a "black box," whereas the latter require much more user intervention based on chemical insight. In multireference methods, one typically chooses an active space, in which a full variational optimization is performed; in practice, this means that one works with linear combinations of Slater determinants containing excited-state configurations (single, double, etc.), and the single-particle orbitals and the expansion coefficients need to be optimized simultaneously, which makes these methods very time-consuming. The computational cost increases exponentially with the size of this active space, which in turn is strongly problem-dependent. The CASPT2 method is viewed by many as the de facto standard in quantum chemistry for calculating electronic spectra, and is often used to produce benchmark results for small molecules. On the other hand, the computational cost of the single-reference methods scales as some power of the number of electrons N.

9.2.2 Vertical excitation energies

Benzene as a test case. As a first example, let us consider the benzene molecule. Figure 9.4 shows a comparison of experimental and theoretical spectra calculated using the LDA Kohn–Sham excitations and the ALDA/LDA (Vasiliev *et al.*, 2002). At first glance, the agreement seems excellent, but let us take a closer look at the individual excitations. Table 9.3 shows eight low-lying singlet and triplet excitation

Table 9.3 Low-lying excitation energies (in eV) of benzene (C_6H_6) calculated with TDDFT using various xc functionals with the basis set 6-31++G(3df,3pd), and geometry optimized using the respective functionals with the same basis (Tao *et al.*, 2008*b*). CASPT2, TDHF, and experimental results from Packer *et al.* (1996). The m.a.e. for TDHF excludes the lowest ($^3B_{1u}$) triplet transition, which is unstable.

Symmetry	LSDA	PBE	TPSS	PBE0	B3LYP	CASPT2	TDHF	Exp.
$^3B_{1u}$	4.47	3.98	3.84	3.68	3.84	3.89	—	3.94
$^3E_{1u}$	4.82	4.61	4.67	4.75	4.72	4.49	4.70	4.76
$^1B_{2u}$	5.33	5.22	5.32	5.52	5.41	4.84	5.82	4.90
$^3B_{2u}$	5.05	4.89	4.98	5.12	5.07	5.49	5.57	5.60
$^1B_{1u}$	6.07	5.94	6.00	6.18	6.05	6.30	5.88	6.20
$^1E_{1g}$	6.12	5.89	5.99	6.38	6.11	6.38	6.54	6.33
$^1A_{2u}$	6.70	6.43	6.50	6.90	6.62	6.86	6.94	6.93
$^1E_{2u}$	6.71	6.44	6.50	6.95	6.65	6.91	7.11	6.95
m.a.e.	0.30	0.37	0.33	0.18	0.27	0.09	0.26*	

energies of the benzene molecule, calculated with various xc functionals (Tao *et al.*, 2008*b*). As an overall measure of the accuracy of the calculations, the mean absolute error (m.a.e.) was also calculated for each functional. Based on this measure, the nonhybrid xc functionals (LSD, PBE, and TPSS) perform at about the same level, with an m.a.e. of 0.3-0.4 eV. The hybrid functionals (PBE0 and B3LYP) used in this study perform somewhat better, with an m.a.e. ranging from 0.18 to 0.27 eV. As we will see in later examples, this behavior is quite typical.

Not unexpectedly, the high-level wave-function-based CASPT2 calculations give the best results, outperforming the best TDDFT calculations by a factor of two. TDHF, on the other hand, performs very inconsistently: the lowest ($^3B_{1u}$) triplet excitation is unstable (i.e., it lies below the HOMO), but the other triplet excitations are in fortuitous agreement with experiment. The lowest TDHF singlet excitation is too high by 1 eV. We should also mention that the CIS method [which is equivalent to the TDA for TDHF; see eqn (7.168)] performs very poorly for benzene, giving excitation energies that are typically too high by an amount on the order of 1 eV (Stratmann *et al.*, 1998).

Taking a closer look at individual excitations, one sees that the nonhybrid functionals typically underestimate the excitation energies; hybrid mixing leads to systematically higher excitation energies. The improvement is more pronounced for the singlet excitations than for the triplet excitations. The $^1B_{2u}$ state is predicted to be systematically too high by all xc functionals, hybrid or nonhybrid.

The trends that we observe for benzene also show up for larger polycyclic aromatic hydrocarbons (PAHs). An detailed study of naphthalene can be found in the review by Elliott *et al.* (2009), and a systematic study of the lowest excitation energies of many different PAHs was performed by Parac and Grimme (2003).

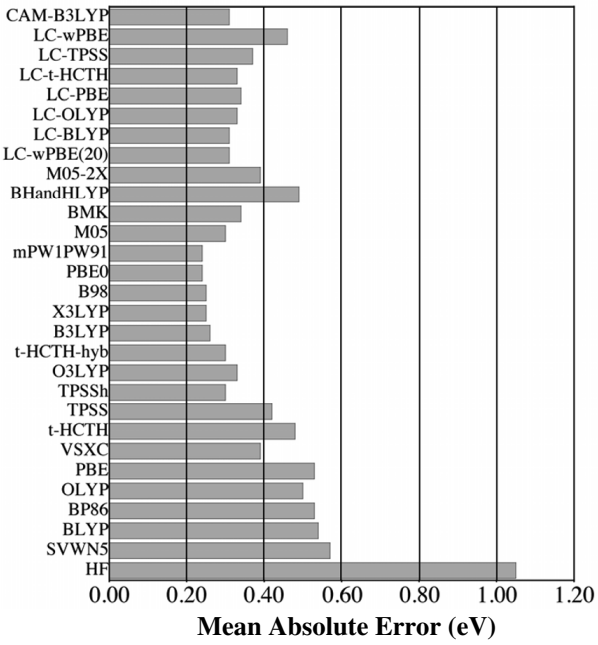

Fig. 9.5 Mean absolute error for the lowest vertical excitation energies of a test set of 28 medium-sized organic molecules (103 excited states), compared with theoretical benchmarks. [Reproduced with permission from ACS from Jacquemin *et al.* (2009), ©2009.]

Extended test sets. A statistically meaningful analysis of the performance of xc functionals can be carried out using test sets—large sets of molecules (often hundreds), including a variety of organic and inorganic species. The reference data is obtained from experiment or from very accurate wave-function-based theories; in the latter case, only small molecules can be included. On the other hand, experimental spectroscopic data for molecules often includes environmental effects such as the effects of temperature, pressure, or solvents. This can make a comparison with theory quite challenging.

Figure 9.5 shows the m.a.e. for 28 xc functionals and for the HF theory, obtained by calculating 103 low-lying vertical excitation energies for a test set of 28 medium-sized organic molecules (Jacquemin *et al.*, 2009), compared against accurate theoretical benchmarks (Schreiber *et al.*, 2008; Silva-Junior *et al.*, 2008). The Kohn–Sham ground states were obtained with the same xc functionals that were used, in the adiabatic approximation, for the TDDFT calculations. No geometry optimization was performed; identical molecular geometries were used for each xc functional.

We see immediately that TDHF gives very large errors (over 1 eV), almost always overestimating the transition energies; any TDDFT calculation reduces the error by at least a half. Among the xc functionals, we can distinguish between pure density functionals (LDA and GGA), meta-GGAs, hybrid GGAs (containing a portion of the exact exchange), and long-range-corrected hybrids (see Section 2.3). The LDA and

GGAs all give an m.a.e. of order 0.5 eV. Meta-GGAs (VSXC and TPSS) give better agreement (about 0.4 eV).

For the test set considered here, the best choice is clearly given by the hybrid GGAs (B3LYP, X3LYP, B98, mPW1PW91, and PBE0), containing between 22% and 25% of the exact exchange.[6] In this case, the m.a.e. is reduced to less than 0.25 eV.

The long-range-corrected hybrids give a slightly higher error, owing to a general overestimation of the transition energies. This is mainly due to the choice of the test set, in which charge-transfer excitations are not significantly represented. As we will see in Section 9.4, the advantage of long-range-corrected hybrids emerges for such excitations in larger molecules.

Similar conclusions were reached for a much larger test set of 614 excited singlet states (Jacquemin *et al.*, 2009), as well as for a large test set of organic indigoid dyes (Perpète and Jacquemin, 2009); it also turns out that most hybrid functionals perform a little less well for triplet states (Jacquemin *et al.*, 2010).

There are numerous applications and comparative studies of TDDFT for various classes of molecular systems—far more than we can list here. Some representatives are studies of organic dyes (Guillaumont and Nakamura, 1976; Goerigk and Grimme, 2010; Send *et al.*, 2011), conjugated oligomers and polymers (Tao *et al.*, 2008*a*, 2009), transition metal complexes (Rosa *et al.*, 2004; Neese, 2006; Li *et al.*, 2009), and biomolecules (Castro *et al.*, 2009*a*).

The examples and applications that we have discussed here were all for closed-shell molecules. Open-shell molecules are no less important—they play a role in many photochemical and spectroscopic processes. However, the electronic structure and excitations of open-shell systems are in general much more complicated than for closed-shell systems, and pose new challenges for DFT and TDDFT (Casida *et al.*, 2006). For instance, there are situations in which the triplet excitation energy comes out below the ground-state energy (using approximate xc functionals); this is known as the *triplet instability*, and corresponds to an imaginary solution of the Casida equation. In such cases, the TDA can be much better behaved (Casida *et al.*, 2000). Another possibility is to treat open-shell molecules by using generalized (TD)DFT approaches for systems with noncollinear spins ("spin-flip TDDFT"). We will not discuss open-shell systems any further here, and refer readers to Appendix G for more details on noncollinear-spin TDDFT.

9.2.3 Excited-state forces and geometries

Static DFT is concerned with the ground-state electronic structure of materials. An important aspect is determining the associated geometries, such as bond lengths and bond angles in molecules, and lattice parameters in solids. In addition, vibrational frequencies are of interest; they are obtained by perturbing the system around the ground-state configuration (Baroni *et al.*, 2001).

To obtain the analogous quantities for excited states requires calculating the derivatives of excited-state energies with respect to the external perturbations. For instance, forces and force constants are obtained as the first and second derivatives, respectively,

[6] This can be considered good news, since the same admixture of exact exchange also leads to the best geometries in ground-state calculations.

Table 9.4 Various excited-state properties of selected diatomic molecules, calculated using various xc functionals (Furche and Ahlrichs, 2002).

System	State	LSDA	BLYP	BP86	PBE	PBE0	B3LYP	Exp.
			Adiabatic excitation energies (eV)					
BH	$1\,^1\Pi$	2.49	2.71	2.72	2.66	2.64	2.68	2.87
NH	$1\,^3\Pi$	3.63	3.91	4.02	3.98	3.96	3.87	3.70
CO	$1\,^3\Pi$	5.73	5.49	5.40	5.43	5.49	5.59	6.04
CO	$1\,^1\Pi$	7.84	7.79	7.83	7.82	8.06	8.00	8.07
NO	$1\,^2\Sigma^+$	—	5.50	5.75	5.45	6.22	6.09	5.45
			Equilibrium bond lengths (pm)					
BH	$1\,^1\Pi$	123	121	122	123	121	121	122
NH	$1\,^3\Pi$	106	106	105	105	104	104	104
CO	$1\,^3\Pi$	120	121	121	121	120	120	121
CO	$1\,^1\Pi$	122	124	124	123	122	123	124
NO	$1\,^2\Sigma^+$	—	107	107	107	105	105	106
			Dipole moments (D)					
BH	$1\,^1\Pi$	0.51	0.44	0.52	0.49	0.49	0.49	0.58
NH	$1\,^3\Pi$	1.37	1.31	1.29	1.28	1.27	1.30	1.31
CO	$1\,^3\Pi$	1.24	1.36	1.34	1.30	1.58	1.57	1.37
CO	$1\,^1\Pi$	0.29	0.26	0.25	0.23	0.50	0.49	0.34
NO	$1\,^2\Sigma^+$	—	1.21	1.71	1.54	1.48	1.17	1.10
			Vibrational frequencies (cm^{-1})					
BH	$1\,^1\Pi$	2281	2306	2263	2267	2389	2406	2251
NH	$1\,^3\Pi$	3015	2937	3000	3015	3219	3123	3231
CO	$1\,^3\Pi$	1831	1729	1762	1769	1836	1792	1743
CO	$1\,^1\Pi$	1611	1474	1513	1524	1591	1543	1518
NO	$1\,^2\Sigma^+$	—	2393	2397	2443	2574	2552	2374

of the molecular energy with respect to the nuclear coordinates; dipole moments are calculated by taking the first derivative with respect to a static electric field. All of these excited-state properties can, in principle, be obtained exactly with TDDFT, using the matrix elements and eigenvectors of the Casida equation as input. However, we will refrain from going into any of the technical details.

Several computationally efficient implementations for calculating the derivatives of excited-state energies with TDDFT have been put forward in the literature, using various types of basis sets (Van Caillie and Amos, 1999, 2000*a*; Furche and Ahlrichs, 2002; Hutter, 2003; Doltsinis and Kosov, 2005; Rappoport and Furche, 2005; Scalmani *et al.*, 2006; Sitt *et al.*, 2007; Liu and Liang, 2011). There are also TDDFT methodolo-

gies for vibrational Raman spectra (van Gisbergen *et al.*, 1996; Van Caillie and Amos, 2000*b*; Quinet *et al.*, 2005; Rappoport and Furche, 2007).

Let us now look at some examples. Table 9.4 shows various excited-state properties of some heteroatomic diatomic molecules: adiabatic excitation energies, bond lengths, dipole moments, and vibrational frequencies (Furche and Ahlrichs, 2002). Notice that the adiabatic excitation energies are different from the vertical excitation energies: the former are with respect to the relaxed excited-state configuration, whereas the latter assume the same configuration for the ground and excited states.

For all xc functionals considered, the relative errors in the excited-state structures, dipole moments, and vibrational frequencies are smaller than the errors in the excitation energies. For the examples of Table 9.4, we find that B3LYP typically gives less than 1% error in the bond lengths. Similarly, dipole moments and vibrational frequencies are typically correct to within a few percent. In general, the degree of accuracy for excited-state forces and geometries is basically the same as that which is achievable with the same functionals for the ground state.

9.3 Double excitations

9.3.1 What do we mean by single and multiple excitations?

Let us begin this section by asking the following question: is there a well-defined meaning to the concept of "single," "double," or other "multiple" excitations in an interacting N-electron system? The answer, it turns out, depends on the situation and requires a bit of explanation.

Noninteracting systems. The situation is clear for noninteracting systems, where the wave function is a single Slater determinant and one can use a single-particle picture in an unambiguous way for describing transitions. As shown on the right-hand side of Fig. 9.6, each excitation is characterized by a transition of one or more electrons from occupied to empty single-particle levels, while the other electrons stay where they are. In the ground state, all single-particle levels are filled up to the HOMO, with energy ε_H. A single excitation promotes one electron to an empty level in the LUMO or higher. A double excitation moves two electrons to empty levels, and so on. Figure 9.6 gives a few examples of low-lying excitations.

Thus, the concept of single and multiple excitations is well defined for noninteracting electrons: each excitation can be uniquely categorized through the configuration of the single-particle states that make up the Slater determinant of the final state. Notice that this holds both for truly noninteracting physical systems and for "effective" noninteracting systems such as Kohn–Sham or Hartree–Fock systems as long as the electronic states are single Slater determinants.[7]

In the presence of interaction, things are a bit more complicated, and we will see that the concept of single and double excitations becomes somewhat fuzzy.

[7]Notice that, in this way, one obtains the excitation energies as differences between single-particle eigenvalues, which in general is incorrect; see Section 9.1.1 for the Kohn–Sham case. The point being made here is about the assignment, namely, the noninteracting single-particle excitation spectrum is easily classified into single, double, and other excitations.

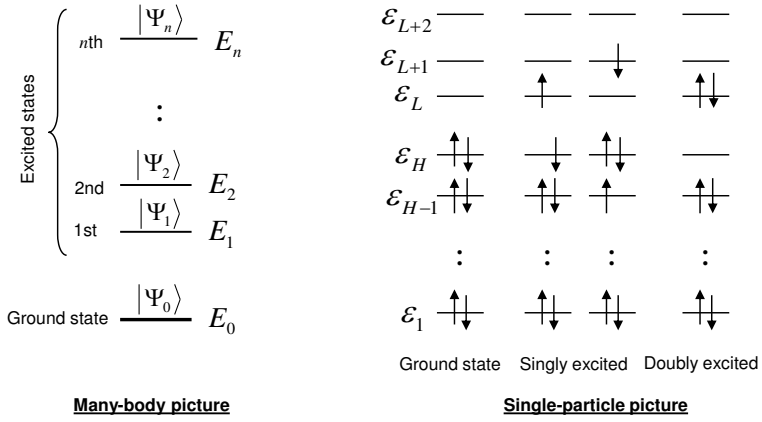

Fig. 9.6 Schematic illustration of the electronic ground and excited states of an N-electron system, in the many-body picture and in the single-particle orbital picture (where two examples of low-lying singly excited states are given, and one of a doubly excited state).

Interacting systems. The electronic ground and excited states of an interacting many-body system are defined as solutions of the static many-body Schrödinger equation $\hat{H}_0\Psi_n = E_n\Psi_n$. The excitation energies of the system are rigorously obtained as differences between the energy eigenvalues, $\Omega_n = E_n - E_0$, and they show up as poles in the density–density response function in the Lehmann representation [see eqn (7.19)]. The many-body excitation spectrum is schematically illustrated on the left-hand side of Fig. 9.6. The interacting wave functions are too complicated to be represented in a simple pictorial way—the best we can do is to simply draw a line for each level to indicate its energy. In this picture, electronic transitions take place between two many-body states, without making reference to individual electrons.

To categorize the excitations in an interacting system, further analysis of the wave functions with respect to a reference single-particle basis is necessary. Let us assume that we perform a full CI expansion of the many-body eigenstates Ψ_n,

$$\Psi_n = \sum_j c_{nj}\Phi_j \,, \tag{9.2}$$

where the Φ_j are a complete set of single Slater determinants. In quantum chemistry, the Φ_j are usually taken to be HF eigenstates of the system under study; in principle, however, any complete, orthonormal set of antisymmetric N-electron wave functions can be used to expand Ψ_n.

The conventional definition of single and multiple excitations is given with reference to the full expansion (9.2) (or a truncated expansion in practice), assuming that the Φ_j are single Slater determinants. If we ignore special situations involving degeneracy or near-degeneracy, it is usually the case that the dominant contribution to the many-body ground state Ψ_0 in eqn (9.2) is the ground-state Slater determinant Φ_0.

We speak of a "single excitation" if the expansion (9.2) of the excited many-body state Ψ_n is dominated by a particular singly excited Slater determinant. Similarly, a

"double excitation" refers to a many-body state that is dominated by a doubly excited Slater determinant, and so on. However, keep in mind that any full CI expansion will always have contributions from Slater determinants with single, double, triple, and any other multiple excitation. Several points need to be emphasized:

- One should properly refer to an excited many-body state as being of "predominantly m-fold excited character," rather than simply calling it an m-fold excitation. The latter terminology should be reserved for noninteracting systems only; interacting many-electron states are mixtures of differently excited single-particle Slater determinants.
- One often encounters situations where a clear assignment cannot be made, i.e., where there is more than one dominant term in the expansion in Slater determinants. As an example, there are many-body states that have both singly and doubly excited character, as we will see below.
- Even if an assignment (e.g., singly excited) can be made, it depends on the particular set of Slater determinants used as a reference. If a different set, say Φ'_j, is used in eqn (9.2), the character of the excitation may change. In other words, the single-particle basis with respect to which a many-body state Ψ_j is called "m-fold excited" should be specified.

9.3.2 Performance of TDDFT for double excitations

The Kohn–Sham noninteracting response function χ_s (7.80) has poles at the Kohn–Sham single excitations. Compared with the many-body response function (7.19), χ_s has fewer poles, since it does not account for double and multiple excitations (understood in the appropriate sense, discussed above). Solving the Casida equation (7.134) in a finite basis and using the adiabatic approximation for $f_{\rm xc}$, as is done in essentially all applications of TDDFT to molecules, will not change the number of poles, but just shift them. To obtain double excitations, a frequency-dependent $f_{\rm xc}(\omega)$ is needed which will generate additional solutions of the Casida equation.

Notwithstanding this simple counting argument, the statement "TDDFT in the adiabatic approximation does not give double excitations" needs to be taken with a grain of salt. Even simple adiabatic xc kernels such as $f_{\rm xc}^{\rm ALDA}$ do contain some correlation; the resulting TDDFT excitation energies therefore correspond to transitions involving multiply-excited determinants, using the quantum chemistry point of view of the previous subsection. For that reason, adiabatic TDDFT may actually be quite good at capturing excitations with a significant (but less than 50%) double-excitation character (Hirata and Head-Gordon, 1999; Hsu *et al.*, 2001).

But let us now consider the Be atom, as an example with clear-cut double excitations (Tozer and Handy, 2000). Experimentally, one finds two low-lying excitations of ^1D symmetry, one of which has double-excitation character ($2p^2$ at 7.00 eV) and the other one of which has single-excitation character ($2s3d$ at 7.99 eV). TDDFT produces just one line at 7.3 eV,[8] which is around the average of the two excitations. This behavior of adiabatic TDDFT is quite typical for systems with pairs of single and double excitations of the same symmetry (another example is methylene).

[8]This number was obtained using an asymptotically corrected GGA (Tozer and Handy, 2000).

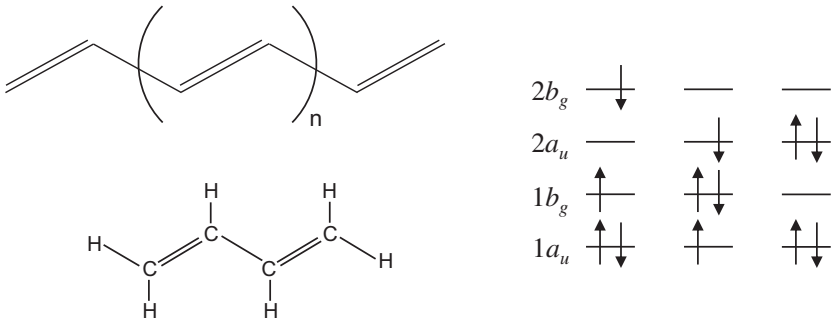

Fig. 9.7 Left: chemical structure of *trans*-polyenes (top) and one of their representatives, butadiene (bottom). Right: subspace of excited-state configurations which dominate in the optically dark 2^1A_g low-lying excitation in polyenes. In adiabatic TDDFT, only the first two excitations (HOMO $\rightarrow$ LUMO+1 and HOMO$-1 \rightarrow$ LUMO) contribute. The HOMO$^2 \rightarrow$ LUMO^2 excitation is mixed in using the dressed TDDFT approach (Cave *et al.*, 2004).

An important class of representatives of closed-shell molecules with low-lying doubly excited states is linear polyenes (see Fig. 9.7). Let us first clarify the notation: the excited states of *trans*-polyenes belong to the molecular symmetry group C_{2h} and are labeled according to their irreducible representations as A_g, B_g, A_u, and B_u.[9] The ground state of linear polyenes, such as butadiene (Fig. 9.7), is 1^1A_g. The lowest excited state is experimentally found to be the 2^1A_g dark state, which cannot be accessed by the usual optical spectroscopic techniques, but requires indirect techniques such as two-photon absorption. The optically allowed 1^1B_u state has a higher energy.

This sounds highly counterintuitive: how can a doubly excited state have a lower energy than a singly excited one (see also the example of the Be atom discussed above)? Naively, one would expect that, at least to lowest order in the Coulomb interaction, double excitations would be roughly twice as energetic. The resolution of this puzzle is as follows (Starcke *et al.*, 2006):

1. A large singlet–triplet splitting pushes the 1^1B_u singlet excited state up in energy.
2. There exist singly excited configurations of A_g symmetry (here, HOMO $\rightarrow$ LUMO $+1$ and HOMO $-1 \rightarrow$ LUMO) that mix with the doubly excited configuration (HOMO$^2 \rightarrow$ LUMO^2), which results in an overall lowering of the energy of the 2^1A_g state. See the right-hand side of Fig. 9.7, and also the next subsection.

Adiabatic xc kernels can accomplish the first effect, but the mixing of configurations requires a strong frequency dependence, as we will show below when we discuss the dressed TDDFT approach.

A universal, frequency-dependent xc functional which successfully describes double excitations in finite systems has so far been elusive, but much progress has been made. In Part III of this book, we describe several nonadiabatic TDDFT approaches which

[9] A full characterization of the states involves an additional label (+ or −), indicating symmetric or antisymmetric linear combinations of degenerate configurations (Starcke *et al.*, 2006). This index is often neglected in the literature, and we shall do the same here in the interests of notational simplicity.

have led to the construction of frequency-dependent xc kernels (Ullrich and Burke, 2004; Hellgren and von Barth, 2008, 2009), and we will discuss their successes and failures. Some recently developed nonadiabatic xc kernels (Romaniello *et al.*, 2009; Gritsenko and Baerends, 2009) have already shown promising results for double excitations in molecular model systems.

9.3.3 Dressed TDDFT approach

Above, we have given a simple counting argument, based on Casida's equations in a finite basis, for why double and multiple excitations require an expression for $f_{\rm xc}$ that is frequency-dependent. In this section, we go further and show explicitly what this frequency dependence looks like under certain assumptions that become exact in the appropriate limit. We shall follow here the work of Maitra *et al.* (2004).

The basic assumption is that we are dealing with a small manifold of excited states of a physical system which are well separated from all other excited states, and which can be characterized as mixtures of close-lying Kohn–Sham singly and doubly excited Slater determinants. To be specific, let us consider the case of a manifold of dimension two, consisting of a singly excited Kohn–Sham Slater determinant $\Phi_{ai} \equiv \Phi_S$ (where the single-particle orbital φ_i^0 is replaced with φ_a^0) and a doubly excited Slater determinant $\Phi_{bcjk} \equiv \Phi_D$ (where two orbitals, φ_j^0 and φ_k^0, are replaced with φ_b^0 and φ_c^0). Within this subspace, the interacting wave functions are expressed as

$$\Psi_l = c_S^{(l)}\Phi_S + c_D^{(l)}\Phi_D\,, \qquad l = 1, 2\,. \tag{9.3}$$

The approximate excitation energies of the interacting system are easily obtained by diagonalizing the many-body Hamiltonian (3.1), $\hat{H} = \hat{T}+\hat{V}+\hat{W}$, in this 2×2 subspace:

$$\begin{pmatrix} H_{SS} & H_{SD} \\ H_{DS} & H_{DD} \end{pmatrix} \begin{pmatrix} c_S^{(l)} \\ c_D^{(l)} \end{pmatrix} = E_l \begin{pmatrix} c_S^{(l)} \\ c_D^{(l)} \end{pmatrix}. \tag{9.4}$$

The resulting energy eigenvalues follow from the secular equation

$$(H_{SS} - E_l)(H_{DD} - E_l) - |H_{SD}|^2 = 0\,, \tag{9.5}$$

and the mixing coefficients $c_S^{(l)}$ and $c_D^{(l)}$ are then obtained from eqn (9.4).

Let us now rewrite eqn (9.5) in the following manner:

$$E_l = H_{SS} + \frac{|H_{SD}|^2}{E_l - H_{DD}}\,. \tag{9.6}$$

By setting $E_l = \Omega_l + H_{00}$, where H_{00} is the expectation value of $\hat{H}$ in the ground-state Kohn–Sham Slater determinant, we get an expression for the transition energy Ω_l:

$$\Omega_l = (H_{SS} - H_{00}) + \frac{|H_{SD}|^2}{\Omega_l - (H_{DD} - H_{00})}\,. \tag{9.7}$$

Notice that here we use H_{00} and not the true ground-state energy of the system, which is consistent with the level of approximation that went into calculating the excitation energies within a 2×2 Kohn–Sham subspace.

What we now want to do is to compare eqn (9.7) with the dressed SPA,

$$\Omega = \omega_{ia} + 2\langle S|f_{\rm H} + f_{\rm xc}(\Omega)|S\rangle \,, \tag{9.8}$$

and extract an expression for the frequency-dependent xc kernel. We separate the frequency-dependent xc kernel into an adiabatic and a dynamical part, $f_{\rm xc}(\Omega) = f_{\rm xc}^{\rm A} + f_{\rm xc}^{\rm dyn}(\Omega)$, and identify the adiabatic part as

$$H_{SS} - H_{00} = \omega_{ia} + 2\langle S|f_{\rm H} + f_{\rm xc}^{\rm A}|S\rangle \tag{9.9}$$

and the dynamic part as

$$2\langle S|f_{\rm xc}^{\rm dyn}(\Omega)|S\rangle = \frac{|H_{SD}|^2}{\Omega - (H_{DD} - H_{00})} \,. \tag{9.10}$$

This important result shows that the xc kernel has a strong frequency dependence in the vicinity of a double excitation. More than that, it also leads to a simple practical scheme for calculating double excitations with TDDFT:

1. First, calculate the TDDFT excitation spectrum of the system using an adiabatic xc kernel.
2. Check the Kohn–Sham spectrum for whether there are any close-lying single and double excitations that are well isolated from the rest of the spectrum. This is a sign that the related TDDFT excitation energies should have a significant double-excitation character.
3. Recalculate these excitation energies only, by using eqns (9.8)–(9.10).

Let us now return to the case of polyenes. Here the situation is slightly more involved since there are two Kohn–Sham single excitations and one double excitation which have to be mixed (Cave *et al.*, 2004; Mazur and Włodarczyk, 2008). From Fig. 9.7 the two single excitations are $1b_g \to 2b_g$ (Φ_{S_1}) and $1a_u \to 2a_u$ (Φ_{S_2}), and the double excitation is $1b_g^2 \to 2a_u^2$ (Φ_D). Let us define the matrix

$$\mathbb{K}_{\rm dyn}(\Omega) = \frac{1}{\Omega - (H_{DD} - H_{00})} \begin{pmatrix} |H_{S_1D}|^2 & H_{S_1D}H_{DS_2} \\ H_{S_2D}H_{DS_1} & |H_{S_2D}|^2 \end{pmatrix} \,, \tag{9.11}$$

which generalizes the dressed xc matrix element (9.10). $\mathbb{K}_{\rm dyn}$ is then included as an additional term in the adiabatic TDA, eqn (7.155), which defines the dressed TDA (D-TDA) as follows:

$$[\mathbb{A}_{\rm adia} + \mathbb{K}_{\rm dyn}(\Omega)]\mathbf{X} = \Omega\mathbf{X} \,. \tag{9.12}$$

Results for the 2^1A_g excitation of butadiene and hexatriene are shown in Table 9.5. Compared with the benchmark CASPT2 results, the uncorrected TDDFT results give a substantial overestimation of this doubly excited state by about 0.7 eV. The uncorrected TDA improves things but is still too high. The best answers are obtained with the D-TDA; there is a slight difference in how the D-TDA is implemented (self-consistently or not), but the results remain within 0.2 eV of CASPT2, which is quite impressive.

Table 9.5 2^1A_g vertical excitation energies for butadiene and hexatriene (in eV). The TDDFT calculations were performed with the B3LYP functional.

System	TDDFT[a]	D-TDDFT[a]	TDA[b]	D-TDA[a]	D-TDA(sc)[b]	CASPT2[c]
C_4H_6	7.02	5.93	6.56	6.28	6.02	6.27
C_6H_8	5.83	4.85	5.69	5.16	4.92	5.20

[a]Cave *et al.* (2004).
[b]Mazur and Włodarczyk (2008).
[c]Serrano-Andrés *et al.* (1993).

It should also be pointed out that the dressing procedure which we have outlined here is consistent when employed with the SPA or the TDA. One can try and include the correction $\mathbb{K}_{\rm dyn}$ in the Casida equation (where it is added to both $\mathbb{A}_{\rm adia}$ and $\mathbb{B}_{\rm adia}$). This gives the D-TDDFT results in Table 9.5, which are too low. Dressing the full Casida equation (or the SMA in the case of one singly excited level) thus results in an overcorrection, due to a nonlinearity that results in a certain degree of double counting of the mixing of single and double excitations (Mazur and Włodarczyk, 2008).

The dressed TDDFT approach is therefore a simple and pragmatic recipe to improve TDDFT calculations of excitations with significant double-excitation character. It needs to be pointed out, however, that it does not constitute a universal xc functional, and requires the user to examine each molecular spectrum case by case. We should also mention that the dressed TDDFT approach arises as a special case in the framework of a generalization of Casida's equation using propagator corrections (this is also known as the superoperator approach) (Casida, 2005).

9.4 Charge-transfer excitations

In this section, we consider a class of excitation processes in which charge physically moves from one region to a second region which is spatially separated from the first. Such processes can occur in a wide range of systems, such as in complexes of two or more molecules, or between different moieties (i.e., functional groups) within the same molecule. In general, excitation processes in which one can identify donor and acceptor regions or subsystems are called charge-transfer excitations. A schematic illustration is given in Fig. 9.8. The same figure also shows an example of a charge-transfer excitation involving two parts of the zincbacteriochlorin–bacteriochlorin (ZnBC–BC) complex (Dreuw and Head-Gordon, 2004). This system belongs to an important class of model systems for studying the function of light-harvesting complexes in plants and bacteria. An understanding of the charge-transfer properties of such (relatively) simple model complexes is important for elucidating photosynthetic processes in nature.

Unfortunately, it turns out that standard TDDFT fails in describing charge-transfer excitations. Dreuw and Head-Gordon (2004) found that the excitation energy in the ZnBC–BC example is drastically underestimated by around 2 eV. This failure is by no means an exception, but turns out to be symptomatic of the performance of standard TDDFT for charge-transfer excitations (Hieringer and Görling, 2006; Autschbach, 2009). In this section we will discuss why, and what can be done about it.

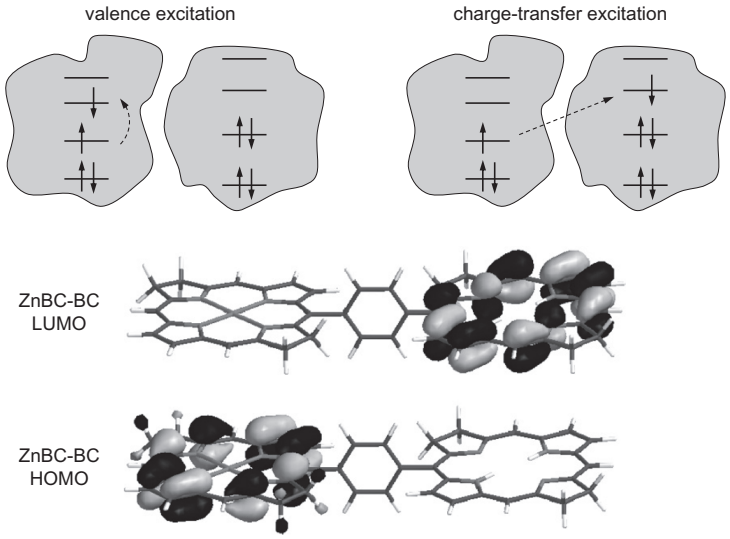

Fig. 9.8 Schematic illustration of valence and charge-transfer excitations of a system consisting of two fragments. The zincbacteriochlorin–bacteriochlorin complex exhibits a charge-transfer excitation, and the HOMO and LUMO levels are shown here. [Adapted with permission from ACS from Dreuw and Head-Gordon (2004), ©2004.]

9.4.1 Limit of large separation

We begin our discussion by considering the case where the donor and acceptor subsystems are separated by a large distance R. In this limit, the lowest charge-transfer energy Ω_{ct} can be obtained from elementary arguments. The minimum energy required to remove an electron from the donor is given by the donor's ionization potential I_d, but when the electron attaches to the acceptor, some of that energy is regained via the acceptor's electron affinity A_a. Once the electron has moved from donor to acceptor the two systems feel the electrostatic interaction energy $-1/R$ of the induced electron–hole pair. Altogether, for $R \to \infty$ we obtain

$$\Omega_{ct}^{\text{exact}} = I_d - A_a - \frac{1}{R}\,. \tag{9.13}$$

Now let us compare this with TDDFT. For the sake of this argument, it is sufficient to consider TDDFT in its simplest form, the SPA [eqn (7.159)], which assumes that the charge-transfer excitation under consideration is sufficiently far away from any other excitations of the total system:

$$\Omega_{ct}^{\text{SPA}} = \varepsilon_L^a - \varepsilon_H^d + 2\int d^3r \int d^3r'\; \varphi_L^a(\mathbf{r})\varphi_H^d(\mathbf{r}) f_{\text{Hxc}}(\mathbf{r},\mathbf{r}',\omega)\varphi_L^a(\mathbf{r}')\varphi_H^d(\mathbf{r}')\,, \tag{9.14}$$

where H and L denote the highest occupied and lowest unoccupied orbitals, respectively, of the donor and acceptor systems. Notice that $\varphi_L^a(\mathbf{r})$ and $\varphi_H^d(\mathbf{r})$ have exponentially vanishing overlap in the limit of large separation, which means that the double

integral in eqn (9.14) becomes zero—this, of course, assumes that the xc kernel remains finite at the charge-transfer excitation frequency, which is certainly the case for all standard approximations; we will come back to this point shortly and construct explicit forms of the xc kernel for which this matrix element does not vanish. But for all standard (semi)local, adiabatic xc kernels, TDDFT simply collapses to the difference between the bare Kohn–Sham eigenvalues,

$$\Omega_{ct}^{\mathrm{SPA}} \longrightarrow \varepsilon_L^a - \varepsilon_H^d \,. \tag{9.15}$$

Compared with the exact expression (9.13), this result is deficient in two respects. First of all, it misses the $-1/R$ component of Ω_{ct}. Secondly, from Section 2.2 we know that

$$I_d = -\varepsilon_H^d \,, \qquad\qquad A_a = -\varepsilon_L^a - \Delta_{\mathrm{xc}}^a \,, \tag{9.16}$$

which holds true for the exact Kohn–Sham eigenvalues, and where Δ_{xc}^a is the xc correction to the Kohn–Sham gap of the acceptor subsystem. In practice, the standard (semi)local approximations of DFT tend to give Kohn–Sham eigenvalues that are too low and completely miss the discontinuity Δ_{xc}^a. This explains why TDDFT often drastically underestimates charge-transfer excitations when conventional xc functionals are used.[10] A simple approximate scheme has been proposed to improve TDDFT charge-transfer excitation energies by manually shifting the donor and acceptor Kohn–Sham eigenvalue spectra relative to each other to account for the missing Δ_{xc}^a (Tozer, 2003).

9.4.2 Long-range (mostly hybrid) xc functionals

If one uses a TDHF approach to calculate excitation energies instead of using TDDFT (see Section 7.7), making the TDA and considering only the two relevant levels d and a, one finds in the limit of large separations that

$$\begin{aligned} \Omega_{ct}^{\mathrm{TDHF}} &= \varepsilon_L^{a,\mathrm{HF}} - \varepsilon_H^{d,\mathrm{HF}} - \int d^3r \int d^3r' \, \frac{\varphi_L^a(\mathbf{r})\varphi_L^a(\mathbf{r})\varphi_H^d(\mathbf{r}')\varphi_H^d(\mathbf{r}')}{|\mathbf{r}-\mathbf{r}'|} \\ &\longrightarrow \varepsilon_L^{a,\mathrm{HF}} - \varepsilon_H^{d,\mathrm{HF}} - \frac{1}{R} \,, \end{aligned} \tag{9.17}$$

i.e., the exchange integral is responsible for the $-1/R$ term. Furthermore, the Koopmans theorem implies $\varepsilon_L^{a,\mathrm{HF}} - \varepsilon_H^{d,\mathrm{HF}} \approx I_d - A_a$, so that the TDHF theory reproduces the charge-transfer excitation energy at large separation qualitatively correctly (Gimon *et al.*, 2009).[11]

It is therefore hardly surprising that the standard hybrid xc functionals, which contain a fraction of the exact HF exchange, will give at least some improvement over pure TDDFT methods when it comes to the description of charge-transfer processes.

[10] The argument immediately carries over from the SPA to the full Casida equation, since the relevant matrix elements $K_{ia\sigma,i'a'\sigma'}$ all involve nonoverlapping orbitals and thus vanish exponentially. A detailed analysis can be found in Hieringer and Görling (2006), where it is shown that this general problem also occurs for excitation processes between two nonoverlapping subsystems in which no net charge transfer takes place.

[11] Recall that the unoccupied HF energy eigenvalues correspond to electron attachment energies, whereas the unoccupied Kohn–Sham eigenvalues correspond to single-electron excitation energies.

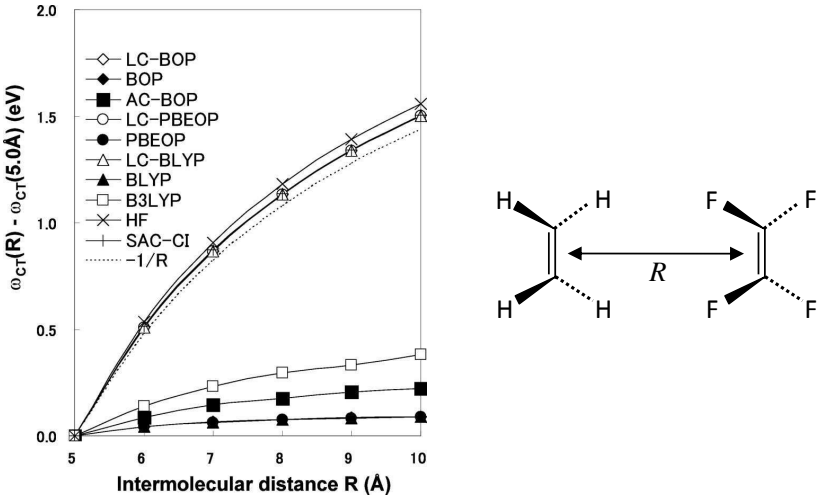

Fig. 9.9 Lowest charge-transfer excitation energy of the ethylene–tetrafluoroethylene dimer as a function of intermolecular distance R. The long-range-corrected (LC) hybrid functionals produce the correct behavior at large R. [Adapted with permission from AIP from Tawada *et al.* (2004), ©2004.]

This is particularly the case if the donor and acceptor regions are not too far separated so that the long-range behavior is not quite so dominant. An example of a successful TDDFT calculation using B3LYP is the work by Rappoport and Furche (2004), which resolved a long-standing debate regarding the occurrence of dual fluorescence and the excited-state geometry in 4-(dimethyl)aminobenzonitrile, a relatively small molecule exhibiting photoinduced intermolecular charge transfer. For larger systems, however, B3LYP and other standard hybrid functionals fail to cure the significant underestimation of charge-transfer energies, as shown by Dreuw and Head-Gordon (2004) for the ZnBC–BC example of Fig. 9.8.

The hybrid functional of Zhao and Truhlar (2006*b*, 2006*a*) contains full HF exchange and a matching meta-GGA xc functional, which depends on 35 fitting parameters that are determined via molecular test sets. At large separations, it reproduces the HF asymptotics and thus performs well for Rydberg and charge-transfer excitations.

In Section 2.3.3, we discussed range-separated hybrid functionals and saw that they produce the correct asymptotic behavior at large distances (where HF exchange takes over), while treating short-range correlations using the standard LDA or GGA. Figure 9.9 shows an example where several hybrid functionals were applied to charge-transfer excitations of a C_2H_4–C_2F_4 dimer at varying intermolecular distances (Tawada *et al.*, 2004). For comparison, TDHF and SAC-CI (symmetry-adapted cluster CI) results are also indicated. It is striking that the range-separated hybrids (here labeled LC, which stands for "long-range-corrected") agree perfectly with the correct behavior of eqn (9.13), whereas all other functionals—regular GGAs as well as hybrids—drastically underestimate the charge-transfer excitation energy of the complex.

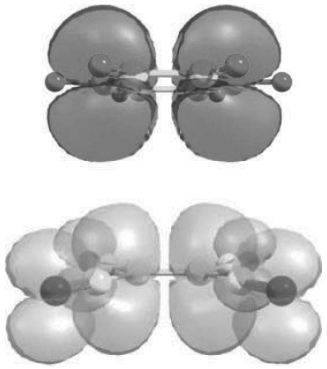

Fig. 9.10 Difference between the excited-state and ground-state densities in the benzene–TCNE complex (dark color, negative density difference; light color, positive density difference). [Adapted with permission from ACS from Stein *et al.* (2009), ©2009.]

Another example is given in Fig. 9.10, which shows the difference between the excited-state and ground-state densities in the benzene-tetracyanoethylene (TCNE) complex. Stein *et al.* (2009) calculated the lowest charge-transfer excitation energies in this and similar complexes (with an aromatic donor such as benzene, and TCNE as the acceptor). Using B3LYP, they found an excitation energy of 2.1 eV, which compares poorly with the experimental value of 3.59 eV. The nonempirical[12] range-separated hybrid functional of Livshits and Baer (2007), on the other hand, gave 3.8 eV, in good agreement with experiment. Similar trends were observed for all other complexes studied, and the oscillator strengths were also improved.

It thus appears that charge-transfer excitations, which not too long ago had been considered to be a typical failure of TDDFT, have now fallen within the reach of systematic quantitative studies thanks to new classes of hybrid xc functionals featuring full HF exchange at large distances. In Chapter 11, we will discuss another TDDFT approach which is suitable for charge-transfer excitations, based on a TDOEP treatment of exact exchange.

9.4.3 Constructing the exact xc kernel

Since TDDFT is formally exact, it is clear that the correct behavior (9.13) of charge-transfer excitations can be captured, at least in principle, with a suitably chosen xc kernel $f_{\rm xc}(\mathbf{r},\mathbf{r}',\omega)$, without the need to incorporate any nonlocal HF exchange. This question was first addressed by Gritsenko and Baerends (2004) by explicit construction. To start with, let us write down the SMA for the lowest charge-transfer excitation,

$$\left(\Omega_{ct}^{\rm SMA}\right)^2 = (\varepsilon_L^a-\varepsilon_H^d)^2+4(\varepsilon_L^a-\varepsilon_H^d)\int d^3r\int d^3r'\,\varphi_L^a(\mathbf{r})\varphi_H^d(\mathbf{r})f_{\rm Hxc}(\mathbf{r},\mathbf{r}',\omega)\varphi_L^a(\mathbf{r}')\varphi_H^d(\mathbf{r}'), \tag{9.18}$$

[12]In this hybrid functional, the range-separation parameter μ is determined self-consistently by enforcing eqn (2.46). In the case of charge-transfer excitations, the condition (2.46) is separately imposed on the donor and acceptor systems, which then yields an optimal μ by minimizing the error.

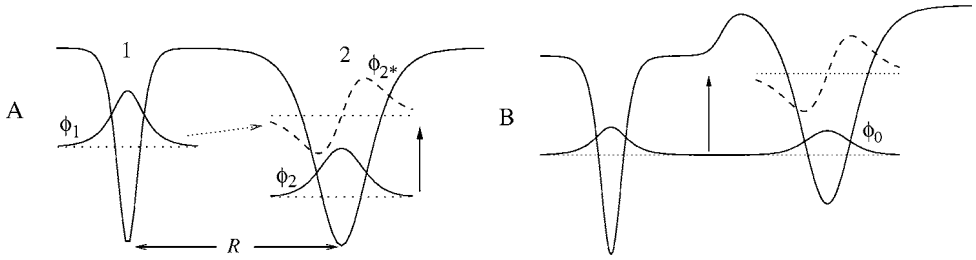

Fig. 9.11 A: schematic illustration of a long-range charge-transfer excitation. B: In exact DFT, the HOMOs of the two molecular fragments are lined up, and the Kohn–Sham effective potential develops a characteristic step. The HOMO and LUMO of the total system are delocalized over both fragments. [Adapted with permission from AIP from Maitra and Tempel (2006), ©2006.]

which generalizes the SPA (9.14) given above. As we showed, TDDFT just reduces to the bare Kohn–Sham excitation energies if the orbitals $\varphi_L^a(\mathbf{r}$ and $\varphi_H^d(\mathbf{r})$ are nonoverlapping, unless the xc kernel somehow succeeds in making the double integral on the right-hand side of eqn (9.18) finite. Let us define the two Coulomb matrix elements

$$K_{adad}^{\mathrm{C}} = \int d^3r \int d^3r' \; \varphi_L^a(\mathbf{r})\varphi_H^d(\mathbf{r}) \frac{1}{|\mathbf{r}-\mathbf{r}'|} \varphi_L^a(\mathbf{r}')\varphi_H^d(\mathbf{r}') \longrightarrow 0\,, \tag{9.19}$$

$$K_{aadd}^{\mathrm{C}} = \int d^3r \int d^3r' \; \varphi_L^a(\mathbf{r})\varphi_L^a(\mathbf{r}) \frac{1}{|\mathbf{r}-\mathbf{r}'|} \varphi_H^d(\mathbf{r}')\varphi_H^d(\mathbf{r}') \longrightarrow -\frac{1}{R}\,. \tag{9.20}$$

It is easy to verify that the following choice for the xc kernel will give $\Omega_{ct}^{\mathrm{SMA}} = \Omega_{ct}^{\mathrm{exact}}$ at large separations R:

$$f_{\mathrm{xc}}(\mathbf{r},\mathbf{r}') = \frac{1}{2K_{adad}^{\mathrm{C}}|\mathbf{r}-\mathbf{r}'|} \left\{ \Delta_{\mathrm{xc}}^a + K_{aadd}^{\mathrm{C}} + \frac{[\Delta_{\mathrm{xc}}^a - K_{aadd}^{\mathrm{C}}]^2}{2(\varepsilon_L^a - \varepsilon_H^d)} \right\}. \tag{9.21}$$

Since K_{adad}^{C} appears in the denominator of eqn (9.21), this expression diverges exponentially for large R. Together with suitable estimates of Δ_{xc}^a, the xc kernel (9.21) can be implemented as a simple asymptotic correction for long-range excitations (Gritsenko and Baerends, 2004).

The arguments we have given so far were all based on a scenario where the excitation involves two states that are localized in different regions of the system. But let us now examine a completely different situation, which applies to charge-transfer excitations between open-shell fragments (Maitra, 2005, 2006*a*), as illustrated in Fig. 9.11. We consider a simple case in which two different atoms, 1 and 2, are separated by a large distance R, and we assume that there are only two active electrons. In exact DFT, the singlet ground state is described by a doubly occupied Kohn–Sham orbital that is delocalized over the entire system. To achieve this, the exact Kohn–Sham potential develops a step between 1 and 2 such that the HOMO levels of the two isolated atoms are aligned. In this way, it is ensured that the system ends up with neutral fragments upon complete dissociation (Perdew *et al.*, 1982).

This leads to the curious situation that neither the HOMO (the bonding orbital) nor the LUMO (the antibonding orbital) of the total system is localized on one of the fragments! Furthermore, the highest occupied and first excited Kohn–Sham orbitals are nearly degenerate (except for a very small tunnel splitting ω_s), which means that the bare Kohn–Sham energy difference vanishes for large R. In this scenario, the lowest charge-transfer excitation must somehow emerge from within the subspace spanned by the HOMO and LUMO; what is essential here is that bonding–antibonding double excitations must be included.

Let us briefly sketch the derivation of Maitra (2005). The idea is to construct the exact kernel at the charge-transfer excitation using its definition (7.77),

$$f_{\rm Hxc}(\mathbf{r},\mathbf{r}',\omega) = \chi_s^{-1}(\mathbf{r},\mathbf{r}',\omega) - \chi^{-1}(\mathbf{r},\mathbf{r}',\omega)\,. \tag{9.22}$$

We thus need the interacting and noninteracting response functions in the reduced subspace spanned by the three nearly degenerate singlet two-electron Kohn–Sham states whose spatial parts are

$$\Phi_0 = \phi_0^+(\mathbf{r})\phi_0^+(\mathbf{r}')\,, \tag{9.23}$$

$$\Phi_S = 2^{-1/2}\left[\phi_0^+(\mathbf{r})\phi_0^-(\mathbf{r}) + \phi_0^-(\mathbf{r})\phi_0^+(\mathbf{r}')\right], \tag{9.24}$$

$$\Phi_D = \phi_0^-(\mathbf{r})\phi_0^-(\mathbf{r})\,, \tag{9.25}$$

where

$$\phi_0^\pm(\mathbf{r}) = \frac{\varphi_1(\mathbf{r}) \pm \varphi_2(\mathbf{r})}{\sqrt{2(1\pm S_{12})}} \tag{9.26}$$

and S_{12} is the exponentially small overlap integral between the atomic orbitals φ_1 and φ_2 on atoms 1 and 2. The spin parts of Φ_0, Φ_S, and Φ_D are all given by $(|\uparrow\downarrow\rangle - |\downarrow\uparrow\rangle)\sqrt{2}$.

From eqn (7.80), we easily derive

$$\chi_s(\mathbf{r},\mathbf{r}',\omega) = \frac{2\omega_s}{\omega^2-\omega_s^2}\,Q_s(\mathbf{r},\mathbf{r}')\,, \tag{9.27}$$

where $Q_s(\mathbf{r},\mathbf{r}') = [\varphi_1^2(\mathbf{r}) - \varphi_2^2(\mathbf{r})][\varphi_1^2(\mathbf{r}') - \varphi_2^2(\mathbf{r}')]/4$. To obtain a similar expression for the interacting response function, one needs to diagonalize the true Hamiltonian in the basis (9.23)–(9.25), which results in the following three interacting states (again, spatial part only):

$$\Psi_0 = 2^{-1/2}\left[\varphi_1(\mathbf{r})\varphi_2(\mathbf{r}') + \varphi_2(\mathbf{r})\varphi_1(\mathbf{r}')\right], \tag{9.28}$$

$$\Psi_{2\to1} = \varphi_1(\mathbf{r})\varphi_1(\mathbf{r}')\,, \tag{9.29}$$

$$\Psi_{1\to2} = \varphi_2(\mathbf{r})\varphi_2(\mathbf{r}')\,. \tag{9.30}$$

Here, Ψ_0 is the expected Heitler–London ground state, and $\Psi_{2\to1}$ and $\Psi_{1\to2}$ are charge-transfer states with energies $\omega_1 = I_2 - A_1 - 1/R$ and $\omega_2 = I_1 - A_2 - 1/R$ relative to the ground state. With this, we find the interacting response function as

$$\chi(\mathbf{r},\mathbf{r}',\omega) = \frac{2\omega_1}{\omega^2-\omega_1^2}\,Q(\mathbf{r},\mathbf{r}') + \frac{2\omega_2}{\omega^2-\omega_2^2}\,Q(\mathbf{r},\mathbf{r}')\,, \tag{9.31}$$

where $Q(\mathbf{r},\mathbf{r}') = 2\varphi_1(\mathbf{r})\varphi_2(\mathbf{r})\varphi_1(\mathbf{r}')\varphi_2(\mathbf{r}')$. Inserting everything into eqn (9.22) gives

$$f_{\rm Hxc}(\omega) = \frac{1}{2}\left[\frac{\omega^2-\omega_s^2}{\omega_s}\,Q_s^{-1} - \frac{(\omega^2-\omega_1^2)(\omega^2-\omega_2^2)}{\omega_2(\omega^2-\omega_1^2)+\omega_1(\omega^2-\omega_2^2)}\,Q^{-1}\right]. \tag{9.32}$$

We now make use of the f-sum rule, which implies $\omega_s Q_s = (\omega_1+\omega_1)Q$ within the present finite space. Lastly, we insert the Hxc kernel (9.32) into the SMA

$$\omega^2 = \omega_s^2 + 4\omega_s[\phi_0^+\phi_0^-|f_{\rm Hxc}|\phi_0^+\phi_0^-] \tag{9.33}$$

[using an obvious notation for the double matrix element of the Hxc kernel, see eqn (9.18)] and demand that we get the two exact charge-transfer excitations $\omega=\omega_1$ and $\omega=\omega_2$ as solutions. This gives the following final expression for the double matrix element between the bonding and antibonding Kohn–Sham levels:

$$\omega_s[\phi_0^+\phi_0^-|f_{\rm Hxc}|\phi_0^+\phi_0^-] = \omega_{av}^2 + \frac{\omega_1\omega_2-\omega_s^2}{4} + \frac{\omega_1\omega_2\omega_{av}^2}{\omega^2-\omega_1\omega_2}\,, \tag{9.34}$$

where $\omega_{av} = (\omega_1-\omega_2)/2$. We thus see that the exact Hxc kernel is strongly nonadiabatic, with a pole at $\omega=\sqrt{\omega_1\omega_2}$. In the light of the previous discussion in Section 9.3, this does not come as a surprise, since charge-transfer excitations between open-shell fragments involve near-degenerate double excitations in the Kohn–Sham system. What TDDFT needs to do in this case is to "undo" this near-degeneracy—also known as *static correlation*—in order to restore the correct charge-transfer excitation energies. To accomplish this, the frequency dependence of the xc kernel is essential.[13] None of the currently available approximate (nonhybrid) xc kernels are capable of accomplishing this difficult task.

9.5 The Sternheimer equation

So far, we have discussed applications of linear-response TDDFT to calculating excitation energies using the Casida equation. In the final two sections of this chapter, let us consider two alternative approaches based on somewhat different philosophies. The basic idea is to calculate excitation spectra without using expressions that mandate sums over unoccupied Kohn–Sham states—this has obvious practical advantages. As we will see, the Sternheimer equation and the real-time propagation approach accomplish this in different ways, and under certain circumstances these approaches are advantageous compared with solving the Casida equation.

Let us begin by writing the frequency-dependent density response, eqn (7.79), in the following way:

$$n_1(\mathbf{r},\omega) = \sum_{k=1}^{N}\left[\varphi_k^{0*}(\mathbf{r})\varphi_k^1(\mathbf{r},\omega) + \varphi_k^0(\mathbf{r})\varphi_k^{1*}(\mathbf{r},-\omega)\right]\,, \tag{9.35}$$

where

[13] Even worse, *all* excitations in stretched heteroatomic molecules consisting of open-shell fragments are plagued by this problem and require a nonadiabatic TDDFT treatment (Maitra, 2006*a*).

$$\varphi_k^1(\mathbf{r},\omega) = \sum_{j=1}^{\infty} \int d^3r' \, \frac{\varphi_j^0(\mathbf{r})\varphi_j^{0*}(\mathbf{r}')\varphi_k^0(\mathbf{r}')}{\omega - \omega_{jk} + i\eta} \left[v_1(\mathbf{r}',\omega) + \int d^3x \, f_{\mathrm{Hxc}}(\mathbf{r}',\mathbf{x},\omega) n_1(\mathbf{x},\omega) \right] . \tag{9.36}$$

In principle, to obtain $\varphi_k^1(\mathbf{r},\omega)$ one needs to evaluate an infinite sum over all occupied and unoccupied states. However, there is an elegant way to circumvent this task. By acting with $(\omega - \hat{H}_0 + \varepsilon_k + i\eta)$ on eqn (9.36) and using the static Kohn–Sham equation $\hat{H}_0\varphi_j^0(\mathbf{r}) = \varepsilon_j\varphi_j^0(\mathbf{r})$, it is easy to see that eqn (9.36) can be recast as follows:[14]

$$\left(\omega - \hat{H}_0 + \varepsilon_k + i\eta\right) \varphi_k^1(\mathbf{r},\omega) = \left[v_1(\mathbf{r},\omega) + \int d^3r' \, f_{\mathrm{Hxc}}(\mathbf{r},\mathbf{r}',\omega) n_1(\mathbf{r}',\omega) \right] \varphi_k^0(\mathbf{r},\omega) \, , \tag{9.37}$$

where we have used the completeness of the infinite set of ground-state Kohn–Sham orbitals. Equation (9.37) is known as the frequency-dependent or modified Sternheimer equation (Sternheimer, 1954; Mahan and Subbaswamy, 1990; Yabana *et al.*, 2006; Andrade *et al.*, 2007). Its advantage is that it allows one to calculate the frequency-dependent density response (9.35) without reference to unoccupied states: all one needs to do is solve N linear differential equations for the $\varphi_k^1(\mathbf{r},\omega)$ over a range of frequencies, which can be done by standard methods. Notice that the right-hand side of eqn (9.37) depends on $n_1(\mathbf{r},\omega)$, which means that eqns (9.35) and (9.37) have to be solved together in some form of iterative procedure until self-consistency is reached. From the density response one can then calculate the desired spectroscopic observables such as the dynamical dipole polarizability tensor $\boldsymbol{\alpha}(\omega)$ (see Section 7.2).

The Sternheimer approach to linear-response TDDFT has the advantage that it involves only occupied states, and therefore scales as N^2 when implemented in real space. A disadvantage is that convergence may be difficult to achieve close to a resonance; one then needs a small but finite imaginary part $i\eta$ to avoid a divergence, and the equations become complex. The method is therefore not ideal if only a few low-lying excitations are desired with high computational precision, but is most suitable if one is seeking to compute dynamic polarizabilities over a wide frequency range.

We should also mention a related but somewhat different version of linear-response TDDFT (Walker *et al.*, 2006; Rocca *et al.*, 2008), based on a continued-fraction superoperator scheme, which can be solved very efficiently using Lanczos techniques and therefore seems to be promising for the calculation of optical spectra of large systems.

As of today, there have been only a few applications of the Sternheimer approach in TDDFT for calculating dynamic polarizabilities and hyperpolarizabilities of atoms and molecules (Senatore and Subbaswamy, 1987; van Gisbergen *et al.*, 1997; Iwata *et al.*, 2001; Andrade *et al.*, 2007). On the other hand, the method has been very popular in static DFT, where it is also known under the name of density-functional perturbation theory (Baroni *et al.*, 2001) and is widely used to calculate phonon spectra and other response properties of materials.

[14] Notice that we could have replaced $\varphi_k^1(\mathbf{r},\omega)$ in eqn (9.35) with $\widetilde{\varphi}_k^1(\mathbf{r},\omega)$, which is obtained by limiting the sum over j in eqn (9.36) to the unoccupied orbitals only; the terms with $j \leq N$ cancel out in eqn (9.35). $\widetilde{\varphi}_k^1(\mathbf{r},\omega)$ is the first-order change in $\varphi_k^0(\mathbf{r})$ caused by a frequency-dependent perturbation $v_1(\mathbf{r},\omega) + \int d^3r' \, f_{\mathrm{Hxc}}(\mathbf{r},\mathbf{r}',\omega) n_1(\mathbf{r}',\omega)$. Working with $\widetilde{\varphi}_k^1(\mathbf{r},\omega)$, however, complicates eqn (9.37) by introducing projection operators (Andrade *et al.*, 2007).

9.6 Optical spectra via time propagation schemes

Spectral information about a system can be extracted from the frequency-dependent response function, as we have demonstrated throughout this chapter. Alternatively, the same information may be obtained from real-time propagation. In this section we present the basic ideas and applications of this method, and discuss its pros and cons.

9.6.1 Formal aspects and initial excitation mechanism

As explained in Chapter 7, an electronic excitation at a frequency Ω is associated with a specific charge-density fluctuation, which can be viewed as an electronic eigenmode of the system. The eigenmode profile $n_1(\mathbf{r}, \Omega)$ of each excitation is unique and can be calculated from the solutions of the Casida equation (7.133), where we have dropped the spin index for simplicity. If such an eigenmode were set in motion in any system (say, a molecule) by whatever means, it would keep oscillating forever at the frequency Ω without any external driving field to keep it going. The time-dependent density of such an eigenmode is

$$n_1(\mathbf{r}, t) = n_1(\mathbf{r}, \Omega) e^{-i\Omega t} \,, \tag{9.38}$$

and the associated dipole power spectrum (see Section 7.2) has a single sharp peak at the frequency Ω. In other words, if we are given the time-dependent density $n_1(\mathbf{r}, t)$ over a sufficiently long time interval that we can accurately calculate the Fourier transform of the dipole moment $\mathbf{d}(t) = \int d^3r\, \mathbf{r} n(\mathbf{r}, t)$, we can go back and obtain from it the associated excitation energy Ω of the system.

The argument can easily be extended to the case where the system is in a state where several excitations are present simultaneously, i.e., where there is a superposition of eigenmodes. The time-dependent density can then be written as

$$n_1(\mathbf{r}, t) = C_1 n_1(\mathbf{r}, \Omega_1) e^{-i(\Omega_1 t + \alpha_1)} + C_2 n_1(\mathbf{r}, \Omega_2) e^{-i(\Omega_2 t + \alpha_2)} + \dots \,. \tag{9.39}$$

Fourier transformation of the oscillating dipole moment produces discrete peaks at the excitation frequencies Ω_i of the coexisting modes. If every possible mode were present, we would therefore be able to get the complete excitation spectrum of the system.

So far, so good—but the question is, how do we prepare the system in a superposition of eigenmodes? The answer turns out to be surprisingly simple. To give an everyday analogy from the area of acoustics, consider a bell that is given a single sharp blow with a hammer. The bell then starts to sound with a characteristic combination of the fundamental and overtones, and the associated frequency spectrum can be extracted from the measured sound profile. The spectral shape will depend somewhat on how the bell was hit with the hammer, but that doesn't affect the positions of the peaks.

So, what is the "hammer" in TDDFT? Basically, any sudden perturbation at time $t = 0$, such as a sudden switching or a force impulse, and letting the system freely propagate afterwards. To see how this works, consider again the first-order electronic dipole polarization induced by an externally applied electric field that was given in eqn (7.42). From this, we can express the dipole polarizability as

$$\alpha_{\mu\nu}(\omega) = \frac{p_{1\mu}(\omega)}{E_\nu(\omega)} \,, \tag{9.40}$$

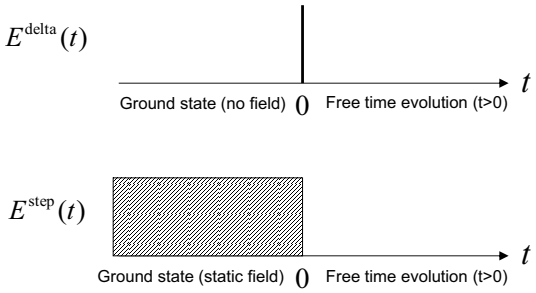

Fig. 9.12 Illustration of the electric fields (9.41) and (9.46) used to trigger dipole oscillations in a system. In both cases, the excitation spectrum is obtained by free time propagation for $t > 0$ and Fourier transformation of the resulting time-dependent dipole moment.

where $E_\nu(\omega)$ can in principle be the Fourier transform of any time-dependent electric field, not just a monochromatic one as we assumed in Section 7.2. For the purpose of triggering as many excitations as possible, it will be advantageous to choose an initial excitation which covers a broad spectral range. Let us now discuss two important examples.

Impulsive electric field. We first consider the extreme case of an external electric field that has the shape of a delta impulse in time:

$$E_\nu^{\text{delta}}(t) = \mathcal{I}\,\delta(t)\,, \tag{9.41}$$

where $\mathcal{I}$ is the magnitude of the electric-field impulse. The Fourier transform of this, $E_\nu(\omega) = \mathcal{I}$, is the same for all frequency components, and should therefore excite all electronic eigenmodes of the system alike. For a system that is in the ground state for $t < 0$, we find[15]

$$\alpha_{\mu\nu}^{\text{delta}}(\omega) = \frac{1}{\mathcal{I}} \int_0^\infty dt\, p_\mu^{\text{delta}}(t) e^{i\omega t}\,. \tag{9.42}$$

When treated as an external time-dependent potential, a delta impulse presents some practical difficulties when one is solving the TDKS equation numerically, because one always needs to work with finite time steps; fortunately, there is a much more convenient alternative (Yabana *et al.*, 2006). Let us assume that we start with the system in its ground state at time $t_0 = 0^-$, infinitesimally before time $t = 0$. To obtain the TDKS orbitals infinitesimally later, at time $t = 0^+$ following excitation with the pulsed field (9.41), we use the time evolution operator (3.12) and write

$$\varphi_j(\mathbf{r}, 0^+) = \exp\left\{-i \int_{0^-}^{0^+} dt' [\hat{H}_0 + \mathcal{I}\,\delta(t') r_\mu]\right\} \varphi_j(\mathbf{r}, 0^-)\,, \tag{9.43}$$

[15] We assume here that the system is unpolarized in its ground state. A generalization to the case of polar systems is straightforward.

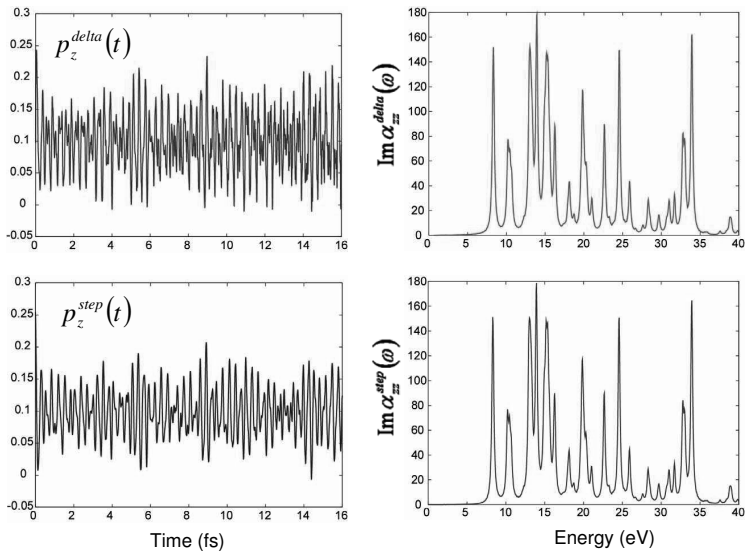

Fig. 9.13 Time-dependent dipole polarization $p_z(t)$ and imaginary part of the frequency-dependent polarizability $\alpha_{zz}(\omega)$ (both in arbitrary units) for a CO molecule excited with a delta impulse field or a suddenly switched-off field along the molecular axis. The dipole polarizations are quite different, but the resulting polarizabilities are almost indistinguishable. [Figure courtesy of J. J. Rehr.]

where $\hat{H}_0$ is the ground-state Kohn–Sham Hamiltonian, whose eigenfunctions are given by $\varphi_j(\mathbf{r}, 0^-) = \varphi_j^0(\mathbf{r})$. Notice that we can use $\hat{H}_0$ in eqn (9.43) because the time propagation interval is infinitesimally short. This gives

$$\varphi_j(\mathbf{r}, 0^+) = e^{-i\mathcal{I}r_\mu}\, \varphi_j^0(\mathbf{r})\,, \tag{9.44}$$

i.e., the effect of the initial pulsed electric field is to add the same space-dependent phase factor to all initial Kohn–Sham orbitals. This does not alter the initial density but produces an initial current along the r_μ direction:

$$j_\mu(\mathbf{r}, 0^+) = -\mathcal{I}n_0(\mathbf{r})\,. \tag{9.45}$$

In other words, all electrons experience an instantaneous boost at the initial time and are then allowed to move freely.

Sudden switching. In this case, a static uniform electric field is switched off at the initial time:

$$E_\nu^{\mathrm{step}}(t) = \begin{cases} E_0 & \text{for } t < 0 \\ 0 & \text{for } t > 0\,. \end{cases} \tag{9.46}$$

This means that one first needs to calculate the Kohn–Sham ground state of the system in the presence of the field[16] and then propagate the TDKS equation for $t > 0$ without the field. The system is initially in a polarized state, and then oscillates freely after the electric field is gone.

The Fourier transform of eqn (9.46) is $E_\nu(\omega) = E_0/i\omega$. We obtain the dipole polarizability as

$$\alpha^{\rm step}_{\mu\nu}(\omega) = \frac{p^{\rm step}_\mu(t=0)}{E_0} + \frac{i\omega}{E_0}\int_0^\infty dt\, p^{\rm step}_\mu(t) e^{i\omega t}\,, \tag{9.47}$$

where the first term on the right-hand side accounts for the fact that the system starts out from a polarized ground state.

The electric fields (9.41) and (9.46) are schematically illustrated in Fig. 9.12. In Fig. 9.13 we give an example of the dipole excitation spectrum of the CO molecule, calculated with respect to the molecular axis using the two excitation mechanisms. The resulting spectra are almost indistinguishable, in spite of the fact that the time-dependent dipole oscillations look quite different. This shows that the time propagation method is robust with respect to the choice of excitation mechanism, as long as the initial switching process is sufficiently rapid and the following time propagation runs over a sufficiently long interval, so that a clean spectrum can be obtained.

In order to probe the linear-response regime only, the strength of the excitation should be as low as possible, but not too weak, so that the signal is not buried in numerical noise. Since time propagation treats all orders of the perturbation on an equal footing, this approach is also suitable for studying nonlinear response properties. We will return to this point later.

9.6.2 Applications

Let us now ask: under what circumstances is it preferable to use time propagation methods, as opposed to the Casida equation (or other linear-response-based methods), to describe the excitation properties of a given system?

- The Casida equation is generally the superior method for low-lying, well-separated excitation energies of molecular systems. One of its main bottlenecks is that it depends on unoccupied states; this can lead to slow convergence with respect to the basis size, especially for higher excitation energies.
- Time propagation methods are particularly advantageous if they are carried out on real-space grids. The problem of the unoccupied states is then easily dealt with, since one is not limited by the choice of basis; instead, the unoccupied states come in automatically during the time evolution of the system. Time propagation methods are most convenient if one wants an excitation or photoabsorption spectrum over a large spectral range, including the continuum and autoionizing states.

[16] Strictly speaking, the ground state of any finite system is not stable against tunneling ionization if a uniform electric field is present, since there exists an asymptotic region where the Coulomb barrier is suppressed, no matter how weak the field. In practice, this is not a problem, because one works with finite grids or finite basis sets so that this asymptotic region does not play a role; alternatively, the field can be chosen to have a cutoff at a finite range.

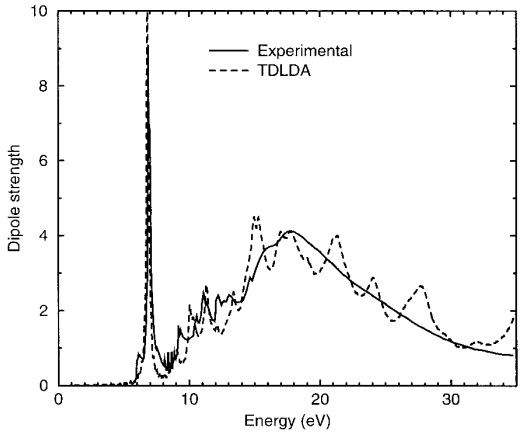

Fig. 9.14 Optical absorption of the benzene molecule, calculated using the ALDA and real-time propagation. [Adapted with permission from John Wiley & Sons from Yabana and Bertsch (1999*b*), ©1999.]

They are also preferable for metallic systems and clusters, which are dominated by collective excitations.

- In practice, one can achieve a numerical scaling of TDDFT in the Casida formalism of N^2 to N^3, depending on the details of the implementation. A substantial part of the computational cost goes into building the matrix that needs to be diagonalized. The numerical scaling of the time propagation method, on the other hand, is somewhere around N to N^2; an important cost factor that needs to be added is that the time propagation can require a small time step.

At the end of the day, there is no clear winner when it comes to an all-purpose approach for calculating excitation properties of finite molecular systems; each approach has its pros and cons, which need to be weighed against the demands for numerical accuracy and resolution of the spectral features, and numerical efficiency. However, one major advantage of the time propagation method is that it is very straightforward to go over to the nonlinear regime. In Chapter 16, we will see that one can describe highly nonlinear, strong-field processes using essentially the same codes that are used to obtain linear excitation spectra.

Let us conclude this section by looking at some applications. The first example is shown in Fig. 9.14, where the optical absorption (measured as dipole strength) of the benzene molecule is given. The calculation, using the ALDA on a real-space grid (Yabana and Bertsch, 1996, 1999*b*; Yabana *et al.*, 2006) compares very favorably with experiment over a wide energy range.

Real-time TDDFT calculations have also been carried out for larger systems (Marques *et al.*, 2003; Takimoto *et al.*, 2007; Botti *et al.*, 2009). Figure 9.15 shows the optical absorption of boron fullerenes as an example of large inorganic systems. Here, the real-time calculations were performed using the PBE xc functional.

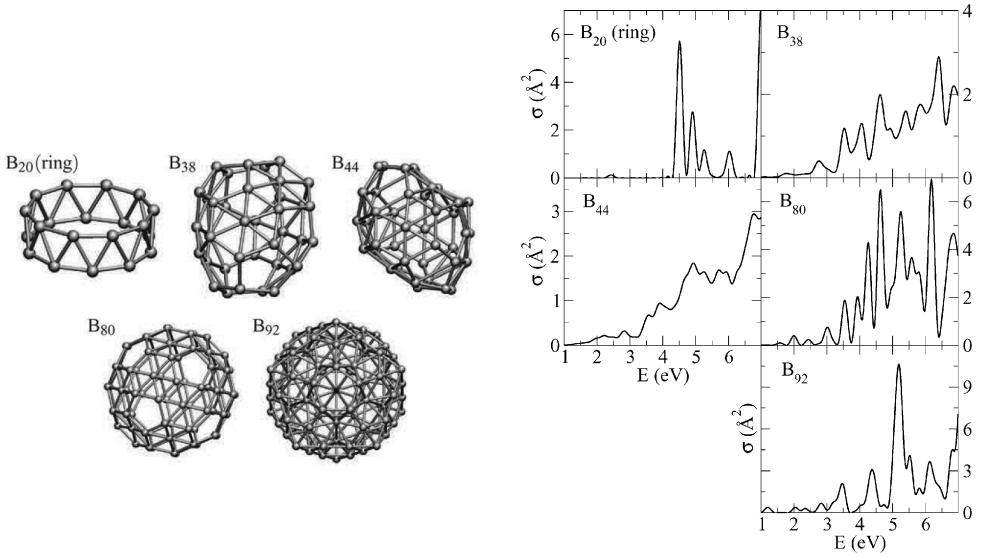

Fig. 9.15 Absorption cross section (in Å^{-2}) of various boron cages. [Adapted with permission from the PCCP Owner Societies from Botti *et al.* (2009), ©2009.]

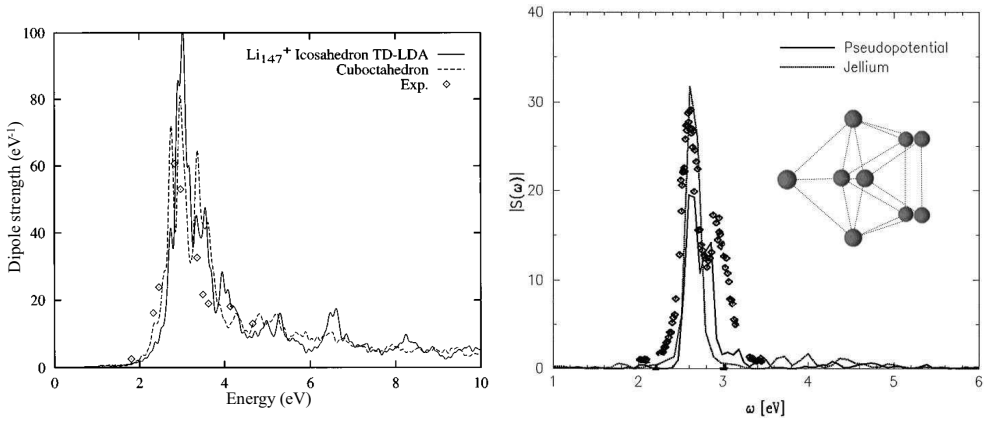

Fig. 9.16 Dipole spectra of an Li_{147}^{+} cluster (left) and an Na_{9}^{+} cluster (right). [Adapted with permission from the APS from Yabana and Bertsch (1996), ©1996, and from Elsevier from Calvayrac *et al.* (2000), ©2000.]

Among the first applications of the TDKS scheme were calculations of the excitation spectra of metallic clusters (Yabana and Bertsch, 1996; Ullrich *et al.*, 1997; Calvayrac *et al.*, 2000). The examples shown in Fig. 9.16 are typical of the optical spectra of clusters of alkali metal atoms: they are dominated by a strong plasmon peak at an energy on the order of 3 eV, and have some smaller spectral features at

higher energies. The agreement with experimental data is generally excellent (as far as high-resolution spectroscopic data is available for clusters), even using very simple ALDA calculations. The basic features of the optical response of metal clusters can be captured even at the level of simple spherical or deformed jellium models, owing to the delocalized character of the valence electrons.

Exercise 9.1 In Section 9.3.3, we derived the matrix elements of the dressed xc kernel (9.10) for double excitations by direct diagonalization in a reduced two-level subspace. The frequency dependence of this kernel can also be derived in an alternative way (Maitra *et al.*, 2004). Consider, as in eqn (9.3), a subspace consisting of two wave functions, where the exact wave functions are mixtures of singly and doubly excited Slater determinants:

$$\Psi_1 = \sqrt{1-m^2}\Phi_S + m^2\Phi_D \,, \qquad \Psi_2 = -m^2\Phi_S + \sqrt{1-m^2}\Phi_D \,,$$

where $0 < m < 1$. The Lehmann representations of the noninteracting and interacting response functions can be written as

$$\chi_s(\mathbf{r},\mathbf{r}',\omega) \approx \frac{A(\mathbf{r},\mathbf{r}')}{\omega-\omega_{ia}} \,, \qquad \chi(\mathbf{r},\mathbf{r}',\omega) \approx A(\mathbf{r},\mathbf{r}')\left(\frac{1-m^2}{\omega-\Omega_1}+\frac{m^2}{\omega-\Omega_2}\right) \,,$$

where $A(\mathbf{r},\mathbf{r}') = \varphi_1^0(\mathbf{r})\varphi_a^0(\mathbf{r})\varphi_i^0(\mathbf{r}')\varphi_a^0(\mathbf{r})$. Use the definition $f_{\rm Hxc} = \chi_s^{-1} - \chi^{-1}$ in eqn (9.8) and show that this produces $\langle ia|f_{\rm Hxc}(\omega)|ia\rangle$, with the same frequency dependence as eqn (9.10).

Exercise 9.2 Verify eqn (9.21), the expression for the xc kernel that produces the correct SMA long-range charge-transfer excitations.

Exercise 9.3 Go over the steps of the derivation of the frequency-dependent xc kernel in eqn (9.32), and verify eqn (9.34) for the double matrix element between the bonding and antibonding states.

Exercise 9.4 Static Kohn–Sham theory produces the exact ground-state density $n_0(\mathbf{r})$. We also know that the static many-body Hamiltonian and, hence, all of its eigenstates Ψ_j can be formally expressed as implicit functionals of n_0. But how can one actually find the excited-state densities $n_j(\mathbf{r}) = \langle\Psi_j|\hat{n}(\mathbf{r})|\Psi_j\rangle$ in practice? There is no Hohenberg–Kohn theorem for excited states (Gaudoin and Burke, 2004), so static DFT methodologies don't really help.

Find a procedure by which the exact excited-state densities $n_j(\mathbf{r})$ for arbitrary excited states can be found using TDDFT. Assume that the exact excitation energy $E_j - E_0$ is known from linear-response TDDFT, and come up with some time propagation scheme, using a suitable time-dependent driving field, that allows you to extract $n_j(\mathbf{r})$ from the time-dependent response of the system.

Exercise 9.5 This is a numerical exercise, based on the homemade computer code for 1D lattice systems of Exercise 4.2. The task is to find the excitation spectrum of a noninteracting system using a time propagation scheme.

Consider a one-electron system subject to a soft-core attractive Coulomb potential (see Exercise 4.5) corresponding to a 1D hydrogen atom. Implement the two excitation methods of Section 9.6.1, the impulsive field and the sudden switching, and carry out the subsequent numerical time propagation. Calculate the time-dependent dipole moment, and from this obtain the frequency-dependent dipole polarizability through Fourier transformation. Plot the resulting excitation spectra, and compare your results with the single-particle excitation energies that you obtained from solving the static Schrödinger equation.